

Stochastic dynamics of small ensembles of non-processive molecular motors: the parallel cluster model

Thorsten Erdmann,¹ Philipp J. Albert,¹ and Ulrich S. Schwarz¹

*BioQuant, Heidelberg University, Im Neuenheimer Feld 267,
69120 Heidelberg, Germany and Institute for Theoretical Physics,
Heidelberg University, Philosophenweg 19, 69120 Heidelberg,
Germany*

(Dated: 26 September 2018)

Non-processive molecular motors have to work together in ensembles in order to generate appreciable levels of force or movement. In skeletal muscle, for example, hundreds of myosin II molecules cooperate in thick filaments. In non-muscle cells, by contrast, small groups with few tens of non-muscle myosin II motors contribute to essential cellular processes such as transport, shape changes or mechanosensing. Here we introduce a detailed and analytically tractable model for this important situation. Using a three-state cross-bridge model for the myosin II motor cycle and exploiting the assumptions of fast power stroke kinetics and equal load sharing between motors in equivalent states, we reduce the stochastic reaction network to a one-step master equation for the binding and unbinding dynamics (*parallel cluster model*) and derive the rules for ensemble movement. We find that for constant external load, ensemble dynamics is strongly shaped by the catch bond character of myosin II, which leads to an increase of the fraction of bound motors under load and thus to firm attachment even for small ensembles. This adaptation to load results in a concave force-velocity relation described by a Hill relation. For external load provided by a linear spring, myosin II ensembles dynamically adjust themselves towards an isometric state with constant average position and load. The dynamics of the ensembles is now determined mainly by the distribution of motors over the different kinds of bound states. For increasing stiffness of the external spring, there is a sharp transition beyond which myosin II can no longer perform the power stroke. Slow unbinding from the pre-power-stroke state protects the ensembles against detachment.

I. INTRODUCTION

Numerous processes in single cells and tissues require the generation of mechanical force and directed motion. Most of these processes are based on the activity of molecular motors interacting with the filaments of the cytoskeleton, that is, motors from the dynein-, kinesin- and myosin-families interacting with microtubule or actin filaments¹. Examples include separation of chromosomes and closure of the constriction ring during cell division, intracellular transport of cargo vesicles and organelles, contraction of muscle cells, large-scale rearrangements in a developing tissue, and wound closure after tissue injury. The mechanical energy used in these processes is gained by hydrolysis of ATP and drives a cycle of conformational changes in the allosteric motor molecules. Over the last decades, the way single motor molecules work has been dissected in great quantitative detail^{2,3}. However, it remains a formidable challenge to understand how molecular motors work in the physiological context of cells and tissues, where they usually collaborate in groups⁴. Here we theoretically address one crucial aspect of this situation, namely force generation in small ensembles of non-processive motors.

A large research effort has been focused on processive motors which stay attached to the substrate sufficiently long as to not lose contact for many motor cycles⁵. For example, the two motor heads of conventional kinesin typically take more than 100 steps of 8 nm length before the motor unbinds from its microtubule track^{6,7}. Although this property would enable processive motors to work alone, experimental evidence suggests that also processive motors in a physiological context often collaborate in small groups⁸. The main benefit here is that attaching several motors to the same cargo increases the walk length dramatically⁹ and allows the cargo to pass over defects on the track and change reliably between tracks of finite length¹⁰. Furthermore, because the velocity of a processive motor typically decreases with the applied load, groups of motors sharing an external load are able to transport cargo at larger velocities or to exert larger forces on a cargo or an elastic element. As an example for the latter, it has been shown that the force necessary to pull membrane tubes from a lipid vesicle can only be produced by groups of processive motors^{11,12}.

In contrast to processive motors, non-processive motors cannot do useful work single-handedly and therefore necessarily have to operate in groups in order to generate persistent motion or appreciable levels of force. The paradigm for a non-processive motor acting in ensembles is myosin II in cross-striated skeletal muscle¹³. In the muscle sarcomere, hundreds of myosin II motors are assembled in so-called thick filaments. The arrangement of myosin II in a thick filament is of

bipolar order, that is, the myosin II motors in the two halves of a thick filament are oriented in opposing direction. The myosin II motors in either half of a thick filament walk as an ensemble on so-called thin filaments, actin filaments which are anchored in the two Z-discs bounding the sarcomere. The arrangement of thick and thin filaments is symmetric with respect to the mid-plane of the sarcomere so that motor activity leads to muscle contraction. Investigation of the structure of muscle has been facilitated by the remarkable precision of the spatial arrangement of myosin II motors in the sarcomere. For example, in frog skeletal muscle each half of a thick filament contains 294 myosin II motors which are arranged at a very regular distance of 14.5 nm¹⁴.

Even before myosin II had been biochemically characterized, the first theoretical description of muscle contraction was already based on the non-equilibrium binding and unbinding kinetics of myosin to actin which effectively rectified thermal fluctuations of an elastic element¹⁵. In this early model, myosin was described as an actin binding site fluctuating in a harmonic potential and binding preferentially ahead of and unbinding preferentially behind its equilibrium position, thus inducing a net force displacing the actin filament. Precise measurements of contraction speed as function of force in combination with X-ray diffraction and detailed modeling allowed to identify the chemical and mechanical details of the myosin II hydrolysis cycle and led to the development of the crossbridge model^{16,17}, which provided a molecular mechanism for the principle of preferential binding and unbinding proposed by Huxley¹⁵. Those advances inspired theoretical models analyzing the statistical physics of large ensembles of myosin II motors simultaneously pulling on a single filament^{18,19}. With these models it has been shown that in order to describe the response of skeletal muscle to varying loading conditions it is essential that the unbinding rate of myosin II from actin is a decreasing function of the applied load. In contrast to, e.g., the processive motor kinesin, this make myosin II a catch bond rather than a slip bond^{20,21} and leads to the recruitment of additional crossbridges under load. Experimentally, this has been confirmed in a combination of mechanical and X-ray techniques¹⁴.

Apart from muscle tissue, groups of myosin II molecular motors are also active in the organization of the actin cytoskeleton of non-muscle tissue cells like fibroblasts. Increasing evidence shows that non-muscle myosin II motors acting in small groups play a crucial role in cell adhesion and migration, with dramatic implications for development, health and disease²². For example, myosin II motors contribute to the retrograde flow of the actin cytoskeleton away from the leading edge during cell spreading and migration²³ as well as to the maintenance of cortical tension underlying cell shape, movement and division^{24,25}. Adherent tissue cells in culture tend to form

contractile actin bundles called *stress fibers* which play an important role in force generation and mechanosensing²⁶. There exist several kinds of stress fibers and only some of them (most notably ventral stress fibers) bear some similarity with skeletal muscle in being characterized by a sarcomeric organization with alternating regions of the crosslinker α -actinin and myosin II²⁷.

While skeletal and cardiac muscle show a large degree of order, smooth muscle is characterized by far more disordered actin-myosin assemblies. Nevertheless, in all types of muscle, myosin II motors work in large groups. The organization of cytoskeletal actin and myosin structures is, in general, far more disordered and far more dynamic than the actin-myosin assemblies in all types of muscle tissue. Most importantly, the number of myosin II motors in the ensembles is much smaller: non-muscle myosin II is usually organized in minifilaments with a bipolar structure similar to thick filaments but comprising only 10-30 myosin II motors, as has been estimated from the size of minifilaments in electron micrographs²⁸. The exact numbers of myosin II motors in different actin modules will vary depending on the cellular conditions under which minifilaments are formed. Recently, contractile actin bundles have been reconstituted *in vitro*²⁹⁻³¹. It was demonstrated that for sufficiently large concentration, myosin II minifilaments are able to contract parallel bundles as well as networks of actin filaments with random polarity. In these experiments, the number of myosin II molecules in the minifilaments depends on the type of myosin II and the preparation of the minifilaments and was estimated to range from 56 for non-muscle myosin II³⁰ to several 100 for muscle myosin II. Due to the small duty ratio of (smooth) muscle myosin II of 0.04³⁰ compared to a duty ratio of 0.23 for non-muscle myosin II³¹, however, the number of myosin II attached to the substrate should be comparable for muscle and non-muscle minifilaments. For a minifilament with 200 muscle myosin II molecules, the number of attached motors may well be as low as 8²⁹.

For the small number of myosin II motors in cytoskeletal minifilaments, stochastic effects are expected to become important and have indeed been observed in measurements of the tension generated by myosin II motors in reconstituted assays. In three bead assays, an actin filament is held in two optical traps and myosin II attached to the surface of a third bead is allowed to bind to the actin filament. At elevated myosin II concentrations^{20,32,33}, several myosin II are able to bind simultaneously and the displacement of the actin filament against the trap force is observed. In active gels, which are *in vitro* mixtures of actin filaments, actin crosslinkers and myosin II minifilaments, the fluctuating tension in the actin network induced by the activity of myosin II minifilaments is measured^{31,34}. In motility assays, myosin II motors are distributed over a surface

and the movement of an actin filament against an external force is followed³⁵⁻³⁷. Such reconstituted assays characteristically reveal noisy trajectories with a gradual build-up of tension followed by an abrupt release, which is likely due to the detachment of the whole ensemble of myosin II motors, allowing the actin filament to slip. However, a detailed and analytically tractable model for this important situation is still missing.

In order to interpret experimental data from cellular and reconstituted assays in terms of molecular properties, theoretical models are required which allow to calculate experimentally accessible quantities like duty ratio and force-velocity relation for small and variable number of motors in an ensemble. At the same time, known molecular characteristics, in particular the catch bond character of myosin II and conformational changes as the power stroke, should be included in the model. Such a model should not only permit to estimate the number of motors present in the experiment, but also provide a deeper understanding of the generic principles governing the statistics of motor ensembles. Here, we present such a model for the non-processive molecular motor myosin II. A short account of some of our results has been given previously³⁸.

Our work is motivated by the long tradition in modeling force generation in skeletal muscle. Generic models for molecular motors investigate the fundamental conditions for the generation of directed motion in a thermal environment but do not take specific properties of molecular motors into account. In ratchet models, a particle switches between diffusive movement in a flat potential and in a periodic potential³⁹. By breaking detailed balance for the transitions between the two potential landscapes, directed motion of the particle can ensue. Ratchet models allow to study generic effects of cooperativity of a large number of motors such as the emergence of directed motion in symmetric systems or spontaneous oscillations^{39,40}. Diffusion and switching of the particles is usually described in the framework of a Fokker-Planck equation. Within this framework, the effect of a finite ensemble size has been included by assuming a fluctuating drift velocity with a noise intensity that increases with decreasing ensemble size³⁶. This approach allows to observe effects specific for finite sized ensembles, such as the reversal of the direction of motion⁴¹. Beginning with the work of Huxley¹⁵, some molecular characteristics were introduced by assuming different conformational states of the motor molecules. With the focus on the large assemblies of motors in muscle, analytical progress was usually made using mean-field approximations. A mean-field model for molecular motors with three conformational states, in which the bound motors moved with given velocity was used to calculate the force-velocity relation of an ensemble of motors¹⁸. Adapting the transition rates between the conformational states allowed to study processive as

well as non-processive motors. Onset of oscillatory behavior of the ensembles was investigated in a generic two-state model, in which conformational changes of the motors upon binding and unbinding allowed bound motors to exert force on their environment⁴². Here, the binding and unbinding rates could be adapted to describe different types of motors and different force-velocity relations. In a generalization, an ensemble of molecular motors working against a visco-elastic element was investigated⁴³. Using a similar mean-field approach as Leibler and Huse¹⁸ for a two-state model, the dynamic behavior of ensembles was investigated, revealing limit cycle oscillations induced by the coupling to the visco-elastic element. To describe specific properties of muscle fibers, crossbridge models with varying degree of detail have been used. Using computer simulations on large ensemble of myosin II with a crossbridge model including explicitly the power stroke and load dependent unbinding from the post-power-stroke state, details of the force-velocity relation for muscle fibers could be fitted very accurately to experimental results and collective phenomena such as the synchronization of the power stroke under load or the transient response of muscle to a step change of the external load were investigated^{19,44}. Coupling to an external elastic element allowed to observe oscillations for the crossbridge model⁴⁵. Recently, a detailed crossbridge model for myosin II was used to describe also the activity of small myosin II ensembles in the cytoskeleton⁴⁶. The activity of small groups of myosin II in motility assays was studied using computer simulations. Large ensembles were described in a mean-field approach. By comparison of the results to experiments, parameters of the model could be determined. The focus of the model was on the description of the ATP dependence of the transition rates. Therefore, the crossbridge model included two separate post-power-stroke states of the bound motors but did not include a bound pre-power-stroke state so that it did not explicitly describe the power stroke.

In order to study effects of molecular details for ensembles of myosin II motors, we use a crossbridge model with three states as a starting point, which was originally used for skeletal muscle^{44,45}. Unlike Walcott et al.⁴⁶, we use a pre- and a post-power-stroke state as the two bound states, so that the power stroke of myosin II is included explicitly. To reduce the complexity of the analytical description, we make two approximations: (*i*) we assume that molecular motors in equivalent conformational states have equal strain and (*ii*) we exploit a separation of time scales in the myosin II cycle and assume that there is thermal equilibrium of the bound states. The partial mean-field approximation of the first assumption still distinguishes between the two different bound states. It can be justified by the small duty ratio of myosin II motors which leads to a narrow distribution of the strains of bound motors. The assumption of local thermal equilibrium between

bound states reduces the system to a two-state model. The effective properties of these states, however, still depend on the distribution over the two bound states. The two approximations allow us to derive a one-step master equation for the binding dynamics of the motors, which explicitly includes the effects of strain-dependent rates and small system size. A one-step master equation has been introduced before for transport by finite-sized ensembles of processive motors with slip bond behavior⁹, but not for non-processive motors with catch bond behavior. Together with rules for the displacement of an ensemble upon binding and unbinding, the one-step master equation fully characterizes the dynamics of ensembles. We investigate two paradigmatic loading conditions for the ensemble: constant loading and linear loading, in which the external load depends linearly on the position of the ensemble. For constant external load, we can solve the one-step master equation for the stationary states and derive binding properties and force-velocity relation from these. For linear external load, the movement of the ensemble feeds back to the load dependent binding rates, so that we have to use computer simulations to analyze this case. In both loading scenarios, we find that the motor ensemble adapts its dynamical state to the external conditions in a way which is reminiscent of its physiological function.

II. MODEL

A. Crossbridge model for single non-processive motors

To describe the mechanism of force generation by non-processive molecular motors, we use a crossbridge model for myosin II^{16,19}. Variants of cross-bridge models differ by number and type of conformational states they include^{19,44,46}, depending on the focus of the modeling approach. Here, we distinguish two bound conformations of the motors and one unbound state. The essential mechanical elements of myosin II in our model are depicted schematically in Fig. 1 (a). The motor head binds the motor to the substrate, which in the case of myosin II is an actin filament. The motor head also is the active domain of myosin II which binds ATP or the products of ATP hydrolysis—ADP and a phosphate group P_i . Hinged to the motor head is the rigid lever arm which can exist either in the primed (gray) or the stretched (black) conformation. The lever arm amplifies small conformational changes in the head domain of the motor so that the tip of the lever arm swings forward by a distance d in the transition from primed to stretched conformation. This movement stretches the elastic neck linker, which is modeled as a linear elastic element with spring constant

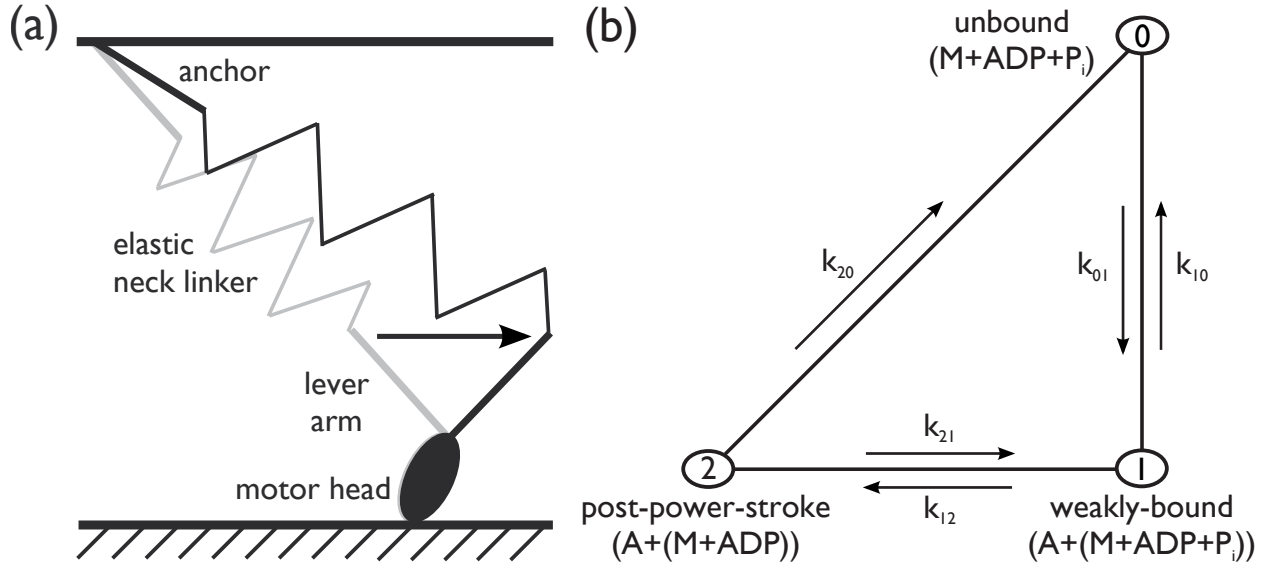


FIG. 1. Crossbridge model for non-processive myosin II motors molecules. (a) Mechanical elements of myosin II. (b) Myosin II motor cycle with three discrete mechano-chemical states. In the unbound state (0) the motor head binds ADP and P_i and the lever arm is in the primed conformation (gray in (a)). Binding to the substrate brings the motor to the weakly-bound (pre-power-stroke) state (1) with unchanged mechanical conformation. After release of the P_i group, the lever arm swings forward into the stretched conformation (black in (a)). This power stroke brings the motor to the post-power-stroke state (2). Replacing ADP by ATP, unbinding from the substrate and ATP hydrolysis brings the motor back to the unbound state (0). Because of the consumption of ATP, the last transition is irreversible. All other transitions are reversible.

k_m . Elastic forces in the neck linker are transmitted to the anchor, through which a myosin II motor can integrate firmly into myosin II motor filaments such as cytoskeletal minifilaments.

Driven by the hydrolysis of ATP, myosin II cycles through a sequence of mechanical and chemical conformations to generate force and directed motion. The exact sequence of reaction steps, the rates of transitions as well as the molecular parameters of myosin II are subject of debate. The basic sequence of conformations we use in our model, however, is well supported by experimental observation. In particular, the reversal of the power stroke under load has been observed for similar types of single headed myosin molecules⁴⁸. In Tab. I we list the values for the most important parameters as determined experimentally or used in earlier models. These parameters depend on the exact experimental conditions, e.g. ATP concentration and spatial arrangement of motors, and also on the exact type of myosin II^{20,31}. In the main body of our paper we use the parameters of the last

| name | symbol | values | model value |
|------------------------|----------------------------|--|---------------------------------|
| thermal energy | $k_B T$ | — | 4.14 pN nm |
| power-stroke distance | d | 8 nm ⁴⁵ , 10 nm ⁴⁶ | 8 nm |
| motor elasticity | k_m | 0.3 pN nm ^{-119,46} , 2.5 pN nm ⁻¹⁴⁵ , 3.0 pN nm ⁻¹⁴⁷ | 2.5 pN nm ⁻¹ |
| transition rates | k_{01} | 6 s ^{-146,47} , 40 s ^{-145,46} | 40 s ⁻¹ |
| | k_{10} | 0 s ⁻¹⁴⁶ , 2 s ⁻¹⁴⁵ | 2 s ⁻¹ |
| | k_{20}^0 | ~ 18 s ⁻¹⁴⁶ , 80 s ⁻¹⁴⁵ , ~ 350 s ⁻¹⁴⁶ , | 80 s ⁻¹ |
| | $k_{12}^0 \simeq k_{21}^0$ | 10 ³ s ⁻¹⁴⁵ | 10 ³ s ⁻¹ |
| post-power-stroke bias | E_{pp} | -60 pN nm ⁴⁵ | -60 pN nm |
| unbinding distance | δ | 0.328 nm ⁴⁵ , 1.86 nm ⁴⁶ , 2.60 nm ⁴⁶ | 0.328 nm |
| unbinding force | F_0 | — | 12.62 pN |

TABLE I. Parameters determining the dynamics of the ensemble non-processive motors. The third column list parameter values used in previous models. The values used in this manuscript are taken from Vilfan and Duke⁴⁵ and are listed in the last column.

column of Tab. I. These are taken from Vilfan and Duke⁴⁵. As shown schematically in Fig. 1 (b), we model the myosin II motor cycle by three discrete mechano-chemical states⁴⁴ with stochastic transitions between them. In the unbound state (0), the motor head is loaded with ADP and P_i and the lever arm is in its primed conformation. The primed conformation is a high energy state, which stores part of the approximately 80 pN nm of energy released in ATP hydrolysis. The motor then reversibly transitions to the weakly-bound state (1) with on-rate k_{01} and off-rate k_{10} . Concomitant with the release of P_i, the lever arm swings to the stretched conformation, thereby releasing most of the energy stored on the primed neck linker, and the motor enters the post-power-stroke state (2). With the stretched lever arm, the motor molecule is close to its conformational ground state and there is a strong free energy bias E_{pp} favoring the post-power-stroke state. Compared to the binding transitions, transitions between the bound states are relatively fast, with unloaded transition rates $k_{12}^0 \simeq k_{21}^0$. Replacing ADP by ATP, unbinding from the substrate and hydrolysis of ATP completes the motor cycle and brings the motor back to the unbound state (0) with primed lever arm. The unloaded off-rate for this last step is k_{20}^0 . Due to the energy released in ATP hydrolysis this transition is considered as irreversible, thus defining the direction of the motor cycle. Most importantly in our context, both power stroke and unbinding from the post-power-stroke state depend on load. The power stroke (1) \rightarrow (2) moves the lever arm forward by the power-stroke distance d and strains the elastic neck linker of a motor. Replacing ADP by ATP and unbinding from (2) requires an additional movement of the lever arm in the same direction as the power stroke, thus

straining the neck linker further by the unbinding distance δ and making unbinding slower under load. The load dependent rates for these transition are denoted without the superscript (see Fig. 2).

B. Parallel cluster model for ensembles of non-processive motors

Because non-processive molecular motors are bound only during a small fraction of the motor cycle they have to cooperate in groups to generate sustained levels of force or persistent motion against an external load. A sufficiently large number of motors ensures permanent attachment of the group while individual motors continuously unbind and rebind as they go through their motor cycle. Fig. 2 (a) illustrates the coupling of myosin II motors in an ensemble working against an external load. With their anchors the motors are firmly integrated into the rigid backbone of the motor filament whereas the motor heads bind to the substrate. In Fig. 2 (a), the motors are oriented such that the lever arm swings towards the right during the power stroke, so that the motors exert force on the motor filament towards the right. The external load pulls the motor filament towards the left, against the motor direction. Because the motors are attached directly to the motor filament, they are working effectively in parallel against the external load. Such parallel arrangement was confirmed experimentally for the myosin II motors in the muscle sarcomere^{30,49}. We will discuss two paradigmatic situations for the external load: (*i*) a constant external load, which is independent of the position of the motor filament, and (*ii*) an elastic external load, which increases linearly with the displacement of the motor filament. For constant external load, the ensemble will eventually reach a steady state of motion with load dependent velocity. For a linear external load, an isometric state with vanishing velocity is expected. Experimentally, the unipolar ensemble of myosin II motors in Fig. 2 (a) would represent one half of a thick filament in the muscle sarcomere or of a minifilament in the cytoskeleton. In this case, the external load is generated by the motors in the other half of the bipolar motor filament or is due to the tension in a surrounding actin network. In reconstituted assays, a constant load could be realized through viscous forces in a flow chamber or applying active feedback control; a linear load might be realized using using elastic elements such as optical traps.

For an ensemble of parallel motors in mechanical equilibrium, the external load F_{ext} is balanced by the sum of elastic forces $F_n = k_m \xi_n$ in the neck linkers of all bound motors:

$$F_{\text{ext}} = \sum_{\text{bound}} F_n = k_m \sum_{\text{bound}} \xi_n. \quad (1)$$

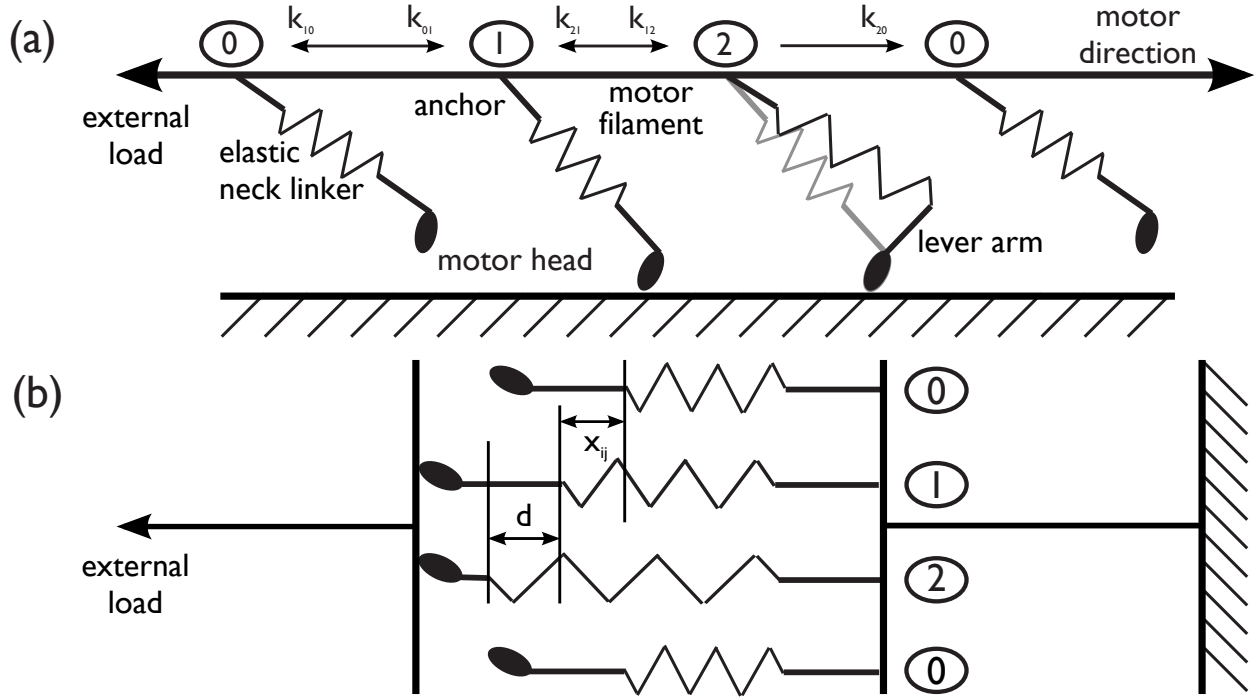


FIG. 2. (a) Mechanical coupling of an ensemble of myosin II motors. The motors pull on the motor filament towards the right against the external load pulling to the left. The external load is balanced by the elastic forces in the neck linkers of the bound motors. Typical cases for the external load are (i) constant load and (ii) linear load increasing with the displacement of the motor filament. The mechanical coupling of the motors through the rigid motor filament induces a dynamic coupling due to the strain dependence of the transition rates. (b) In the *parallel cluster model* (PCM) all motors in a given mechano-chemical state are assumed to have the same strain. Weakly-bound motors have the strain x_{ij} . The power stroke corresponds to a shortening of the bound molecular motor so that motors in the post-power-stroke state have the strain $x_{ij} + d$. The arrangement of the motors is equivalent to adhesion clusters of parallel bonds, where the closed bonds can be in two different conformations.

In this expression, k_m is the elastic constant of the neck linkers, ξ_n their elongation (or strain) and the index n runs over all motors which are bound to the substrate. An imbalance of forces induces a change of the position of the motor filament. This changes the strain ξ_n of all bound motors simultaneously until the balance of forces in Eq. (1) is restored. In addition, a linear external load would be changed by the displacement of the motor filament. In the following, we assume that the relaxation time towards mechanical equilibrium is negligible in comparison with the time scale for stochastic transitions, so that the mechanical state of an ensemble always obeys the force

balance in Eq. (1). Anchoring of the motors to the rigid motor filament in combination with the condition of the force balance introduces a tight mechanical coupling between motors: a stochastic transition of one motor changes the force balance and hence the strain of all bound motors. Thus, the strain ξ_n of a bound motor does not only depend on the state of the motor itself but results from the past activity of the motor ensemble. Specifically, ξ_n is determined by the displacement of the motor filament after binding of a motor. Therefore, Eq. (1) determines the sum but not the individual strains of the motors: while the sum over the strain of the bound motors vanishes at vanishing external load, the individual strains ξ_n will in general not. The distribution of the ξ_n will be determined by the randomly distributed times during which a motor remains bound to the substrate and the displacement of the motor filament during these times.

Because the rates for the stochastic transitions (1) \leftrightarrow (2) and (2) \rightarrow (0) depend on the strain of a motor, the mechanical coupling leads to a dynamical coupling of the motors, as illustrated in Fig. 2 (a). A stochastic description of the ensemble dynamics as a Markov process would thus require not only the mechano-chemical state but also the strain of every motor as state variables. Denoting the total number of motors in an ensemble by N_t , the state space for an ensemble with N_t motors would then encompass 3^{N_t} discrete states and N_t independent, continuous variables ($N_t - 1$ considering Eq. (1)). This complexity prohibits analytical solutions and previous approaches either used mean field models or computer simulations (see e.g.^{18,19,44}). Here, we use mean-field elements to arrive at an analytically tractable model, which preserves the molecular details contained in the crossbridge model and allows to study stochastic effects due to finite ensemble size. We make the assumption that all motors in the same mechano-chemical state have the same strain. This assumption is the essence of our *parallel cluster model* (PCM); its validity will be discussed in Sec. III A 5 and demonstrated by comparison with computer simulations. As illustrated in Fig. 2 (b), the PCM effectively describes the ensemble of molecular motors as an adhesion cluster of parallel bonds⁵⁰⁻⁵². In this picture, the power stroke shortens the closed bonds by the power-stroke distance d . Therefore, closed bonds can be in two conformations with different lengths in which they carry different loads. All motors in a given conformation, however, carry an equal share of the external load and have the same strain. Thus, all motors in a given mechano-chemical state are mechanically equivalent within the PCM so that the state of a motor ensemble of N_t motors can be characterized by the number of motors in each of the mechano-chemical states. We use the number i of bound motors ($0 \leq i \leq N_t$) and the number j ($0 \leq j \leq i$) of motors in the post-power-stroke state. The number of motors in the weakly-bound state then follows as $i - j$ and the number of

unbound motors is $N_t - i$. The strain of the motors in the weakly-bound state (1) is referred to as x_{ij} , where the indices indicate the dependence on the ensemble state (i, j) . Since the power stroke stretches the neck linker by d , the strain of the motors in the post-power-stroke state (2) is given by $x_{ij} + d$. With $i - j$ motors with strain x_{ij} and j motors with strain $x_{ij} + d$, the force balance in the PCM reads

$$F_{\text{ext}} = k_m [(i - j)x_{ij} + j(x_{ij} + d)] = k_m [ix_{ij} + jd]. \quad (2)$$

This expression can be solved for the strain x_{ij} of the weakly-bound motors. For constant external load, $F_{\text{ext}} = \text{const}$, Eq. (2) yields

$$x_{ij} = \frac{(F_{\text{ext}}/k_m) - jd}{i}. \quad (3)$$

For linear external load, we have to introduce an external coordinate describing the position of the motor ensemble. We define z as the average position of the bound motor heads. The position of the motor filament then is given by $z - x_{ij}$. The definition of ensemble position is described in detail in Sec. II E. With the external elastic constant k_f , the linear external load is $F_{\text{ext}} = k_f(z - x_{ij})$.

Inserting this into Eq. (2) yields

$$x_{ij} = \frac{(k_f/k_m)z - jd}{i + (k_f/k_m)} \quad (4)$$

for the strain of the weakly-bound motors. Here, we define the strain of a weakly-bound motor to be positive when the neck linker is stretched in the direction of the external load (towards the left in Fig. 2 (a)) whereas the average position z of bound motor heads increases in the motor direction (towards the right in Fig. 2 (a)) (see Sec. II E). If all bound motors are in the weakly-bound state ($j = 0$), the strain $x_{ij} = x_{i0}$ is positive, that is, the neck linkers pull on the motor filament against the external load. When the external load is not too large, the strain of the weakly-bound motors can become negative, if sufficiently many motors have gone through the power stroke. In this case, the neck linkers of the weakly-bound motors pull the motor filament against the motor direction, thereby supporting the external load. Because $j \leq i$, the strain $x_{ij} + d$ of motors in the post-power-stroke state is always positive. It is this pulling of post-power-stroke motors which eventually drives force generation and motion by the ensemble.

The major benefit of the PCM lies in the fact, that it eliminates the history dependence of the strain and introduces x_{ij} as a state function. Within the PCM, the strain of all motors follows from the current ensemble state (i, j) and the external load F_{ext} . For constant external load, $F_{\text{ext}} = \text{const}$ takes the role of a parameter and the ensemble dynamics is fully characterized by (i, j) . For linear

external load, $F_{\text{ext}} = k_f(z - x_{ij})$ is changed through the activity of motors so that additional rules for the position z of the ensemble are required to fully characterize the dynamics of an ensemble.

C. Local thermal equilibrium of bound motors

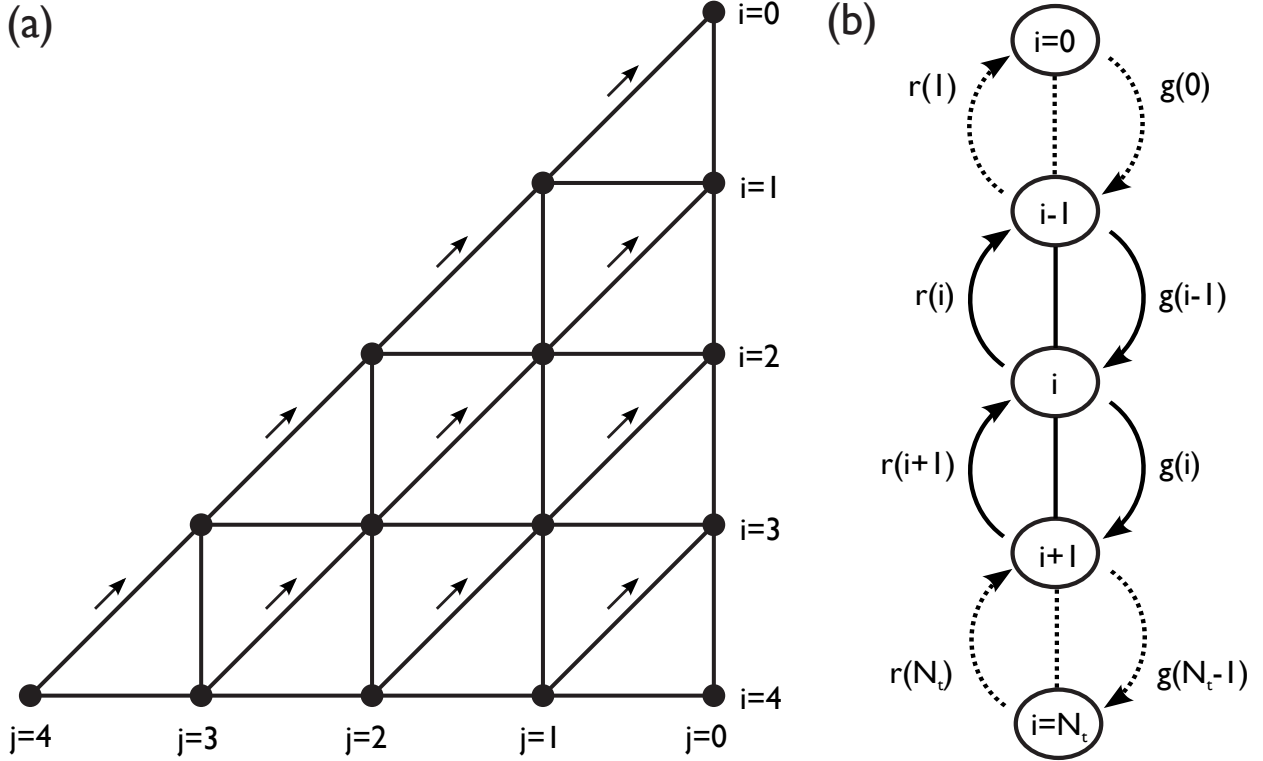


FIG. 3. (a) Two-dimensional stochastic reaction network for transitions between the states (i, j) of an ensemble within the PCM. Binding to and unbinding from the weakly-bound state changes the number of bound motors i (vertical lines). The power stroke changes the number of motors in the post-power-stroke state j (vertical lines). Unbinding from the post-power-stroke state changes both i and j (diagonal lines). This is the only irreversible transition and is marked by an arrow. (b) *Local thermal equilibrium* (LTE) projects all states with different j but given i onto a single state so that the state of an ensemble is described by the number i of bound motors alone. Transitions are described by effective reverse and forward rates.

For an ensemble with N_t myosin II motors, the number i of bound motors ranges from 0 to N_t . The number j of motors in the post-power-stroke state ranges from 0 to i . Fig. 3 (a) shows the corresponding network of states (i, j) which are connected by the possible stochastic transitions. Binding to and unbinding from the weakly-bound state change i by ± 1 without changing j (verti-

cal transitions). The power stroke and its reversal change j by ± 1 but leave i constant (horizontal transitions). Unbinding from the post-power-stroke state reduces i and j simultaneously (diagonal transitions). This is the only irreversible transition in the network and is marked by an arrow. In total there are $(N_t + 1)(N_t + 2)/2$ states and $3N_t(N_t + 1)/2$ transitions (of which $N_t(N_t + 1)$ are reversible) in this network.

To further reduce the complexity of the model, we take advantage of the strong separation of time scales between the slow binding and unbinding transitions and the transitions between the bound states, which are at least an order of magnitude faster^{19,45} (see Tab. I). Following previous modeling approaches, we assume that a *local thermal equilibrium* (LTE) is maintained within the bound states⁴⁵. For a given number i of bound motors, the conditional probability to find j motors in the post-power-stroke state and $i - j$ in the weakly-bound state is given by the Boltzmann distribution

$$p(j|i) = \frac{1}{Z_i} \exp(-E_{ij}/k_B T) . \quad (5)$$

Here, Z_i is the appropriate partition sum for given i ,

$$Z_i = \sum_{j=0}^i \exp(-E_{ij}/k_B T) . \quad (6)$$

The energy $E_{ij} = jE_{pp} + E_{ij}^{\text{el}} + E_{ij}^{\text{ext}}$ of an ensemble in state (i, j) is the sum of the free energy bias $E_{pp} \simeq -60 \text{ pN nm} < 0$ towards the post-power-stroke state for j motors, the elastic energy E_{ij}^{el} stored in the neck linkers and a possible external contribution E_{ij}^{ext} . The elastic energy of the neck linkers is given by

$$E_{ij}^{\text{el}} = \frac{k_m}{2} [(i - j)x_{ij}^2 + j(x_{ij} + d)^2] . \quad (7)$$

The strain x_{ij} is given by Eq. (3) for constant and Eq. (4) for linear external load. The external contribution to the energy vanishes for constant external load, $E_{ij}^{\text{ext}} = 0$. For linear external load, E_{ij}^{ext} is given by the energy stored in the external harmonic potential,

$$E_{ij}^{\text{ext}} = \frac{k_f}{2} (z - x_{ij})^2 , \quad (8)$$

where x_{ij} is given by Eq. (4) and $z - x_{ij}$ is the position of the motor filament.

Combining Eqs. (3) and (7) reveals that for constant external load, the elastic energy of the neck linkers is identical in states (i, j) and $(i, i - j)$. E_{ij}^{el} is minimal when all bound motors are either weakly-bound ($j = 0$) or in the post-power-stroke state ($j = i$). Intermediate states with $0 < j < i$ have a larger elastic energy because bound motors in opposite conformations are pulling against

each other. Because of this symmetry of E_{ij}^{el} , the free energy bias E_{pp} translates directly into a strong bias of the LTE distribution towards the post-power-stroke state so that almost all bound motors are in the post-power-stroke state. The symmetry of the elastic energy is not affected by the exact value of the constant external load, which merely changes the absolute values of E_{ij}^{el} , so that the bias of the LTE distribution persists for arbitrary values of a constant external load.

A linear external load is increased by the power stroke of a motor. Therefore, elastic energy E_{ij}^{el} and external energy E_{ij}^{ext} tend to increase with an increasing number of post-power-stroke motors and introduce a bias towards the weakly-bound state, opposite to the free energy bias E_{pp} . To demonstrate this, we compare the energy in the extreme states $(i, 0)$ and (i, i) . For a given z , E_{ij}^{el} and E_{ij}^{ext} take the smallest value in state $(i, 0)$, in which all bound motors are weakly-bound with strain $x_{i0} = (k_f/k_m)z/(i + k_f/k_m)$. In state (i, i) , all bound motors are in the post-power-stroke state with the strain $x_{ii} + d = (k_f/k_m)(z + d)/(i + k_f/k_m)$. Because $x_{i0} < x_{ii} + d$, the elastic energy in state $(i, 0)$ is smaller than in state (i, i) , $E_{i0}^{\text{el}} < E_{ii}^{\text{el}}$. On the other hand, $x_{i0} > x_{ii}$ and $z - x_{i0} < z - x_{ii}$, so that also the external energy $E_{ij}^{\text{ext}} = (k_f/2)(z - x_{ij})^2$ is smaller in state $(i, 0)$ than in state (i, i) , $E_{i0}^{\text{ext}} < E_{ii}^{\text{ext}}$. The total energy difference is

$$(E_{ii}^{\text{el}} + E_{ii}^{\text{ext}}) - (E_{i0}^{\text{el}} + E_{i0}^{\text{ext}}) = \frac{ik_mk_f}{ik_m + k_f} \frac{d(d + 2z)}{2}. \quad (9)$$

It increases with increasing k_f and z so that the bias of the LTE distribution will shift from the post-power-stroke state to the weakly-bound state at large values of the external elastic constant k_f or the ensemble position z . This transition eventually will stall ensemble movement, because movement is driven by post-power-stroke motors and requires passage through the motor cycle.

D. One-step master equation for binding dynamics

As illustrated in Fig. 3 (b), the assumption of an LTE within the bound motors effectively projects all ensemble states (i, j) with different j but given i onto a single variable. Thus, the state of an ensemble is described by the number i of bound motors alone. In this effectively one-dimensional system, the probability $p_i(t)$ to find i motors bound to the substrate at time t follows the one-step master equation

$$\frac{d}{dt}p_i = r(i + 1)p_{i+1} + g(i - 1)p_{i-1} - [r(i) + g(i)]p_i. \quad (10)$$

Once $p_i(t)$ is known, the probability $p_{ij}(t) = p(j|i)p_i(t)$ to find the ensemble in the state (i, j) at time t is obtained as the product of $p_i(t)$ with the time independent LTE distribution $p(j|i)$ from

Eq. (5). In the one-step master equation, the effective reverse rate $r(i)$ describes the rate at which bound motors unbind from the substrate, that is, $r(i)$ is the rate of the transition $i \rightarrow i - 1$. The effective forward rate $g(i)$ describes the rate at which free motors bind to the substrate, that is, $g(i)$ is the rate of the transition $i \rightarrow i + 1$. The effective transition rates $r(i)$ and $g(i)$ with their dependence on i and F_{ext} define the stochastic dynamics of binding and unbinding in the motor ensemble.

In the state (i, j) of an ensemble, weakly-bound motors unbind with off-rate $k_{10}(i, j)$ and post-power-stroke motors unbind with off-rate $k_{20}(i, j)$. Following previous modeling approaches^{19,44}, we assume that the off-rate from the weakly-bound state is independent of the load on a motor and therefore independent of the state of an ensemble, $k_{10}(i, j) = k_{10} = \text{const}$. Unbinding from the post-power-stroke state requires the lever arm to work against the external load over the unbinding distance δ . Assuming a Kramers-type load dependence, the off-rate from the post-power-stroke state decreases exponentially with the load $F_{ij} = k_{\text{m}}(x_{ij} + d)$ on the neck linker:

$$k_{20}(i, j) = k_{20}^0 \exp(-F_{ij}/F_0). \quad (11)$$

The unbinding force scale $F_0 = k_{\text{B}}T/\delta \simeq 12.6$ pN is set by the thermal energy $k_{\text{B}}T$ and the unbinding distance δ . In state (i, j) , there are $i - j$ weakly-bound motors and j post-power-stroke motors. Because all stochastic transitions proceed independently, the rate for unbinding of a motor in state (i, j) is the sum over the single-motor transition rates:

$$r(i, j) = (i - j)k_{10}(i, j) + jk_{20}(i, j). \quad (12)$$

The effective reverse rate $r(i)$ for the transition $i \rightarrow i - 1$ in the one-dimensional system is then obtained by averaging $r(i, j)$ over j with the LTE distribution from Eq. (5):

$$r(i) = \sum_{j=0}^i r(i, j)p(j|i). \quad (13)$$

Considering the exponential dependence of $k_{20}(i, j)$ on strain and the strain dependence of the LTE distribution, $r(i)$ is a strongly non-linear function of the external load and the number of bound motors. Since the off-rate $k_{20}(i, j)$ decreases under load (see Eq. (11)), the post-power-stroke state of myosin II behaves as a catch bond. Due to the strong bias of the LTE distribution towards the post-power-stroke state, myosin II motors predominantly unbind from the post-power-stroke state. This implies that also the effective reverse rate $r(i)$ decreases under load and the myosin II ensemble as a whole behaves as a catch bond. For constant external load, the bias persists for

arbitrary values of F_{ext} , so that the catch bond character of myosin II motors is found for all values of the external load. For elastic external load, the bias of the LTE distribution passes over to the weakly-bound state for very stiff external springs. This means that myosin II behaves as a catch bond at small values of k_f and z , but unbinds with load-independent rate at large values of k_f or z . For very large loads, it is expected that unbinding of motors is accelerated under load as for slip bonds⁴⁹, but such large loads will not be considered here.

The only pathway for binding is the transition $(0) \rightarrow (1)$ from the unbound state to the weakly-bound state of a motor. Because unbound motors are not subject to any load, the on-rate is assumed to be constant, $k_{01} = \text{const}$. With $N_t - i$ motors binding independently, the effective forward rate is given by

$$g(i) = (N_t - i)k_{01}. \quad (14)$$

The forward rate $g(i)$ increases linearly with the number $N_t - i$ of unbound motors but is otherwise independent of the state of the ensemble. Because there is no dependence on j , averaging with the LTE distribution is not required.

With the definition of the effective transition rates in Eqs. (13) and (14), the one-step master equation of Eq. (10) for the binding dynamics in an ensemble of myosin II motors is fully characterized for the case of constant external load. If the external load depends on the position of the ensemble, as for a linear load, Eq. (10) has to be solved together with additional rules for the movement of the motor ensemble, which will be introduced in the next section.

E. Ensemble movement

With the introduction of the PCM, we have focused on modeling the dynamics of binding and unbinding of molecular motors in an ensemble. The displacement of the ensemble, on the other hand, seems to be eliminated by the analogy to a cluster of parallel adhesion bonds. Nevertheless, there are clear prescriptions for the transformation of binding and unbinding of motors to a displacement of the ensemble. In order to derive these prescriptions and to elucidate the inherent approximations, we take a step back and consider the general case of an ensemble of molecular motors without the approximation of the PCM, that is, we consider an ensemble in which every motor is characterized by an individual value of the strain. The spatial coordination of the motors is schematically depicted in Fig. 2 (a). The anchors are integrated into the motor filament at fixed positions. Because the motor filament is rigid, the relative positions of the anchors are constant

and we can assume that all anchors are at the same position z_{fil} , which is identified with the position of the motor filament. In the following, we consider a reference state in which i motors are bound to the substrate and $N_t - i$ are unbound. The neck linkers of the bound motors have the strains ξ_n , where the index $n \in \{1, \dots, i\}$ labels the bound motors. The position z_n of a bound motor head on the substrate is related to the position z_{fil} of the motor filament via its strain ξ_n as $z_n = z_{\text{fil}} + \xi_n$ for weakly-bound and $z_n = z_{\text{fil}} + \xi_n - d$ for post-power-stroke motors. To abbreviate notation, we define the offset of a motor head from its anchor as $x_n := \xi_n$ for weakly-bound and $x_n := \xi_n - d$ for post-power-stroke motors. Using this definition, the position of a bound motor head can be written as

$$z_n = z_{\text{fil}} + x_n \quad (15)$$

for all bound motors with $n \in \{1, \dots, i\}$. We now define the position of an ensemble as the average position of the bound motor heads:

$$\bar{z} := \frac{1}{i} \sum_{n=1}^i z_n. \quad (16)$$

With this definition, the ensemble position \bar{z} can only change through binding or unbinding of motors, because motor heads are bound at fixed positions on the substrate. By contrast, the position z_{fil} of the motor filament also changes through transitions within the bound states which change the balance of forces in Eq. (1). Only for completely detached ensembles, in which no motor is bound to the substrate, we have to use the position z_{fil} of the motor filament as the ensemble position. Because unbound motors have vanishing strain and unbound motor heads are at the same position as the anchors, z_{fil} is identical to the average position of the unbound motor heads. Inserting z_n from Eq. (15) into Eq. (16), the average position of the bound motor heads is

$$\bar{z} = z_{\text{fil}} + \bar{x}_{ij}. \quad (17)$$

The average offset \bar{x}_{ij} between anchors and motor heads is related to the external load F_{ext} via the balance of forces in Eq. (1) as

$$\bar{x}_{ij} := \frac{1}{i} \sum_{n=1}^i x_n = \frac{(F_{\text{ext}}/k_m) - jd}{i}. \quad (18)$$

Unlike the absolute position \bar{z} and the individual values of x_n or ξ_n , which all result from the history of the ensemble, \bar{x}_{ij} follows from the current state of the ensemble alone. In particular, it depends on the external load F_{ext} , the number i of bound motors and the number j of post-power-stroke motors.

We now calculate how the average position of bound motor heads changes through binding of one additional motor. Assuming that i motors are bound initially with average position \bar{z} and that the new motor binds with vanishing strain at z_{fil} to the substrate, the new average position \bar{z}' of $i + 1$ bound motor heads is

$$\bar{z}' = \frac{i\bar{z} + z_{\text{fil}}}{i + 1} = z_{\text{fil}} + \frac{i}{i + 1}\bar{x}_{ij}. \quad (19)$$

Thus, binding of a motor changes ensemble position by

$$\Delta\bar{z}_{ij}^{\text{on}} := \bar{z}' - \bar{z} = \left[\frac{i}{i + 1} - 1 \right] \bar{x}_{ij} = -\frac{\bar{x}_{ij}}{i + 1}. \quad (20)$$

Like \bar{x}_{ij} , the binding step $\Delta\bar{z}_{ij}^{\text{on}}$ is a function of the ensemble state before binding. After binding, the average offset of the motors is adjusted to

$$\bar{x}'_{i+1j} = \frac{i}{i + 1}\bar{x}_{ij}. \quad (21)$$

Combining this with \bar{z}' confirms that the position of the motor filament remains unchanged, $z'_{\text{fil}} = \bar{z}' - \bar{x}'_{i+1j} = \bar{z} - \bar{x}_{ij} = z_{\text{fil}}$. This is required for consistency, because the balance of forces is not affected by a motor binding with vanishing strain. In a more general description, motors could be allowed to bind with a finite value of the strain chosen from a random distribution with vanishing mean. In this case, Eq. (21) for $\Delta\bar{z}_{ij}^{\text{on}}$ would remain valid in the ensemble average.

Unlike the binding step $\Delta\bar{z}_{ij}^{\text{on}}$, the change of the ensemble position upon unbinding depends on which of the motors unbinds. Assuming that a motor head with offset x_n unbinds from the position $z_n = z_{\text{fil}} + x_n$ on the substrate, the average position \bar{z}'' of the $i - 1$ remaining motor heads is

$$\bar{z}'' = \frac{i\bar{z} - z_n}{i - 1} = \frac{i(z_{\text{fil}} + \bar{x}_{ij}) - (z_{\text{fil}} + x_n)}{i - 1} = z_{\text{fil}} + \frac{i\bar{x}_{ij} - x_n}{i - 1}. \quad (22)$$

Thus, unbinding of a motor from z_n changes the position of the ensemble by

$$\Delta\bar{z}_{ij,n}^{\text{off}} = \bar{z}'' - \bar{z} = \frac{i\bar{x}_{ij} - x_n}{i - 1} - \bar{x}_{ij} = \frac{\bar{x}_{ij} - x_n}{i - 1}. \quad (23)$$

Assuming that all motors are equally likely to unbind, the average of the unbinding step over all bound motors vanishes:

$$\Delta\bar{z}_{ij}^{\text{off}} = \frac{1}{i} \sum_{n=1}^i \Delta\bar{z}_{ij,n}^{\text{off}} = \frac{\bar{x}_{ij} - \bar{x}_{ij}}{i - 1} = 0. \quad (24)$$

For weakly-bound motors this assumption is valid, because the off-rate $k_{10} = \text{const}$ is independent of strain. Post-power-stroke motors, on the other hand, are catch bonds with an off-rate $k_{20}(i, j)$

decreasing exponentially with increasing strain. Therefore, post-power-stroke motors unbind preferentially with small strain and small offset, $x_n < \bar{x}_{ij}$. Averaging the unbinding step $\Delta z_{ij,n}^{\text{off}}$ with the actual off-rates would then lead to a positive displacement $\Delta \bar{z}_{ij}^{\text{off}} \geq 0$. The size of the unbinding step depends on the distribution of strains of the bound motor heads and vanishes when all motors have the same offset. In addition, unbinding of a motor with non-zero strain changes the balance of forces so that the position z_{fil} of the motor filament is changed.

When the last bound motor unbinds and the ensemble detaches completely from the substrate, the motor head relaxes instantaneously from its position $\bar{z} = z_1 = z_{\text{fil}} - x_1$ on the substrate to the position $z_{\text{fil}} = \bar{z} - x_1$ of the motor filament. Because the position of the detached ensemble is described by the position z_{fil} of the motor filament, unbinding of the last motor changes the ensemble position by

$$\Delta \bar{z}_{1j}^{\text{off}} = -x_1 \quad \text{for } j = 0, 1. \quad (25)$$

The dependence on the state of the unbinding motor is included in the definition of the offset x_1 .

Within the PCM, weakly-bound motors have the strain x_{ij} and the strain of post-power-stroke motors is $x_{ij} + d$, so that all bound motors are characterized by the same offset x_{ij} . Therefore, all bound motor heads are at the same position $z = z_{\text{fil}} + x_{ij}$ on the substrate. To apply the general expressions for the displacement to the PCM, the averages \bar{z} and \bar{x}_{ij} are replaced by the quantities z and x_{ij} which are the same for all motors in the PCM ensemble. In a given state (i, j) , binding of a new motor changes the position z of the ensemble by

$$\Delta z_{ij}^{\text{on}} = -\frac{x_{ij}}{i+1}. \quad (26)$$

This is the actual change of the average position of the bound motor heads assuming that the new motor has bound with vanishing strain at the position z_{fil} . As illustrated in Fig. 4, in order to implement the assumption of the PCM, all $i+1$ bound motor heads have to be shifted to the new common position $z' = z + \Delta z_{ij}^{\text{on}}$ on the substrate after binding. This shift is not meant to correspond to an actual physical process but is a theoretical procedure required to maintain the PCM assumption of identical strains of bound motors. As in the general case, the position of the motor filament does not change upon binding of a motor because the balance of forces is unchanged. Because all bound motor heads have the same offset x_{ij} and are at the same position z on the substrate, the position z of the ensemble is unchanged by the unbinding of a motor:

$$\Delta z_{ij}^{\text{off}} = 0 \quad \text{for } i \geq 2. \quad (27)$$

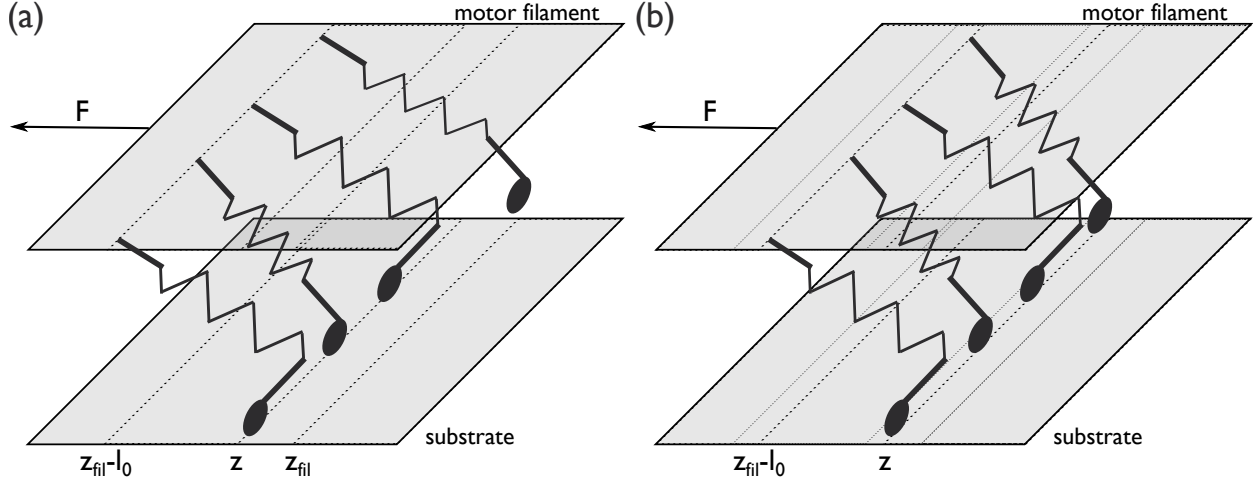


FIG. 4. Change of ensemble position z upon binding of a motor within the PCM. (a) Before binding, all bound motor heads are at the ensemble position z . In the illustrated case, the strain of the weakly-bound motor is negative, $x_{ij} < 0$, so that motor heads will bind at $z_{\text{fil}} = z - x_{ij} > z$ ahead of the current ensemble position. The post-power-stroke motors have positive strain, $x_{ij} + d > 0$, and work against the external load and the elastic force from the weakly-bound motor. For the illustration, motors are depicted with length ℓ_0 so that the anchors are at $z_{\text{fil}} - \ell_0$. (b) After a motor has bound, all bound motor heads are shifted to the new ensemble position z to implement the PCM assumption of equal x_{ij} of all bound motors. Because the external force is distributed over a larger number of bound motors, the position z_{fil} of the motor filament also shifts to larger values.

This is the same result as for the average in Eq. (24). Comparison with the general case reveals that the PCM predicts too small a displacement upon unbinding and will underestimate the velocity of an ensemble when there is a wide distribution of the strains of motors. When the last motor unbinds from the substrate, according to Eq. (25) the position of the motor ensemble changes by the unbinding step

$$\Delta z_{1j}^{\text{off}} = -x_{1j} \quad \text{for } j = 0, 1. \quad (28)$$

Eqs. (26) to (28) completely specify the rules for ensemble movement resulting from the binding dynamics in an ensemble. The ensemble moves forward, when a motor binds while the strain x_{ij} of the weakly-bound motors is negative and moves backwards when x_{ij} is positive. Unbinding of a motor does not change the position unless the last motor unbinds. In this case, the position of the unbinding motor head relaxes to the position of the motor filament.

The velocity v_{ij} of an ensemble in state (i, j) is given by the product of the displacement step induced by a binding or unbinding transition with the rate at which this transition proceeds. Unbound motors bind with the effective forward rate $g(i)$ defined in Eq. (14). Unbinding only changes ensemble position when the last motor unbinds. Weakly-bound motor unbind with the constant off-rate $k_{10} = \text{const}$; post-power-stroke motors unbind with the off-rate $k_{20}(1, 1)$. Thus, the velocity of the ensemble in state (i, j) is

$$v_{ij} = g(i)\Delta z_{ij}^{\text{on}} + [k_{10}\Delta z_{10}^{\text{off}}\delta_{j0} + k_{20}(1, 1)\Delta z_{11}^{\text{off}}\delta_{j1}] \delta_{i1} \quad (29)$$

$$= -g(i)\frac{x_{ij}}{i+1} - [k_{10}x_{10}\delta_{j0} + k_{20}(1, 1)x_{11}\delta_{j1}] \delta_{i1}. \quad (30)$$

The last term applies only to unbinding from the state $i = 1$ and distinguishes between weakly-bound motors ($j = 0$) and post-power-stroke motors ($j = 1$).

To combine the expressions for ensemble displacement and velocity with the solutions of the one-step master equation for the binding dynamics, we have to average over the variable j using the LTE distribution. The offset of the bound motors in state i is given by

$$x_i = \sum_{j=0}^i x_{ij}p(j|i) = \frac{1}{Z_i} \sum_{j=0}^i x_{ij} \exp(-E_{ij}/k_B T). \quad (31)$$

The binding step of the ensemble due to the transition $i \rightarrow i+1$ then becomes

$$\Delta z_i^{\text{on}} = - \sum_{j=0}^i \Delta z_{ij}^{\text{on}} p(j|i) = - \frac{1}{i+1} \sum_{j=0}^i x_{ij} p(j|i) = - \frac{x_i}{i+1} \quad (32)$$

for $i \geq 1$. The unbinding step is $\Delta z_i^{\text{off}} = 0$ for $i \geq 2$ and $\Delta z_1^{\text{off}} = -x_1$ for $i = 1$. Averaging the velocity v_{ij} from Eq. (29) over j yields the velocity in state i :

$$v_i = g(i)\Delta z_i^{\text{on}} - [k_{10}x_{10}p(0|1) + k_{20}(1, 1)x_{11}p(1|1)] \delta_{i1}. \quad (33)$$

The expression for the velocity applies to attached ensembles with at least one bound motor, that is, $i \geq 1$. To complete the description of ensemble movement, the velocity of detached ensembles with $i = 0$ has to be defined. The position of the detached ensemble is described by the position of the motor filament, z_{fil} , which is identical to the position of the unbound motor heads. We assume that the external load F_{ext} moves the motor filament through the viscous environment with effective mobility η . For constant external load, detached ensembles move with constant velocity

$$v_0 = -\eta F_{\text{ext}}. \quad (34)$$

The negative sign follows from the definition of the direction of the external load opposite to the working direction of the motors. Detached ensembles attach to the substrate with forward rate $g(0) = N_t k_{01}$ so that the random attachment times follow an exponential distribution with average $g^{-1}(0)$. For constant velocity $v_0 = \text{const}$, this implies an exponential distribution also for the size of the backsteps. The average backstep size is then given by

$$\Delta z_0^{\text{on}} = \frac{v_0}{g(0)} = -\frac{\eta k_f}{N_t k_{01}}. \quad (35)$$

For a linear external load, $F_{\text{ext}} = k_f z_{\text{fil}}$, the velocity of the detached ensemble depends on the position $z_{\text{fil}} = z$ of the ensemble:

$$v_0(z) = \dot{z}_{\text{fil}} = -\eta k_f z_{\text{fil}}. \quad (36)$$

Therefore, the average backstep size for linear external load depends on the position z_{fil}^0 of the motor filament at detachment:

$$\Delta z_0^{\text{on}} = -\frac{\eta k_f z_{\text{fil}}^0}{N_t k_{01} + \eta k_f}. \quad (37)$$

For a large mobility with $\eta k_f \gg N_t k_{01}$, the average backsteps size is $\Delta z_0^{\text{on}} \approx z_{\text{fil}}^0$, that is, the ensemble is effectively reset to the initial position $z = 0$.

Together, the master equation of Eq. (10) for the stochastic binding dynamics and the rules for the displacement upon binding and unbinding of motors fully characterize dynamics and movement of an ensemble of molecular motors. For constant external load, ensemble movement is slaved to binding and unbinding of motors, because on- and off-rates are independent of the position z of the ensemble. In this case, the master equation can be solved independently for the probability distribution $p_i(t)$ and the average velocity of an ensemble can be inferred from this solution. The average bound velocity, that is, the average velocity of ensembles with at least one bound motor, is given by

$$v_b(t) = \sum_{i=1}^{N_t} v_i \hat{p}_i(t) = \sum_{i=1}^{N_t} v_i \frac{p_i(t)}{1 - p_0(t)}. \quad (38)$$

The probability distribution $\hat{p}_i(t)$ is normalized over the attached states $i \in \{1, \dots, N_t\}$ of the ensemble. The effective velocity of an ensemble, which includes the backward motion (slips) of the unbound ensemble, is given by the average

$$v_{\text{eff}}(t) = \sum_{i=0}^{N_t} v_i p_i(t) \quad (39)$$

over all states $i \in \{0, \dots, N_t\}$. Because $v_0 = -\eta F_{\text{ext}} \leq 0$, the effective velocity is smaller than the bound velocity, $v_{\text{eff}}(t) \leq v_b(t)$. For linear load, also a probability distribution for the unbound velocity would have to be determined. From the average ensemble velocity as function of time, the position $z(t)$ can be calculated as

$$z(t) = z_0 + \int_0^t v_{\text{eff}}(t') dt'. \quad (40)$$

For linear external load, the transition rates characterizing the master equation depend on the position of the motor ensemble, so that the master equation has to be solved together with the displacement of the ensemble, which usually has to be done numerically.

III. RESULTS

A. Constant load

1. Analytical solutions of the one-step master equation

Mathematically, the reduction of the stochastic binding dynamics on the two-dimensional network of states of Fig. 3 (a) to the one-dimensional system of Fig. 3 (b) described by Eq. (10) is a dramatic advance, because many general results are known for one-step master equations⁵³. For constant external load, the transition rates are independent of the position z of the ensemble and stationary solutions of the one-step master equation can be derived analytically. For a single variable and in the absence of sources and sinks, stationarity implies detailed balance, that is, $r(i+1)p_{i+1} = g(i)p_i$. Iterating this condition yields the stationary probability $p_i(\infty)$ to find i bound motors in an ensemble:

$$p_i(\infty) = \frac{\prod_{j=0}^{i-1} \frac{g(j)}{r(j+1)}}{1 + \sum_{k=1}^{N_t} \prod_{j=0}^{k-1} \frac{g(j)}{r(j+1)}}. \quad (41)$$

This distribution immediately allows to calculate the average number of bound motors as

$$N_b = \langle i \rangle = \sum_{i=0}^{N_t} i p_i(\infty). \quad (42)$$

In order to calculate averages restricted to attached ensembles with $i \geq 1$, the stationary probability distribution $p_i(\infty)$ has to be re-normalized for the N_t attached states:

$$\hat{p}_i(\infty) = \frac{p_i(\infty)}{1 - p_0(\infty)} = \frac{\prod_{j=0}^{i-1} \frac{g(j)}{r(j+1)}}{\sum_{k=1}^{N_t} \prod_{j=0}^{k-1} \frac{g(j)}{r(j+1)}}. \quad (43)$$

The average detachment time T_{10} of an ensemble is defined as the mean first passage time of the ensemble from the initial attached state, in which only a single motor is bound ($i = 1$), to complete detachment of the ensemble, where all motors have dissociated ($i = 0$). The mean first passage time T_{10} can be calculated analytically using the adjoint master equation⁵³:

$$T_{10} = \sum_{j=1}^{N_t} \frac{1}{r(j)} \prod_{k=1}^{j-1} \frac{g(k)}{r(k)}. \quad (44)$$

The average attachment time of an ensemble is defined as the mean first passage time T_{01} from the detached state ($i = 0$) to the initial attached state ($i = 1$). This transition involves only a single binding step so that the mean first passage time is given by the inverse of the forward rate $g(0)$:

$$T_{01} = \frac{1}{g(0)} = \frac{1}{N_t k_{01}}. \quad (45)$$

A measure for the ability of ensembles of non-processive motors to generate force and directed motion is the duty ratio of an ensemble. For a single molecular motor, the duty ratio is defined as the fraction of time in the motor cycle, during which the motor is attached to its substrate. Processive motors usually are characterized by large duty ratios close to unity, which allows them to walk along the substrate for many motor cycles. Non-processive motors, on the other hand, are characterized by small duty ratios, which reduces the interference between cooperating motors. For ensembles of molecular motors, we define the ensemble duty ratio ρ_d as

$$\rho_d = \frac{T_{10}}{T_{10} + T_{01}}. \quad (46)$$

This is the ratio of detachment time T_{10} , which is the average time during which an ensemble remains attached to the substrate before detaching again, to the average time it takes to complete one attachment-detachment cycle of an ensemble, which is the sum $T_{10} + T_{01}$ of detachment and attachment time. To allow for efficient motion and force generation, the duty ratio of an ensemble of non-processive motors should be close to unity, comparable to that of processive motors.

The average bound velocity of an ensemble in the stationary state is given by Eq. (38) with the stationary probability distribution from Eq. (43) replacing $\hat{p}_i(t)$, that is,

$$v_b = \sum_{i=1}^{N_t} v_i \hat{p}_i(\infty). \quad (47)$$

Correspondingly, the average effective velocity in the stationary state is found by inserting $p_i(\infty)$ from Eq. (41) in Eq. (39) as

$$v_{\text{eff}} = \sum_{i=0}^{N_t} v_i p_i(\infty). \quad (48)$$

The effective velocity can be also expressed using the ensemble duty ratio:

$$v_{\text{eff}} = \rho_d v_b + (1 - \rho_d) v_0 = \frac{T_{10} v_b + T_{01} v_0}{T_{10} + T_{01}}. \quad (49)$$

Because $v_0 \leq 0$, the effective velocity of an ensemble is always smaller than the bound velocity. The closer the ensemble duty ratio is to unity, the closer is the effective velocity to the bound velocity.

Processive motors can be characterized by their processivity, that is, the average number of steps a motor takes on a substrate before unbinding. For ensembles of non-processive motors, we can use the average walk length d_w between attachment and complete detachment as a measure for the effective processivity. Assuming that relaxation to the stationary distribution $\hat{p}_i(\infty)$ is fast compared to the detachment time T_{10} , the ensemble moves with constant bound velocity v_b from Eq. (47) over the detachment time T_{10} so that the average walk length is given by the product

$$d_w = v_b T_{10}. \quad (50)$$

Unlike processive motors, d_w does not correspond to a fixed number of binding and unbinding steps of motors because the displacement steps depend on the state of the ensemble.

2. Binding dynamics

To demonstrate the stochastic effects resulting from the finite number of motors in an ensemble and the influence of the catch bond character of the post-power-stroke state, we first study the dependence of the binding dynamics on ensemble size N_t and external load F_{ext} .

Fig. 5 (a) shows the average detachment time T_{10} (see Eq. (44)) of an ensemble of myosin II motors as function of ensemble size N_t for different values of the external load per motor F_{ext}/N_t . T_{10} appears to increase exponentially with N_t , where prefactor and scale of the exponential increase with F_{ext}/N_t . An approximation for T_{10} can be derived for vanishing external load under the assumption that all bound motors are in the post-power-stroke state, which is justified by the strong bias of the LTE distribution towards the post-power-stroke state. For $F_{\text{ext}} = 0$, the dynamics of the bound motors is not coupled so that not only the on-rate k_{01} but also the off-rate $k_{20} \simeq k_{20}^0$ is independent of the ensemble state (i, j) . A series expansion of Eq. (44) for T_{10} then leads to

$$T_{10} \approx \frac{1}{k_{01} N_t} \left[\exp \left(\ln \left[\frac{k_{20}^0 + k_{01}}{k_{20}^0} \right] N_t \right) - 1 \right] = T_{01} \left[\exp \left(\ln \left[\frac{k_{20}^0 + k_{01}}{k_{20}^0} \right] N_t \right) - 1 \right]. \quad (51)$$

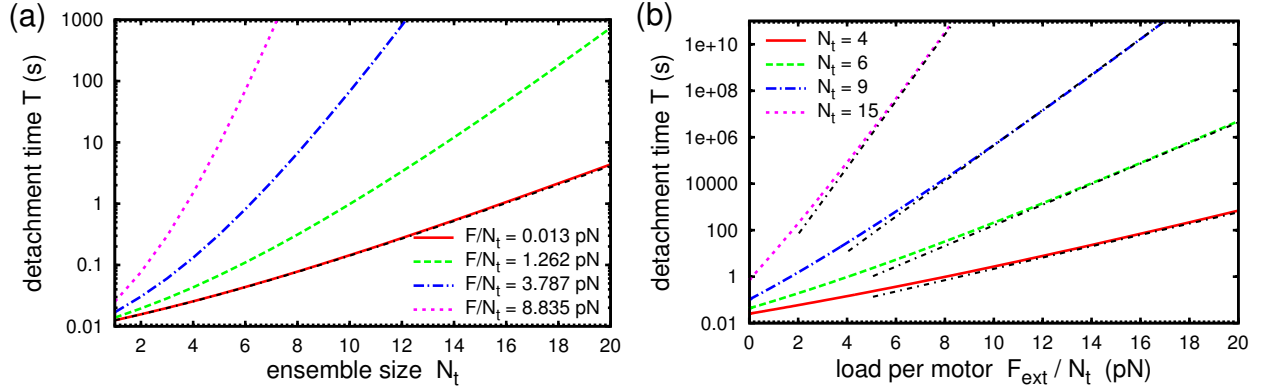


FIG. 5. Analytical results for the parallel cluster model with constant external load: average detachment time T_{10} . (a) T_{10} as function of ensemble size N_t for the values $F_{\text{ext}}/N_t = 0.0126$ pN, 1.262 pN, 3.787 pN and 8.835 pN of the external load per motor. The black, dash-dotted curve is the approximation of Eq. (51) for $F_{\text{ext}}/N_t = 0$. (b) T_{10} as function of the external load per motor F_{ext}/N_t for ensemble sizes $N_t = 4, 6, 9$ and 15 . Black, dash-dotted curves are exponential approximations. Constant parameters are listed in Tab. I.

Comparison with the exact results for $F_{\text{ext}}/N_t = 0.013$ pN in Fig. 5 (a) shows excellent agreement. For finite load, no closed form can be found, because the off-rate $k_{20}(i, j)$ is a strongly non-linear function of the ensemble state (i, j) . A fit of T_{10} to a function of the type of Eq. (51) with adapted prefactor and scale of the exponential yields a better approximation than a pure exponential but deviations at small N_t are still observed, in particular for large external load (not shown).

Fig. 5 (b) shows the average detachment time T_{10} for different ensemble sizes as function of the external load per motor. T_{10} increases exponentially for not too small values of F_{ext}/N_t where the scale of the exponential increases with N_t . This exponential increase is a consequence of the catch bond character of the post-power-stroke state: for all values of a constant external load, the LTE distribution is strongly biased towards the post-power-stroke state, that is, $p(i|i) \lesssim 1$ and $0 \lesssim p(j \neq i|i)$. Hence, unbinding will occur predominantly from the post-power-stroke state so that the effective reverse rate $r(i) \approx p(i|i)k_{20}(i, i) \propto \exp(-F_{\text{ext}}/iF_0)$ decreases exponentially under load. This induces the exponential increase of T_{10} observed in Fig. 5 (b). Only for very large loads beyond $F_{\text{ext}}/N_t \simeq 20F_0$, unbinding from the post-power-stroke state would become slow enough to make unbinding from the weakly-bound state significant so that T_{10} would reach a plateau. At this level of force, however, forced unbinding would have to be taken into account⁴⁹ and we do not consider such large forces in our model. The average attachment time T_{01} of a myosin II

ensemble involves only a single binding step, so that the dependence on F_{ext} and N_t is rather weak: $T_{01} = (k_{01}N_t)^{-1}$ is independent of external load and decreases inversely with ensemble size.

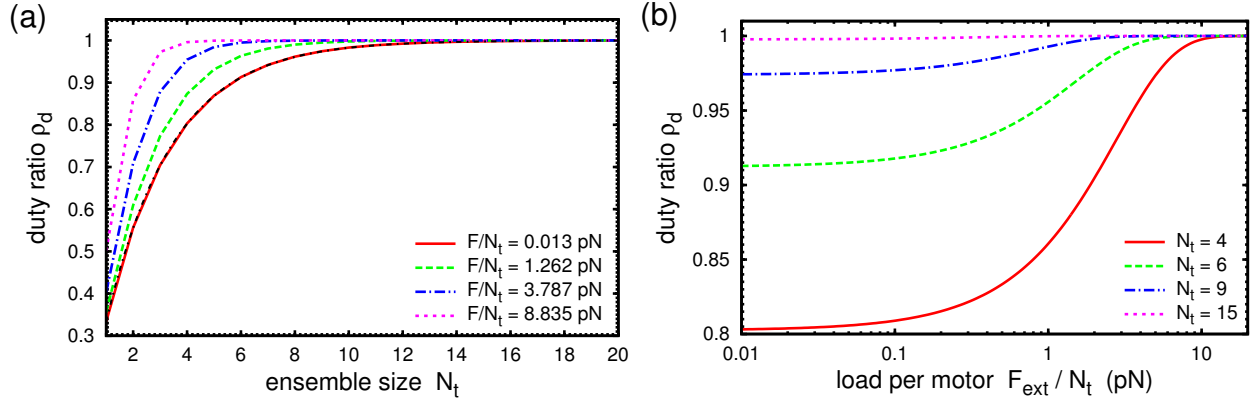


FIG. 6. Analytical results for the parallel cluster model with constant external load: ensemble duty ratio ρ_d . (a) ρ_d as function of ensemble size N_t for the values $F_{\text{ext}}/N_t = 0.0126$ pN, 1.262 pN, 3.787 pN and 8.835 pN of the external load per motor. The black, dash-dotted curve is the approximation of Eq. (53). (b) ρ_d as function of the external load per motor F_{ext}/N_t for ensemble sizes $N_t = 4, 6, 9$ and 15. Constant parameters are listed in Tab. I.

The ability of a molecular motor to generate sustained levels of force or continuous motion depends crucially on its duty ratio. Due to the increase of the detachment time T_{10} and the decrease of the attachment time T_{01} with N_t , the ensemble duty ratio can be adjusted via the ensemble size N_t . The minimal number of motors, which could allow for a duty ratio close to unity and almost continuous attachment of an ensemble, is determined by the inverse of the duty ratio of a single motor. For $F_{\text{ext}} = 0$, the off-rate of myosin II can be approximated as $k_{20} \simeq k_{20}^0 \simeq 80 \text{ s}^{-1}$ because myosin II unbinds almost exclusively from the post-power-stroke state. With the on-rate $k_{01} = 40 \text{ s}^{-1}$, the duty ratio of a single myosin II is

$$\rho_d^{\text{single}} = \frac{T_{10}}{T_{01} + T_{10}} = \frac{k_{01}}{k_{01} + k_{20}^0} \simeq 0.33. \quad (52)$$

This value is significantly larger than the observed duty ratio of skeletal and smooth muscle myosin II but comparable to the duty ratio ($\simeq 0.23$) of non muscle myosin II³¹. For $\rho_d^{\text{single}} \simeq 0.33$, a minimum of $N_t \simeq 3$ motors is required for continuous attachment. However, due to the stochastic binding dynamics and the lack of coordination of individual motors, the ensemble duty ratio will be smaller than the sum over the single motor duty ratios and a larger number of motors will

be required to ensure continuous attachment. For vanishing external load, the approximation of Eq. (51) for the average detachment time T_{10} can be used to derive an approximation for the duty ratio. Inserting Eq. (51) for T_{10} in Eq. (46) for the ensemble duty ratio yields

$$\rho_d \approx 1 - \exp\left(-\ln\left[\frac{k_{20}^0 + k_{01}}{k_{20}^0}\right] N_t\right). \quad (53)$$

With increasing N_t , the duty ratio saturates exponentially from the single motor value $\rho_d = 1 - k_{20}^0/(k_{20}^0 + k_{01})$ for $N_t = 1$ towards $\rho_d \simeq 1$ for large N_t . Fig. 6 (a) shows ρ_d as function of N_t for different values of the external load per motor. Eq. (53) provides an excellent approximation for near-vanishing load. For $F_{\text{ext}}/N_t = 0.013$ pN, the duty ratio is $\rho_d \simeq 0.33$ for a single motor. For $N_t = 3$, the duty ratio is $\rho_d \simeq 0.7 < 1$ and reaches unity for ensemble sizes beyond $N_t \simeq 15$. With increasing external load, the duty ratio is elevated already for $N_t = 1$ and a smaller number of motors is required to reach a duty ratio of $\rho_d \simeq 1$. Fig. 6 (b) shows the ensemble duty ratio (see Eq. (46)) as function of the external load per motor. For $N_t = 4$, $T_{10} \simeq 0.025$ s and $T_{01} \simeq 0.006$ s so that $\rho_d \simeq 0.8$ at $F_{\text{ext}}/N_t = 0$. Due to the exponential increase of T_{10} with F_{ext}/N_t , the duty ratio increases quickly and saturates at $\rho_d \simeq 1$ above $F_{\text{ext}}/N_t \simeq F_0 \simeq 12.6$ pN. With increasing ensemble size N_t the duty ratio increases and the limiting value $\rho_d \simeq 1$ is reached at smaller values of F_{ext}/N_t . For $N_t = 15$ the duty ratio is practically unity for all values of the external load, because $T_{10} \simeq 0.73$ s and $T_{01} \simeq 0.0017$ s so that $\rho_d \simeq 0.998$ at $F_{\text{ext}} = 0$.

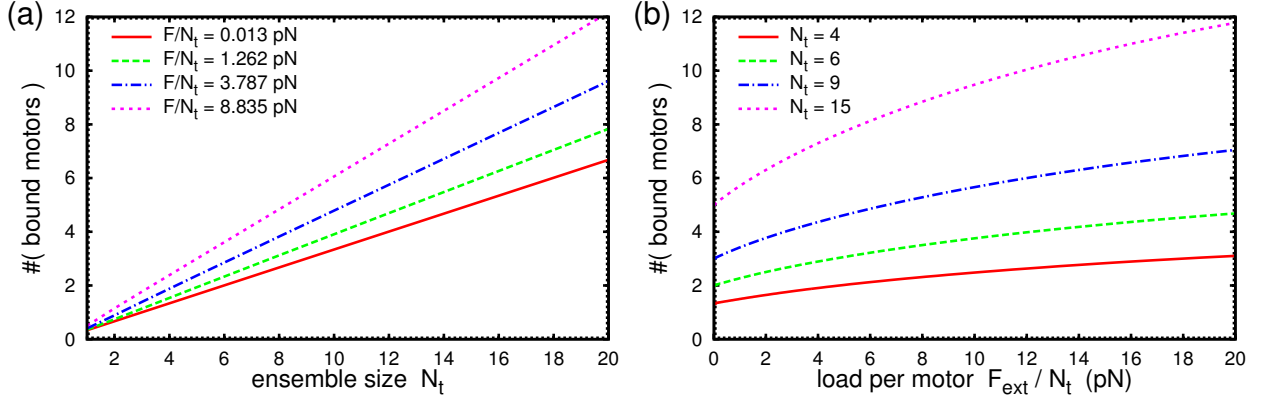


FIG. 7. Analytical results for the parallel cluster model with constant external load: average number of bound motors N_b . (a) N_b as function of ensemble size N_t for the values $F_{\text{ext}}/N_t = 0.0126$ pN, 1.262 pN, 3.787 pN and 8.835 pN of the external load per motor. (b) N_b as function of external load per motor F_{ext}/N_t for ensemble sizes $N_t = 4, 6, 9$ and 15. Constant parameters are listed in Tab. I.

Fig. 7 (a) shows the average number of bound motors N_b as function of ensemble size N_t for

different values of the external load. For all values of the load, N_b increases linearly with N_t , where the increase becomes steeper under larger external load. Fig. 7 (b) shows N_b as function of the external load per motor for different ensemble sizes. At vanishing load, $N_b \simeq \rho_d^{\text{single}} N_t \simeq 0.33N_t$. For $F_{\text{ext}} = 0$, the motors bind independently, because the PCM assumes that motors in equivalent states have equal strains and because most bound motors are in the post-power-stroke state, so that no internal stress is built up between motors in different states. With increasing F_{ext}/N_t , the average number of bound motors increases sub-linearly and plateaus towards N_t for large loads. The recruitment of additional bound motors under increasing load was described theoretically¹⁹ and has been observed experimentally for myosin II in muscle¹⁴. The increase of the average number of bound motors under load observed in Fig. 7 (b), as well as the increase of T_{10} and ρ_d under load, confirms that myosin II as a whole behaves as a catch bond over a large range of values of a constant external load. Thus, the efficiency of an ensemble of non-processive motors for the generation of motion and force, which is determined by detachment time, duty ratio and number of bound motors, can be adjusted by changing the ensemble size N_t or by using the force sensitivity of the motors.

3. Stochastic trajectories

To gain more insight into the movement of an ensemble of non-processive molecular motors and the relation between binding and movement, it is instructive to look at single, stochastic trajectories. We use the Gillespie algorithm⁵⁴ to simulate stochastic binding and unbinding trajectories according to the one-step master equation of Eq. (10) and apply the rules for the displacement upon binding and unbinding to implement ensemble movement. Within the Gillespie algorithm, the transition rates $r(i)$ and $g(i)$ are used to choose time and type of the next stochastic transition from an exponential probability distribution. After a binding transition $i \rightarrow i + 1$ with $i \geq 1$, the position z of the ensemble is changed by $\Delta z_i^{\text{on}} = -x_i/(i + 1)$. For $i = 0$, the position of the detached ensemble is changed by $\Delta z_0^{\text{on}} = -\eta F_{\text{ext}}\tau$ before attachment. Here, τ is a random attachment time with average T_{01} . After an unbinding transition $i \rightarrow i - 1$, z is unchanged for $i \geq 2$. If the last motor unbinds, that is for $i = 1$, ensemble position is changed by $\Delta z_1^{\text{off}} = -x_1$. After adjusting ensemble position, the new value of the strain x_{ij} of weakly-bound motors is determined from the balance of forces in Eq. (1) and the position z_{fil} of the motor filament is set to $z_{\text{fil}} = z - x_{ij}$. With the updated LTE distribution $p(j|i)$, the average strain of weakly-bound

motors, $x_i = \sum_{j=0}^i x_{ij} p(j|i)$, and the transition rates $r(i)$ and $g(i)$ are calculated and new random time and type of the next reaction are chosen.

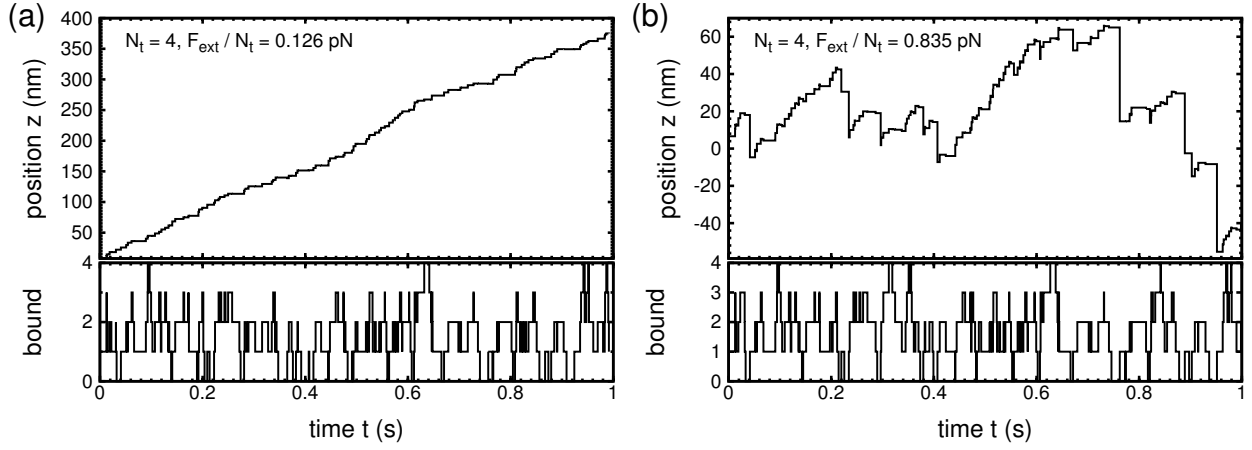


FIG. 8. Stochastic trajectories for constant external load. Ensemble position z (upper panel) and number i of bound motors (lower panel) as function of time t for ensemble size $N_t = 4$ and external load per motor (a) $F_{\text{ext}}/N_t = 0.126$ pN and (b) $F_{\text{ext}}/N_t = 0.835$ pN. In (a) and (b) the detached ensemble slides backwards with mobility $\eta = 10^3$ nm pN $^{-1}$ s $^{-1}$. Constant parameters are listed in Tab. I.

Fig. 8 (a) shows a stochastic trajectory of an ensemble with $N_t = 4$ motors working against the constant external load $F_{\text{ext}}/N_t = 0.126$ pN. The lower panel shows the fluctuating number of bound motors i , the upper panel the ensemble position z . The external load is below the stall force so that the attached ensemble moves forward with a velocity fluctuating around the average bound velocity $v_b > 0$. The number of bound motors fluctuates strongly and the ensemble frequently detaches completely from the substrate. Unlike z , the position $z_{\text{fil}} = z - x_i$ of the motor filament is also changed by a change of the strain x_i of the motors. When a motor binds, the external load is distributed over a larger number of motors, so that the strain is reduced and the motor filament slides forward in addition to the change of z . When a motor unbinds, the strain x_i of the remaining bound motors increases, so that the motor filament slides backwards while z remains constant. Trajectories of $z_{\text{fil}} = z - x_i$ therefore are rather close to z but show stronger fluctuations (not shown). Complete detachment of the ensemble leads to backward steps of average size $\Delta z_0^{\text{on}} = -v_0 T_{01}$. For a small load as in Fig. 8 (a), however, backsteps are too small to be resolved so that detachment events appears as pauses in the trajectory. Fig. 8 (b) shows a stochastic trajectory for an ensemble with $N_t = 4$ motors but at larger external load. At this load, the average bound velocity

is positive so that the net movement of the attached ensemble is forward, although the strain x_1 is positive for a single bound motor so that binding of the second motor leads to a backward step in z . Detachment of the ensemble has become only marginally less frequent under the larger load, but the size of the backward steps has increased (note the larger z scale in (b) compared to (a)) such that the effective velocity is close to zero. Hence the value of the external load is close to the effective stall force, at which the forward movement of the attached ensemble balances the backward slips of the detached ensemble.

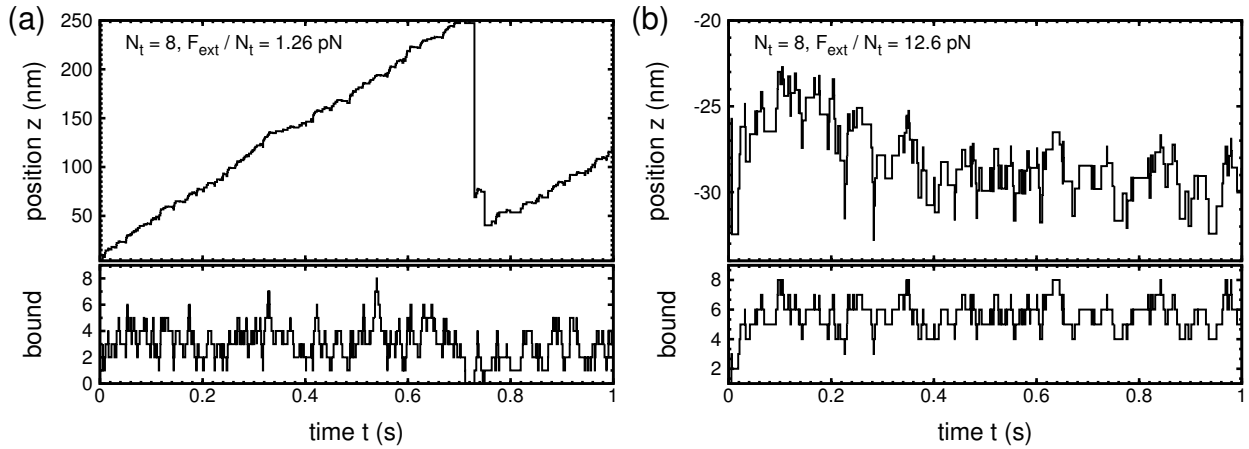


FIG. 9. Stochastic trajectories for constant external load. Ensemble position z (upper panel) and number i of bound motors (lower panel) as function of time t for ensemble size $N_t = 8$ and external load per motor (a) $F_{\text{ext}}/N_t = 1.26$ pN and (b) $F_{\text{ext}}/N_t = 12.6$ pN. In (a) and (b) the unbound ensemble slides backwards with mobility $\eta = 10^3$ nm pN $^{-1}$ s $^{-1}$. Constant parameters are listed in Tab. I.

Fig. 9 (a) shows a stochastic trajectory of an ensemble at larger ensemble size $N_t = 8$. The external load is below the stall force, so that the attached ensemble moves forward with slightly fluctuating velocity. Due to the larger ensemble size, complete detachment occurs less frequently but the large external load leads to large backsteps. In Fig. 9 (b), the ensemble size is the same as in (a) but F_{ext} is increased to a value close to the stall force with $v_b \simeq 0$. Due to the catch bond character of myosin II, the typical number of bound motors is increased and complete detachment is rare. Nevertheless, the ensemble position z fluctuates strongly because binding at small i leads to backsteps $\Delta z_i^{\text{on}} \leq 0$ whereas binding at larger i leads to forward steps $\Delta z_i^{\text{on}} \geq 0$ of the ensemble. At the stall force these two effects balance so that the average bound velocity vanishes, $v_b = 0$.

4. Velocity and walk length

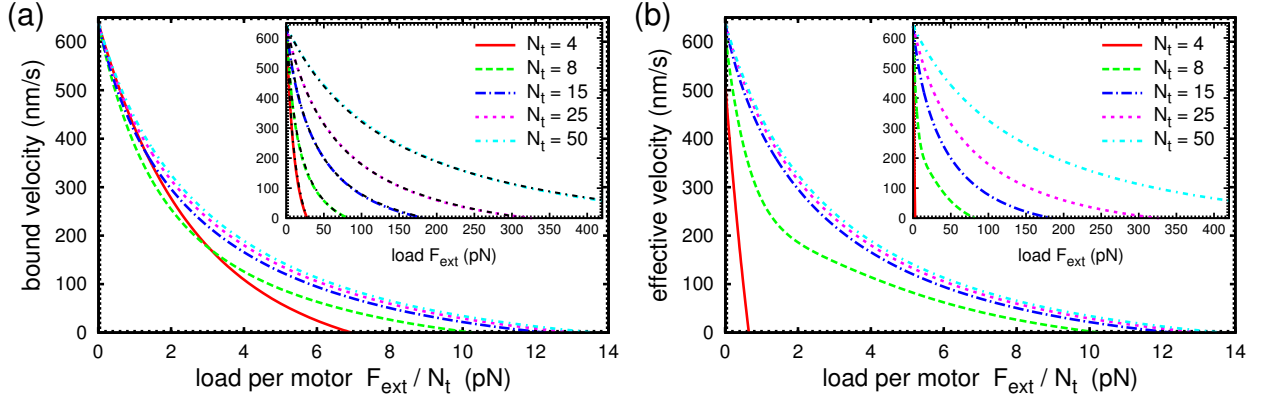


FIG. 10. Analytical results for the parallel cluster model with constant external load. (a) Average bound velocity v_b and (b) average effective velocity v_{eff} as function of the external load per motor F_{ext}/N_t for ensemble sizes $N_t = 4, 8, 15, 25$ and 50 . For v_{eff} the viscous mobility of detached ensembles is $\eta = 10^3 \text{ nm pN}^{-1} \text{ s}^{-1}$. The insets show v_b and v_{eff} as function of external load F_{ext} . Black, dash-dotted curves in the inset of (a) show the Hill-relation from Eq. (54) with $\alpha = 0.46 \text{ pN}, 0.205 \text{ pN}, 0.2 \text{ pN}, 0.215 \text{ pN}$ and 0.215 pN for $N_t = 4, 8, 15, 25$ and 50 . Constant parameters are listed in Tab. I.

Fig. 10 (a) shows analytical results for the average bound velocity v_b (see Eq. (47)) as function of the external load per motor for different ensemble sizes. For $F_{\text{ext}} = 0$, the average bound velocity is $v_b(F_{\text{ext}} = 0) \simeq 640 \text{ nm s}^{-1}$ and is independent of ensemble size N_t . From its maximal value, v_b decreases with increasing F_{ext}/N_t in a concave fashion and becomes negative for loads above the stall force F_s . The concave shape of the force-velocity relation has been explained before by the increase of the average number of bound motors under load^{19,44} which is a consequence of the catch bond character of myosin II. Compared to a system with constant N_b , the increase of N_b reduces the load on the individual bound motors and reduces their strain x_{ij} . According to Eq. (33) for v_i , this increases the velocity at given external load and hence the stall force of the ensemble. Beyond sufficiently large ensemble sizes of $N_t \geq 15$ the force-velocity relation $v_b(F_{\text{ext}}/N_t)$ hardly changes with further increasing N_t . At $N_t = 15$, the stall force per motor is $F_s/N_t \simeq 12.4 \text{ pN}$. With increasing ensemble size, it increases slightly to $F_s/N_t \simeq 13.5 \text{ pN}$ for $N_t = 50$ because the force-velocity relation becomes very shallow near F_s . Smaller ensembles show a more rapid decrease of v_b from the value at $F_{\text{ext}} = 0$ as well as a smaller F_s/N_t . The inset in Fig. 10 (a) shows v_b as function of the absolute load F_{ext} for the same values of N_t as in the main panel. The

analytical results from the model are compared to the effective, Hill-type force-velocity relation⁵⁵

$$v_{\text{hill}}(F_{\text{ext}}) = v_{\text{b}}(F_{\text{ext}} = 0) \frac{F_{\text{s}} - F_{\text{ext}}}{F_{\text{s}} + (F_{\text{ext}}/\alpha)}. \quad (54)$$

For the comparison, the values of $v_{\text{b}}(F_{\text{ext}} = 0)$ and F_{s} are taken from the model results. The parameter α has units of force and is used to fit the curvature of the force-velocity relations. The comparison shows that Eq. (54) describes the force-velocity relation for all N_{t} extremely well. The parameter α is almost identical for ensemble sizes $N_{\text{t}} = 8$ to 50 with a typical value of $\alpha \simeq 0.21$ pN and differs significantly only for $N_{\text{t}} = 4$. For $N_{\text{t}} = 4$, the ensemble detaches frequently so that the off-step $\Delta z_{1j}^{\text{off}}$ from Eq. (28), in which the strain of the last unbinding motor is released and changes the ensemble position, contributes significantly to the bound ensemble velocity. This causes the markedly different dependence on $F_{\text{ext}}/N_{\text{t}}$ with smaller curvature of the force-velocity curve for $N_{\text{t}} = 4$. For $N_{\text{t}} = 1$, this off-step upon unbinding can still generate forward movement.

The good fit of $v_{\text{b}}(F_{\text{ext}})$ by $v_{\text{hill}}(F_{\text{ext}})$ demonstrates the qualitative agreement of the PCM with the experimental force-velocity curve of muscle, for which v_{hill} was originally derived. Our model can now be used to estimate the values for load free velocity and stall force and to elucidate their dependence on the model parameters. For vanishing force, the number of bound motors on average is $N_{\text{b}} \simeq \rho_{\text{d}} N_{\text{t}} \simeq N_{\text{t}}/3$. Since almost all of these motors are in the post-power-stroke state, we find $x_i = -d$ and the binding step of the ensemble is $\Delta z_{N_{\text{b}}}^{\text{on}} = -x_i/(N_{\text{b}} + 1) \simeq d/N_{\text{b}}$. Together with the forward rate $g(N_{\text{b}}) = (N_{\text{t}} - N_{\text{b}})k_{01} = (2N_{\text{t}}/3)k_{01}$ we obtain the bound velocity $v_{\text{b}}(F_{\text{ext}} = 0) \simeq g(N_{\text{b}})\Delta z_{N_{\text{b}}}^{\text{on}} \simeq d[(N_{\text{t}} - N_{\text{b}})/N_{\text{b}}]k_{01} = 2dk_{01} = 640 \text{ nm s}^{-1}$. To estimate the stall force, we again assume that all N_{b} bound motors are in the post-power-stroke state. At the stall force, the strain $x_{N_{\text{b}}} = (F_{\text{s}}/k_{\text{m}}N_{\text{b}}) - d$ should vanish so that $\Delta z_{N_{\text{b}}}^{\text{on}} = 0$. Thus, the stall force follows the relation $F_{\text{s}}/N_{\text{b}} = k_{\text{m}}d \simeq 20$ pN. For $N_{\text{t}} = 15$ at $F_{\text{s}}/N_{\text{t}} \simeq 12.4$ pN the number of bound motors can be read from Fig. 7 (b) as $N_{\text{b}} \simeq 0.68N_{\text{t}}$. This yields the ratio $F_{\text{s}}/N_{\text{b}} \simeq 18.2$ pN, which is consistent with the estimate. The estimate of the stall force shows that F_{s} increases linearly with the number of bound motors. If the number of bound motors remained constant at $N_{\text{b}}(F_{\text{ext}} = 0) \simeq 0.33N_{\text{t}}$, the stall force would be reduced to one half the actual value. On the other hand, the velocity at vanishing external load decreases with the number of bound motors. If N_{b} at $F_{\text{ext}} = 0$ had the same value $N_{\text{b}} = 0.68N_{\text{t}}$ found at $F_{\text{ext}} = F_{\text{s}}$, the unloaded velocity would be reduced to $v_{\text{b}}(F_{\text{ext}} = 0) \simeq 160 \text{ nm s}^{-1}$. In this way, the catch bond character of myosin II motor allows ensembles to adapt the typical number of bound motors to the environmental conditions and to increase the dynamic range of an ensemble. At small external load, a small number of

bound motors is able to generate fast movement of the ensemble. At large external load, a large number of bound motors is needed to overcome the external load and to generate slow forward movement.

Fig. 10 (b) shows the average effective velocity v_{eff} (see Eq. (48)) as function of the external load per motor for different ensemble sizes. For large ensembles with $N_t \geq 15$, the effective velocity is essentially identical to the bound velocity because large ensembles rarely detach from the substrate ($\rho_d \simeq 1$). The difference between v_b and $v_{\text{eff}} \leq v_b$, which is observed for smaller ensemble sizes, is determined by the frequency T_{10}^{-1} of detachment and the size Δz_0^{on} of the backsteps. As shown in Fig. 5, T_{10}^{-1} decreases exponentially with F_{ext} , while Δz_0^{on} increases linearly with F_{ext} (see Eq. (35)). For $F_{\text{ext}} = 0$, detached ensembles do not move so that even very small ensembles (including single motors) effectively move forward. Because the frequency of detachment as well as the average duration $T_{01} = (k_{01}N_t)^{-1}$ of detachment events increases with decreasing N_t , $v_{\text{eff}}(F_{\text{ext}} = 0)$ is smaller for smaller N_t . For $N_t = 4$ it is $v_{\text{eff}}(F_{\text{ext}} = 0) \simeq 513 \text{ nm s}^{-1}$ and v_{eff} decreases very rapidly with increasing external load. The stall force is reduced to $F_s/N_t \simeq 1 \text{ pN}$ compared with the value $F_s/N_t \simeq 7 \text{ pN}$ for the bound ensemble. For $N_t = 8$, the effective velocity initially decreases quickly under load. Once the detachment frequency has decreased sufficiently, the force-velocity relation becomes rather shallow. As detachment becomes very rare under further increasing load, the stall force for $N_t = 8$ is almost identical to the stall force of the bound ensemble with $v_b = 0$. The interplay of the linear increase of the size of the backsteps and the exponential decrease of the detachment frequency under load can also lead to a non-monotonous force-velocity relation.

Fig. 11 (a) shows the average walk length of an ensemble as function of ensemble size for different values of the external load F_{ext}/N_t . The stationary approximation $d_w = v_b T_{10}$ is compared to numerical results from stochastic simulations. After an initial transient, the average walk length increases exponentially with N_t . This increase reflects the exponential increase of the detachment time T_{10} with N_t . The initial transient is due to the variation of v_b for small N_t at given F_{ext}/N_t . With increasing external load, the walk length increases as long as F_{ext}/N_t is below the stall force. For the smallest external load, the walk length reaches $d_w \simeq 500 \text{ nm}$ for $N_t = 15$. For $F_{\text{ext}}/N_t \simeq 1.3 \text{ pN} \simeq 0.1F_s$, the walk length increases to 10^4 nm because the exponential increase of T_{10} outruns the decrease of the velocity. Fig. 11 (b) shows d_w as function of the external load per motor for different ensemble sizes. For $N_t = 4$, the walk length decreases slowly because the quick decrease of v_b under load compensates the increase of the detachment time. For larger N_t ,

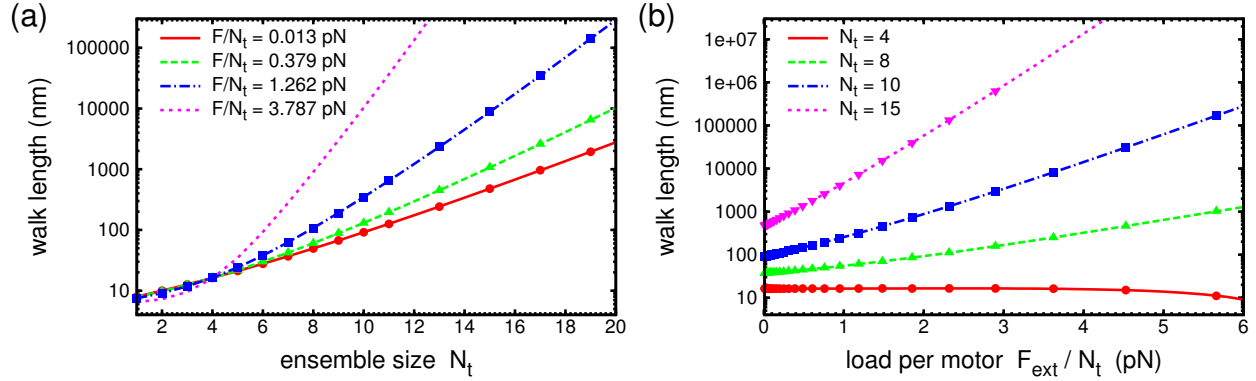


FIG. 11. Comparison of analytical and numerical results for the parallel cluster model with constant external load: Average walk length d_w . (a) d_w as function of N_t for $F_{\text{ext}}/N_t = 0.013$ pN, 0.379 pN, 1.26 pN and 3.79 pN. (b) d_w as function of F_{ext}/N_t for ensemble sizes $N_t = 4, 8, 10$ and 15. The approximation $d_w = v_b T_{10}$ (see Eq. (50)) (curves) is compared to results from stochastic simulations (symbols). Constant model parameters are listed in Tab. I.

d_w increases with F_{ext}/N_t over the range of force shown in the figure. Only when the stall force is reached, the walk length plummets to negative values. The stationary approximation describes the exact numerical results remarkably well over the whole range of ensemble size and external load. This confirms that bound ensembles are characterized by the stationary values for bound velocity v_b and processivity d_w , in analogy to processive motors.

5. Validation of the parallel cluster model

The assumption underlying the parallel cluster model—motors in equivalent mechano-chemical states have identical strains—is not justified a priori. In fact, a finite distribution of strains is expected because motors remain bound at fixed positions on the substrate for random time intervals while the ensemble moves with fluctuating velocity. When the ensemble moves forward, the bound motor which was bound for the longest time should have the largest strain while the motor which has bound most recently should have the smallest strain. For groups of processive motors (see Refs.^{9,56,57}) the load dependence of the velocity seems to provide a natural mechanism for equalizing the load on the motors: as a motor moves ahead of the group it will be subject to a large load; this reduces the velocity of the motor so that the group will catch up with the advancing motor and the loads will be equalized. On the other hand, if a motor trails behind the group it

will be subject to the smallest load and will have the largest velocity so that the trailing motor catches up with the group. Such a mechanism does not seem to be at work for ensembles of non-processive motors, which cannot move along the substrate. However, movement of an ensemble of non-processive motors requires continuous unbinding and binding of the motors. Thereby, the motors remain bound to the substrate for short time intervals and the strain, which was build up while the motor was bound, is released completely before the motor binds again with vanishing strain. Frequent binding and unbinding of motors as a prerequisite of movement in combination with the release of strain after unbinding should result in a narrow distribution of strains of the bound motors, which is the basis for the PCM. Interestingly, equalizing the load in a group of processive motors requires several step of the motors along the substrate, that is, several unbinding and binding events of the individual motor heads, whereas the strain of a non-processive motors is released in a single step. Due to the catch bond character of myosin II it might occur that motors remain bound for long time intervals and build up excessive strains. This, however, should only possible for a small fraction of bound motors, because the majority of motors in the ensemble is required to displace the ensemble and build up the strain. Therefore, most bound motors will still have a narrow distribution of strains.

To validate the assumptions of the PCM, we compare analytical results obtained within the PCM for constant external load to results from computer simulations which do not use the PCM assumption of equal motor strains. Moreover, these simulations do not apply the LTE of bound states but include stochastic transitions between weakly-bound state and post-power-stroke state explicitly. In the simulations, the motor cycle is described by the three distinct mechano-chemical states depicted in Fig. 1. Without LTE, the stochastic transitions in an ensemble with N_t motors proceed on the two-dimensional network of mechano-chemical state shown in Fig. 3 (a). The mechano-chemical state of the ensemble has to be complemented by the strain ξ_n of every bound motor in order to calculate strain dependent transition rates. Every bound motor head is assigned an individual position z_n on the substrate. For given external load F_{ext} and positions z_n , the strain ξ_n for every bound motor is calculated from the balance of forces in Eq. (1). The position z of the ensemble is defined as the average position of the bound motor heads (see Eq. (16)). As in the PCM, detached ensembles slip backwards in the direction of the external load with mobility η .

Transitions between unbound and weakly-bound state are independent of strain so that the transitions $(0) \rightarrow (1)$ and $(1) \rightarrow (0)$ proceed with constant transition rates $k_{01} = \text{const}$ and $k_{10} = \text{const}$, respectively. The values are listed in Tab. I. For transitions $(1) \rightarrow (2)$ and $(2) \rightarrow (1)$

between weakly-bound and post-power-stroke state we assume constant transition rates $k_{12} = k_{12}^0 \exp(-E_{\text{pp}}/2k_{\text{B}}T)$ and $k_{21} = k_{21}^0 \exp(+E_{\text{pp}}/2k_{\text{B}}T)$, respectively. For our simulations we use $k_{12}^0 = k_{21}^0 = 10^3 \text{ s}^{-1}$ but the actual value does not affect the results as long as the forward rate k_{12} is not smaller than the off-rate k_{10} from the weakly-bound state. Because $k_{21}/k_{12} = \exp(E_{\text{pp}}/k_{\text{B}}T)$, a Boltzmann distribution for two states with free energy difference $E_{\text{pp}} < 0$ will establish in equilibrium. Compared to the LTE distribution of Eq. (5), the elastic energy of the motors has been omitted. For constant external load, however, the LTE distribution is dominated by the strong bias E_{pp} towards the post-power-stroke state so that the omission will have little effect on results. Unbinding from the post-power-stroke state is irreversible. The transition $(2) \rightarrow (0)$ proceeds with strain dependent transition rate

$$k_{20}(\xi_n) = k_{20}^0 \exp(-k_{\text{r}}\xi_n/F_0) \quad (55)$$

for $\xi_n \geq 0$ and $k_{20}(\xi_n) = k_{20}^0$ for $\xi_n < 0$, where k_{20}^0 and F_0 from Tab. I are used. Unbinding is slowed down when the neck linker is stretched in the direction of the external force but remains constant when the neck linker is compressed in the opposite direction. The latter case does not occur in the PCM model (as long as the external load is positive) so that the distinction was not necessary. Results of simulations using the Kramers' type off-rate for positive and negative strain are discussed in Appendix A 2. As in the simulations with the PCM, we used the Gillespie algorithm⁵⁴ to simulate the stochastic reactions: the reaction rates for all the motors are used to choose the waiting times between transition and the kind of reaction from the appropriate probability distributions. After every transition, strains ξ_n and transition rates are updated and the next reaction is determined.

Neglecting the change of the elastic energy in the kinetic description of the power stroke seems necessary because of the large value of the stiffness k_{m} of the neck linkers assumed in our model. The neck linker of a motor is stretched when it goes through the power stroke. This step is favorable as long as the increase of the elastic energy of the neck linker is smaller than the (negative) free energy bias $-E_{\text{pp}}$ towards the post-power-stroke state. For a larger number of bound motors, $i \gg 1$, the power stroke stretches the neck linker of a motor approximately by the power-stroke distance $d \simeq 8 \text{ nm}$ and the decrease of the elastic energy of the other bound motors can be neglected. For $k_{\text{m}} \simeq 2.5 \text{ pN nm}^{-1}$, the elastic energy increases by $k_{\text{m}}d^2/2 \simeq 80 \text{ pN nm} > 60 \text{ pN nm} \simeq -E_{\text{pp}}$. For the given elastic constant of the neck linkers, individual motors are effectively unable to perform the power stroke when a large number of bound motors holds the motor filament in place.

Thus, the motor ensemble is stuck kinetically with most motors in the weakly-bound state although the energy of the ensemble as a whole would be reduced by a transition of all bound motors to the post-power-stroke state. To overcome this problem and to make the power stroke favorable also for individual motors in a kinetic description, significantly smaller values of $k_m \simeq 0.3 \text{ pN nm}^{-1}$ have been used^{19,44}. For larger values $k_m \simeq 2.5 \text{ pN nm}^{-1}$ as in our model, the LTE assumption has been used before⁴⁵. For a kinetic description with a large value of the neck linker stiffness, variants of the motor cycle have been used, which do not require an explicit load dependence of the power stroke^{46,47}. This approach, however, does not allow to describe the transition of the LTE distribution to the weakly-bound state when working against very stiff external springs (see Sec. III B 1) or the synchronization of the power stroke against large forces¹⁹.

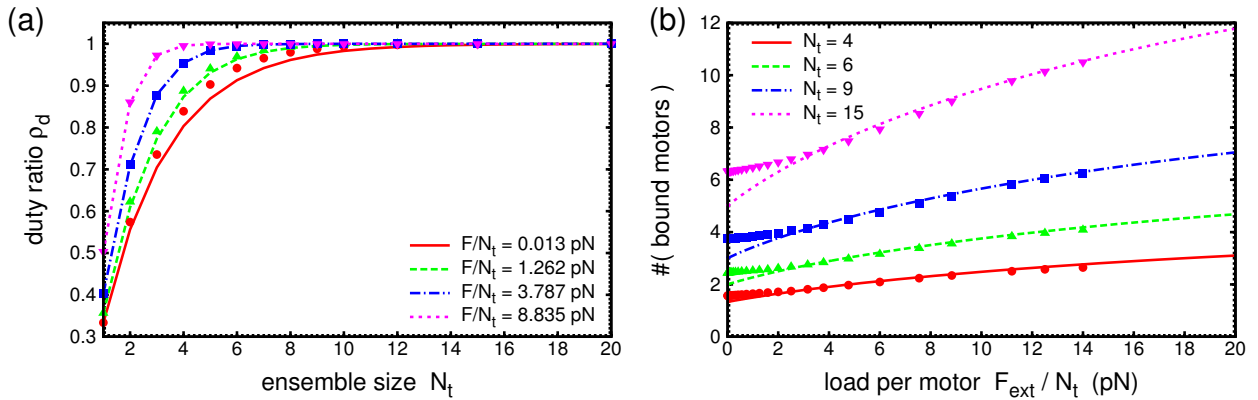


FIG. 12. Validation of the parallel cluster model: comparison of analytical results using the PCM (lines) with computer simulations with individual motor strains (symbols). (a) Duty ratio ρ_d as function of ensemble size N_t for the values $F_{\text{ext}}/N_t = 0.0126 \text{ pN}$, 1.262 pN , 3.787 pN and 8.835 pN of the external load per motor. (b) Average number of bound motors N_b as function of external load per motor F_{ext}/N_t for ensemble sizes $N_t = 4, 6, 9$ and 15 . Constant parameters are listed in Tab. I.

In the following, we compare analytical results from the PCM with numerical results from simulations with individual motor strains. Fig. 12 (a) shows the ensemble duty ratio ρ_d as function of ensemble size for different values of the external load per motor; Fig. 12 (b) shows the average number of bound motors N_b as function of F_{ext}/N_t for different values of N_t . For all ensemble sizes, analytical results from the PCM agree very well with numerical results with individual motor strains. Significant deviations are only observed for small external load where the analytical results underestimate the duty ratio as well as the number of bound motors. These deviations are

caused by the distribution of strains among bound motors. For vanishing and small external load, unbinding of those motors with positive strain will be slowed down while unbinding of those motors with negative strain is unaffected. With increasing external load, the strain of the motors is dominated by the external load and the effects of the distribution of strains become negligible.

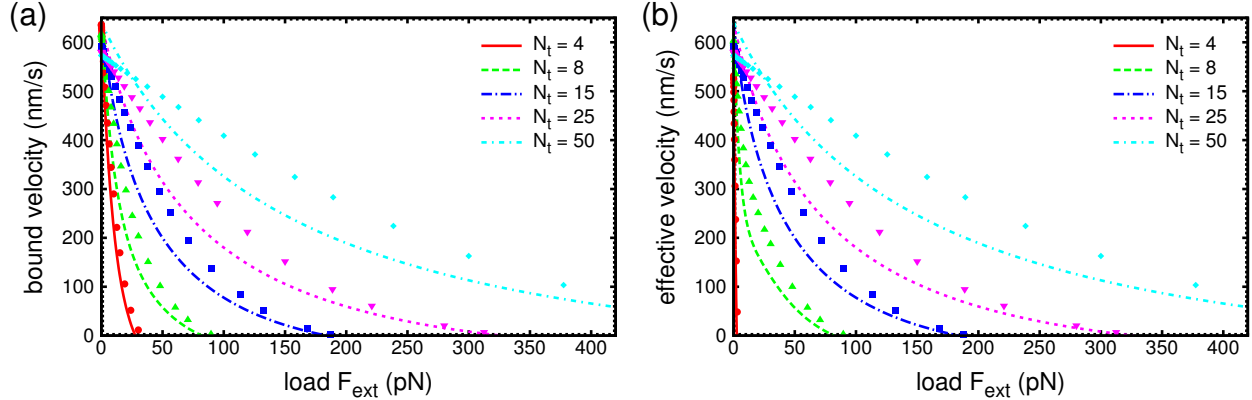


FIG. 13. Validation of the parallel cluster model: comparison of analytical results using the PCM (lines) with computer simulations with individual motor strains (symbols). (a) Average bound velocity v_b and (b) average effective velocity v_{eff} as function of the external load per motor F_{ext}/N_t for ensemble sizes $N_t = 4, 8, 15, 25$ and 50 . The mobility of the free ensemble entering v_{eff} is $\eta = 10^3 \text{ nm pN}^{-1} \text{ s}^{-1}$. Constant parameters are listed in Tab. I.

Fig. 13 compares analytical and simulation results for the bound velocity v_b in (a) and for the effective velocity v_{eff} in (b) as function of external load per motor for different ensemble sizes. The agreement is quite good for small N_t but clear deviations are observed for large N_t at small and intermediate values of F_{ext} . At vanishing and small load, the simulations show a decrease of the bound velocity v_b with increasing N_t . In the PCM, $v_b(F_{\text{ext}} = 0)$ was independent of N_t . The N_t dependence of v_b is caused by the increase of the average number of bound motors at small external load observed in Fig. 12 (b). As demonstrated in the previous section, an increasing number of bound motors reduces the bound velocity at vanishing external load. At intermediate values of F_{ext} , the numerical results for v_b and v_{eff} are larger than predicted by the PCM because the numerical force-velocity relation is less concave than the analytical one. This underestimation of the velocity has been predicted in Sec. II E and is due to the preferential unbinding of post-power-stroke motors with small strain in the presence of a distribution of internal strains. Close to the stall force, the analytical and numerical results again agree very well even for large values of

N_t .

B. Linear load

1. LTE distribution and effective reverse rate

For constant external load, the elastic energy stored in the neck linkers was symmetric against exchanging weakly-bound and post-power-stroke motors, $j \leftrightarrow i - j$. This symmetry was not affected by the value of F_{ext} , so that the LTE distribution remained strongly biased towards the post-power-stroke state for all values of a constant external load. For a linear external load, on the other hand, the elastic energy stored in the neck linkers of bound motors and in the external spring favor the weakly-bound state (see Eq. (9)). Because this contribution to the elastic energy of the ensemble increases with increasing stiffness of the external spring, the bias of the LTE distribution will shift towards the weakly-bound state for large values of k_f . This transition between post-power-stroke and weakly-bound state has been described as a possible basis for unconventional elastic behavior of muscle fibers⁵⁹.

Fig. 14 (a) plots the conditional probabilities $p(i|i)$ (all bound motors in the post-power-stroke state) and $p(0|i)$ (all bound motors in the weakly-bound state) from the LTE distribution of Eq. (5) as function of the external spring constant per bound motor, k_f/i , for the ensemble position $z = 0$ and different numbers of bound motors, i . The probabilities $p(j|i)$ for the intermediate states $0 < j < i$ are negligible due to internal strains built up by bound motors in opposite states working against each other. For small k_f/i , most bound motors are in the post-power-stroke state with $p(i|i) \lesssim 1$. At a critical value of the external spring constant, $k_f^c/i \simeq 7.5 \text{ pN nm}^{-1}$, the bias of the LTE distribution shifts rapidly from the post-power-stroke state to the weakly-bound state. The ratio k_f^c/i is independent of the number of bound motors but the transition becomes sharper with increasing i . The power stroke of a bound motor is driven by the free energy bias $E_{\text{pp}} < 0$ towards the post-power-stroke state. Thus, the transition of the LTE distribution from post-power-stroke to weakly-bound state occurs, when the increase of the elastic energy of an ensemble upon the transition of i bound motors from weakly-bound to post-power-stroke state (see Eq. (9)) exceeds the free energy gain $-jE_{\text{pp}}$ upon this transition. Solving the condition

$$\frac{ik_m k_f^c}{ik_m + k_f^c} \frac{d(2z + d)}{2} = -iE_{\text{pp}} = i|E_{\text{pp}}| \quad (56)$$

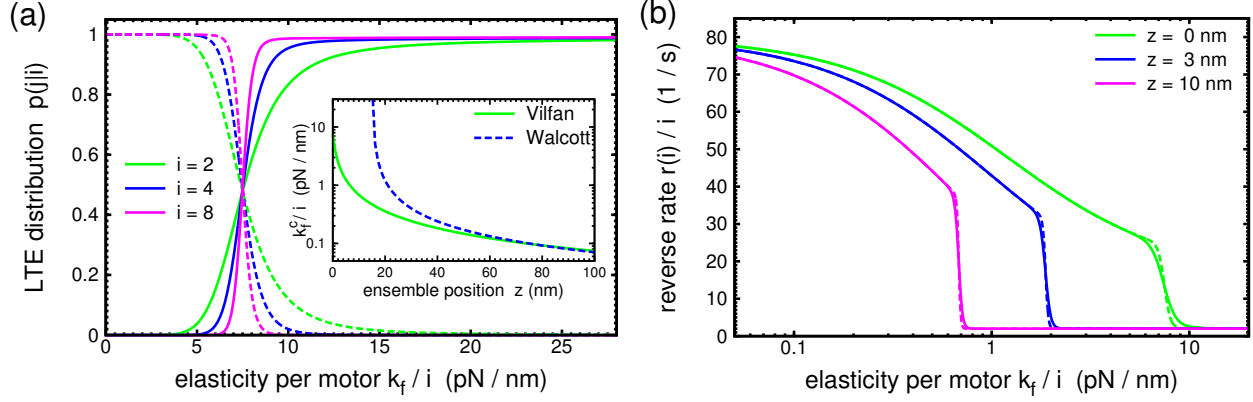


FIG. 14. Transition of LTE distribution: (a) Conditional probabilities $p(0|i)$ (solid lines) and $p(i|i)$ (dashed lines) from the LTE distribution (see Eq. (5)) as function of the external spring constant per bound motor, k_f/i , for $i = 2, 4$ and 8 bound motors and ensemble position $z = 0$. *Inset*: Critical external spring constant per motor, k_f^c/i , as function of ensemble position z . The solid curve uses the model parameters listed in Tab. I. For the dashed curve, the parameters $k_m = 0.3 \text{ pN nm}^{-1}$ and $d = 10 \text{ nm}$ were used as in Walcott et al.⁴⁶. (b) Effective reverse rate per bound motor, $r(i)/i$, (see Eq. (13)) as function of the external spring constant per bound motor, k_f/i , for $i = 4$ (dashed lines) and 8 (solid lines) bound motors and ensemble positions $z = 0 \text{ nm}, 3 \text{ nm}$ and 10 nm . Constant parameters are listed in Tab. I.

for the critical spring constant yields

$$\frac{k_f^c}{i} = k_m \left[\frac{k_m d (2z + d)}{2 |E_{pp}|} - 1 \right]^{-1}. \quad (57)$$

The ratio $k_f^c(z)/i$ is independent of i for all values of z . This is due to the parallel arrangement of the motors under the external load. The inset in Fig. 14 (a) plots $k_f^c(z)/i$ as function of z . Because $k_f \geq 0$, a finite critical elastic constant exists for all $z \geq 0$ only if $k_m d^2 > 2 |E_{pp}|$. This is the case for our model parameters listed in Tab. I. In Walcott et al.⁴⁶, the parameters $d = 10 \text{ nm}$ and $k_m = 0.3 \text{ pN nm}^{-1}$ are used to characterize the power stroke. For these values, $k_m d^2 < 2 |E_{pp}|$ so that the transition of the LTE distribution can only occur above a finite ensemble position $z \geq (|E_{pp}|/k_m d) - d/2$. The corresponding $k_f^c(z)/i$ is also plotted in the inset in Fig. 14 (a). For both parameter sets, the critical spring constant decreases as $k_f^c/i \propto z^{-1}$ for large z so that the external load $k_f^c z/i$ at the LTE transition becomes independent of z .

The LTE transition from post-power-stroke to weakly-bound state affects the binding dynamics of an ensemble quantitatively and qualitatively, because the off-rate from the weakly-bound state

is significantly smaller than the unloaded off-rate from the post-power-stroke state, $k_{10} \ll k_{20}^0$, and because k_{10} is independent of the load on a motor. Fig. 14 (b) plots the effective reverse rate divided by the number of bound motors, $r(i)/i$, as function of k_f/i for different values of i and z . For $k_f/i \rightarrow 0$, motors unbind predominantly from the post-power-stroke state ($p(i|i) \lesssim 1$) and $r(i)/i$ approaches the value of the unloaded off-rate from the post-power-stroke state, $r(i)/i \rightarrow k_{20}^0 \simeq 80 \text{ s}^{-1}$. From this limit, $r(i)/i$ decreases exponentially with k_f/i , because the load on a post-power-stroke motor increases linearly with k_f/i and k_{20} decreases exponentially under load. Below the LTE distribution, it is $r(i)/i \gg k_{10}$. Thus, the effective reverse rate decreases strongly as the LTE distribution shifts towards the weakly-bound state and approaches the off-rate from the weakly-bound state, $r(i)/i \rightarrow k_{10} \simeq 2 \text{ s}^{-1} = \text{const}$ for large $k_f > k_f^c$. The exponential decrease of $r(i)/i$ and the critical elastic constant are independent of i but the transition becomes sharper with increasing i . With increasing z , the initial exponential decrease of $r(i)/i$ becomes faster. Nevertheless, the drop of $r(i)/i$ at the LTE becomes more pronounced because the LTE transition occurs at smaller values of k_f/i , as predicted by Eq. (57).

In an ensemble with N_t molecular motors, the number i of bound motors fluctuates continuously. Because the critical elastic constant $k_f^c(z)$ is proportional to i , the LTE distribution follows the fluctuations of i and alternates between post-power-stroke state (for large i with $k_f/i < k_f^c(z)/i$) and weakly-bound state (for small i with $k_f/i > k_f^c(z)/i$) when the ensemble is in the transition region. Because the transition to the weakly-bound state occurs first for the smallest i and unbinding from the weakly-bound state is significantly slowed down, onset of the LTE distribution will stabilize the ensemble against unbinding. Furthermore, the critical elastic constant is itself a dynamic quantity, because $k_f^c(z)/i$ reduces with increasing ensemble position. Thus, for linear external load two different mechanisms can stabilize an ensemble as it moves to larger z : (i) for ensemble positions below the LTE transition, unbinding is slowed down by the catch bond character of motors in the post-power-stroke state and (ii) above the LTE transition threshold, unbinding is slowed down by the transition to the weakly-bound state. Moreover, because ensemble movement relies on the presence of motors in the post-power-stroke state, ensemble movement feeds back negatively on itself and the ensemble will stall as the LTE transition threshold is reached.

2. Stochastic trajectories

As for the case of constant external load, it is instructive to study individual stochastic trajectories in order to gain more insight into the interplay of ensemble movement and binding dynamics. The stochastic trajectories are generated using the Gillespie algorithm as described for the case of constant load. The upper panel of the stochastic trajectories, is now used to display the the external load $k_f z$, which is proportional to ensemble position but omits the strongly fluctuating contribution of the strain of the motors. The actual external load depends on the number of bound motors and their states: if all bound motors are in the post-power-stroke state, the external load is larger than $k_f z$. If all bound motors are in the weakly-bound state, the external load is smaller than $k_f z$.

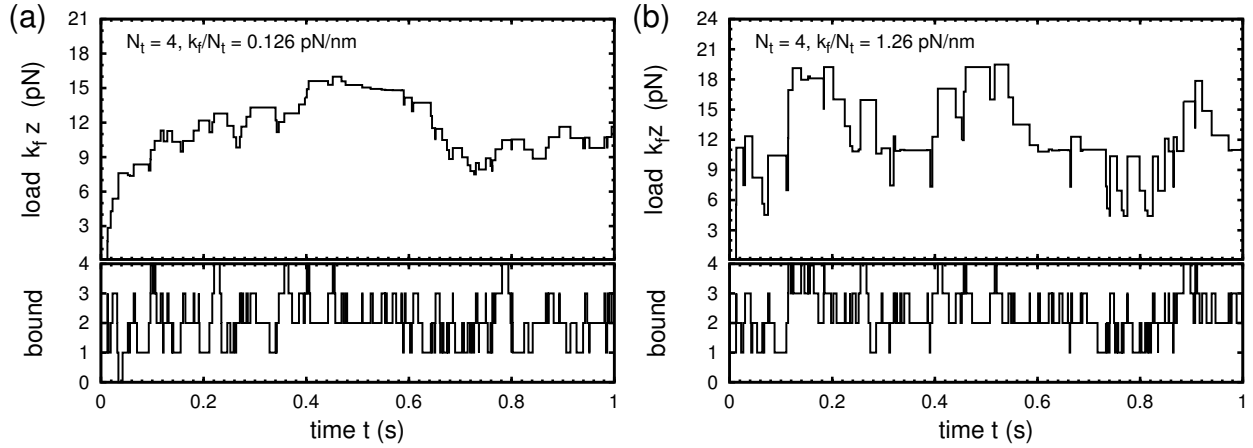


FIG. 15. Stochastic trajectories for linear external load. Elastic load $k_f z$ on the ensemble (upper panel) and number i of bound motors (lower panel) as function of time t for ensemble size $N_t = 4$ and external elastic constant per motor (a) $k_f/N_t = 0.126 \text{ pN nm}^{-1}$ and (b) $k_f/N_t = 1.26 \text{ pN nm}^{-1}$. In (a) and (b) detached ensembles are stationary with mobility $\eta = 0$. Constant parameters are listed in Tab. I.

Fig. 15 (a) shows a stochastic trajectory of an ensemble with $N_t = 4$ motors working against a linear external load with elastic constant $k_f/N_t = 0.126 \text{ pN nm}^{-1}$ ($k_f = 0.504 \text{ pN nm}^{-1}$). At $z = 0$, the ratio k_f/i is below the critical elastic constant $k_f^c/i \simeq 7.5 \text{ pN nm}^{-1}$ for all $i \geq 1$. Therefore, ensemble position initially increases gradually. During this transient movement, the ensemble occasionally detaches completely, because for all $i \geq 1$ unbinding occurs from the post-power-stroke state with large intrinsic off-rate against small external load. After the initial transient, the ensemble reaches a stationary state in which $k_f z$ fluctuates around a constant average. The typical external load $k_f z \simeq 12 \text{ pN}$ in this isometric state corresponds to the ensemble position

$z \simeq 24 \text{ nm}$. For this value of z , the critical elastic constant is lowered to $k_f^c(z)/i \simeq 0.3 \text{ pN nm}^{-1}$. With $k_f = 0.504 \text{ pN nm}^{-1}$, the LTE distribution shifts to the weakly-bound state for $i = 1$ but remains in the post-power-stroke state for $i > 1$. Due to the very slow unbinding of the last ($i = 1$) bound motor from the weakly-bound state, complete detachment of the ensemble is no longer observed in the isometric state, although i continues to fluctuate between $i = 1$ and N_t . This demonstrates the stabilization of the ensemble due to the LTE transition. On the other hand, the LTE transition for $i = 1$ also causes stalling of the ensemble and prevents movement beyond the isometric state. Assuming that all bound motors are in the post-power-stroke state, even for the largest values of z the strain x_{ij} is negative for all $i > 1$ so that the ensemble still steps forward in these states. (Although the size of the steps may be reduced due to the increased probability for weakly-bound motors in the proximity of the LTE transition). Because the ensemble can only step backwards when all bound motors are in the weakly-bound state, the ensemble alternates between forward stepping for large i (k_f/i below the threshold) and backward stepping for small i (k_f/i above the threshold). The isometric state is reached, when these two contributions balance and the ensemble fluctuates around a constant average position. Excursion to large z will shift the LTE to the weakly bound state for higher values of i and induce quick backward movement and restoring of the the isometric state. Excursions to small z , on the other hand, will shift the LTE distribution towards the post-power-stroke state for $i = 1$, thus inducing quick forward movement towards the isometric state. This stalling mechanism is different from the case of constant external load, where the LTE distribution was always in the post-power-stroke state and the stall force was determined by vanishing x_{ij} under large load. Fig. 15 (b) shows a stochastic trajectory of an ensemble with $N_t = 4$ motors working against the larger external elastic constant $k_f/N_t = 1.26 \text{ pN nm}^{-1}$. The isometric load $k_f z \simeq 12 \text{ pN}$ is comparable to the trajectory from (a). Due to the larger elastic constant, however, this corresponds to the smaller ensemble position 2.4 nm . Moreover, small fluctuations in z induce strong fluctuations of $k_f z$. The critical elastic constant for the LTE transition is $k_f^c/i \simeq 2.5 \text{ pN nm}^{-1}$. Again, the value of $k_f \simeq 5.04 \text{ pN nm}^{-1}$ is below the critical elastic constant for $i > 1$ and above for $i = 1$ so that complete detachment is prevented by the LTE transition to the weakly-bound state in the lowest bound state $i = 1$. As in (a), the strain x_{ij} of the bound motors is negative for $i > 1$ (assuming they are all in the post-power-stroke state) so that the stalling of the ensemble is caused by the LTE transition.

For the trajectories with $N_t = 4$ in Fig. 15, the LTE transition occurred only in the lowest bound state $i = 1$. For increasing N_t , more states with $i \geq 1$ undergo the LTE transition and fluctuations

of i in the isometric state are effectively restricted to values above the threshold (compare Fig. 25). For large ensembles as in Fig. 25, the alternating forward and backward motion in the isometric state displays a characteristic pattern of rapid increase of $k_f z$ concomitant with an increase of i , followed by a gradual decrease of $k_f z$ accompanied by a decrease of i . This pattern, which becomes more pronounced for larger values of the external spring constant, is reminiscent of oscillation pattern for ensembles of motors working against an elastic element⁴⁰. A Fourier analysis, however, has not shown any characteristic time scale for the fluctuations.

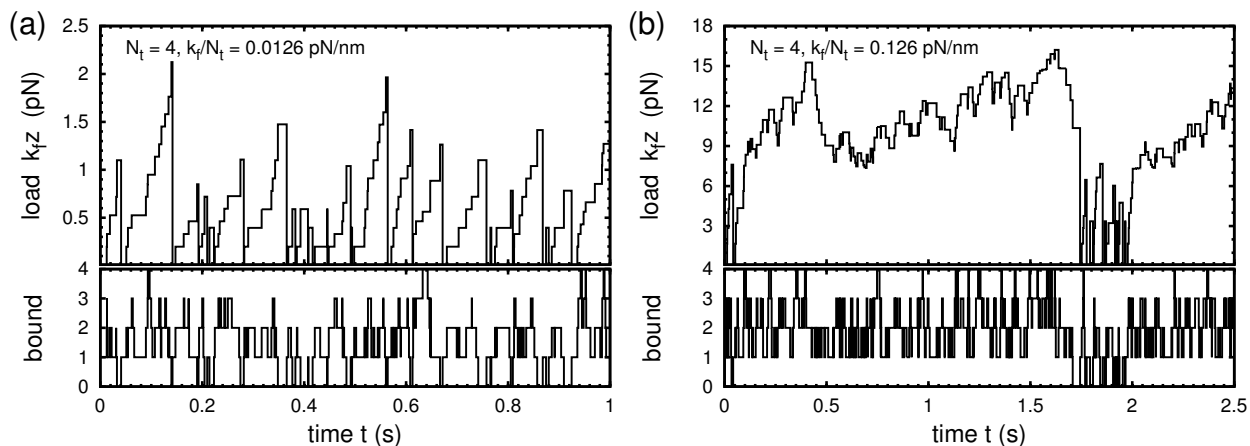


FIG. 16. Stochastic trajectories for linear external load. Elastic load $k_f z$ on the ensemble (upper panel) and number i of bound motors (lower panel) as function of time t for ensemble size $N_t = 4$ and external elastic constant per motor (a) $k_f/N_t = 0.0126 \text{ pN nm}^{-1}$ and (b) $k_f/N_t = 1.26 \text{ pN nm}^{-1}$. In (a) and (b) detached ensembles are reset to $z = 0$ with infinite mobility $\eta = \infty$. Constant parameters are listed in Tab. I.

In the above trajectories, detached ensembles are stationary with mobility $\eta = 0$. Fig. 16 demonstrates the effect of resetting an ensemble to $z = 0$ after detachment. Fig. 16 (a) shows a trajectory for $N_t = 4$ with the small external elastic constant $k_f/N_t = 0.0126 \text{ pN nm}^{-1}$. The small ensemble size and the small external elastic constant allows frequent detachment during the initial, transient movement. Because the position is reset to $z = 0$ after detachment, the ensemble cannot reach the isometric state which would stabilize the ensemble and prevent detachment. Therefore, the stochastic trajectories show a characteristic pattern of gradual linear buildup of load, followed by rapid release upon detachment. This pattern resembles trajectories observed experimentally in three bead assays^{20,32,33}, active gels^{31,34} and motility assays³⁶. Fig. 16 (b) shows a trajectory with larger external elastic constant. During the transient increase of $k_f z$, the ensemble detaches

occasionally and is reset to $z = 0$. Because the isometric ensemble position is smaller for larger k_f/N_t , the isometric state can eventually be reached. This isometric state is not affected by the movement of the detached ensemble. As observed above, complete detachment from the isometric state is rare. As detachment occurs in a rare fluctuation, however, the ensemble detaches several times on its trajectory until the isometric state is again reached.

3. Binding dynamics

To study the interplay of ensemble movement and binding dynamics, we first analyze the dependence of detachment time T_{10} on ensemble size N_t and external elastic constant k_f . Because the one-step master equation Eq. (10) cannot be solved with position dependent transition rates, the detachment time is calculated numerically by averaging the first passage time from $i = 1$ to $i = 0$ over repeated, stochastic trajectories. The trajectories all start at $z = 0$ and are terminated as soon as the ensemble detaches, so that the mobility η has no influence on the result.

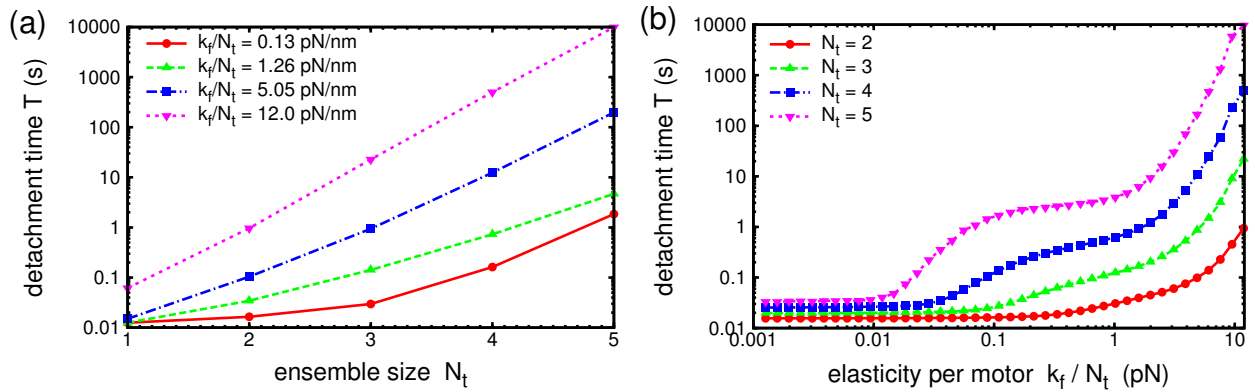


FIG. 17. Numerical results for the parallel cluster model with linear external load: average detachment time T_{10} . (a) T_{10} as function of ensemble size N_t for the values $k_f/N_t = 0.126 \text{ pN nm}^{-1}$, 1.262 pN nm^{-1} , 3.787 pN nm^{-1} and 12.0 pN nm^{-1} of the external elastic constant per motor. (b) T_{10} as function of the external elastic constant per motor k_f/N_t for ensemble sizes $N_t = 2, 3, 4$ and 5 . Constant parameters are listed in Tab. I.

Fig. 17 (a) plots simulation results for the average detachment time T_{10} of an ensemble as function of ensemble size N_t for different values of the external elastic constant k_f/N_t . The largest value of k_f/N_t is above the critical external elastic constant at $z = 0$ so that unbinding proceeds predominantly from the weakly-bound state for all values of N_t and is independent of load. Thus,

T_{10} increases approximately exponentially with increasing N_t and reaches $T_{10} \simeq 10^4$ s already for $N_t \simeq 5$. For constant load, such detachment times required external loads well beyond the stall force. For the smallest value of k_f/N_t , which is well below $k_f^c(z=0)/i$, a transient regime with a very slow increase of T_{10} is observed. Here, the average detachment time results from a combination of fast detachment from the post-power-stroke state during the transient increase of z and slow unbinding from the weakly-bound state (for small values of i) once the isometric state is reached. For sufficiently large N_t , detachment before reaching the isometric state becomes unlikely and T_{10} is determined by slow unbinding from the weakly-bound state. Thus, the increase of T_{10} with N_t becomes similar to the exponential increase observed for large k_f/N_t . For increasing values of k_f/N_t , the transient regime of slow increase of N_t becomes less pronounced and T_{10} increases exponentially for most values of N_t .

Fig. 17 (b) plots T_{10} as function of k_f/N_t for different N_t . The plot reveals three different regimes of the detachment time which corresponds to different detachment mechanisms. At very small k_f/N_t , ensembles detach during the initial increase of z . Here, unbinding of motors proceeds predominantly from the post-power-stroke state under small external load, so that the detachment time is almost independent of k_f/N_t . In an intermediate regime, the detachment time increases significantly. Here, the ensembles can reach the isometric state so that the contribution of slow unbinding from the weakly-bound state becomes more prominent. Because the ensembles adjust themselves dynamically to the isometric state, large ensembles display a plateau region with constant T_{10} . When the external elastic constant approaches the absolute threshold $k_f^c/N_t \simeq 7.5$ pN nm⁻¹ for $z = 0$, the LTE distribution shifts towards the weakly-bound state for an increasing number of states i . This increases the typical number of bound motors and the detachment time increases rapidly (see Fig. 25).

Fig. 18 (a) plots the ensemble duty ratio ρ_d as function of ensemble size N_t for different values of the external elastic constant k_f/N_t . Because the attachment time T_{01} is independent of k_f and decreases with N_t^{-1} , the dependence of ρ_d on k_f and N_t mainly reflects the corresponding dependence of T_{10} . For the largest value with $k_f/N_t > k_f^c/N_t$, the duty ratio at $N_t = 1$ is increased significantly with respect to the duty ratio of a single free motor, $\rho_d^{\text{single}} \simeq 0.33$. Due to the exponential increase of the detachment time, $\rho_d \simeq 1$ is reached already for $N_t \geq 2$. For smaller $k_f/N_t < k_f^c/N_t$, the duty ratio at $N_t = 1$ is close to the duty ratio of a single free motor. This indicates that unbinding proceeds predominantly from the post-power-stroke state. Due to the rapid increase of T_{10} with N_t , permanent attachment with $\rho_d \simeq 1$ is achieved for $N_t \geq 5$. This

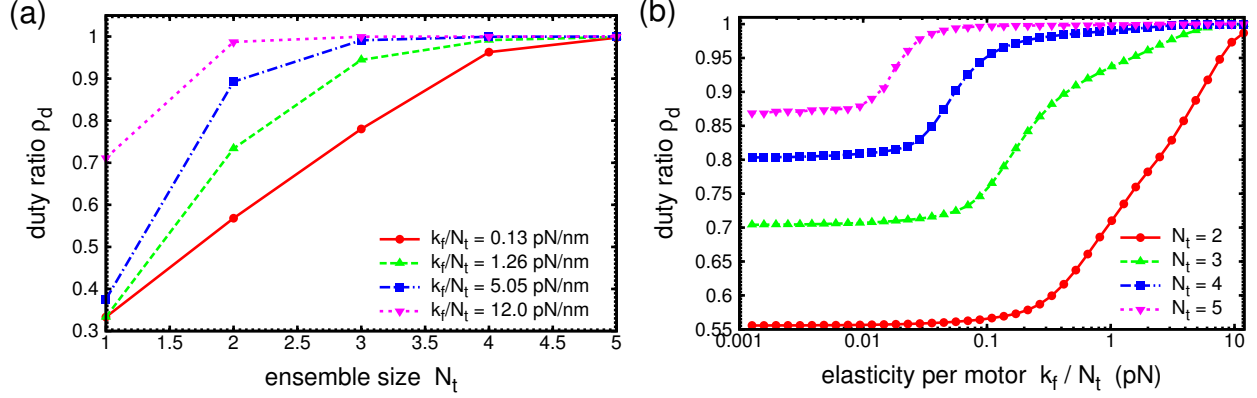


FIG. 18. Numerical results for the parallel cluster model with linear external load: ensemble duty ratio ρ_d . (a) ρ_d as function of ensemble size N_t for the values $F_{\text{ext}}/N_t = 0.13 \text{ pN nm}^{-1}$, 1.26 pN nm^{-1} , 5.05 pN nm^{-1} and 12.0 pN nm^{-1} of the external elastic constant per motor. (b) ρ_d as function of the external elastic constant per motor k_f/N_t for ensemble sizes $N_t = 2, 3, 4$ and 5 . Detached ensembles are stationary with vanishing mobility, $\eta = 0$. Constant parameters are listed in Tab. I.

is significantly smaller than the ensemble size $N_t = 15$ required for permanent attachment under constant external load. Fig. 18 (b) plots ρ_d as function of k_f/N_t for different N_t . In analogy to the detachment time, ρ_d displays two regimes: a constant duty ratio at small k_f/N_t followed by a rapid increase at intermediate values of k_f/N_t . Because $\rho_d \simeq 1$ is already reached here, the strong increase of T_{10} for $k_f/N_t \gtrsim k_f^c/N_t$ cannot be resolved.

To calculate the average number of bound motors $N_b = \langle i \rangle$, we average i over long trajectories in which the ensembles are allowed to detach from the substrate. The detached ensembles are stationary with vanishing mobility, $\eta = 0$, so that the isometric state of the ensembles is probed. Fig. 19 (a) plots the average number N_b of bound motors as function of ensemble size N_t for different values of the external elastic constant per motor k_f/N_t . For all the values of k_f/N_t the average number of bound motors increases linearly with N_t . The slope becomes steeper with increasing k_f/N_t but saturates for very large k_f/N_t . Only for small values of k_f/N_t there is a short transient with a slower increase of N_b . Fig. 19 (b) plots N_b as function of the external elastic constant per motor k_f/N_t for different values of N_t . For $k_f/N_t < k_f^c(z=0)/N_t$, the average number of bound motors is constant. Here, the ensembles adjust themselves to an isometric state at finite ensemble position $z > 0$. As the value of k_f/N_t exceeds the critical values $k_f^c(z=0)/N_t$, the average number of bound motors increases steeply. Here, the LTE transition to the weakly-bound

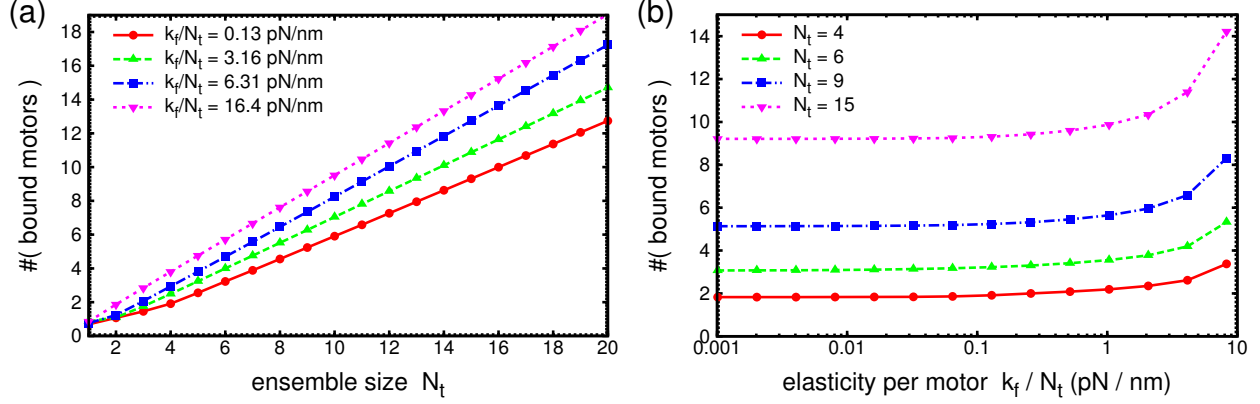


FIG. 19. (a) Numerical results for the parallel cluster model with linear external load: average number N_b of bound motors. (a) N_b as function of ensemble size N_t for the values $k_f/N_t = 0.13 \text{ pN nm}^{-1}$, 3.16 pN nm^{-1} , 6.31 pN nm^{-1} and 16.4 pN nm^{-1} of the external elastic constant per motor. (b) N_b as function of external elastic constant per motor k_f/N_t for the ensemble sizes $N_t = 4, 6, 9$ and 15 . Detached ensembles at stationary with $\eta = 0$. Constant parameters are listed in Tab. I.

state occurs already at $z = 0$ and for an increasing number of states i (see Fig. 25).

4. Average external load

For linear external load, analogous to the force-velocity relation as a characteristic for the dynamic properties of an ensemble under constant external load, is the average external load $\langle F_{\text{ext}} \rangle = \langle k_f z \rangle$ of the ensemble in the stationary state. As explained in the context of the stochastic trajectories, this quantity differs from the actual load in the external elastic element by leaving out the strain x_{ij} of the motors.

As for the average number of bound motors, the average external load is determined by averaging over long trajectories with multiple unbinding events. In Fig. 20, the detached ensembles are stationary with mobility $\eta = 0$, so that the average load in the isometric state is probed. Fig. 20 (a) plots the average external load $\langle F_{\text{ext}} \rangle$ in the stationary state of an ensemble as function of ensemble size N_t for different values of the external elastic constant per motor, k_f/N_t . Below the critical value for the LTE transition, $k_f/N_t < k_f^c/N_t$, the average external load increases with N_t . For very small external elastic constants, $k_f/N_t < 1 \text{ pN nm}^{-1}$, the curves are almost identical for different k_f , but begin to decrease for $k_f/N_t > 1 \text{ pN nm}^{-1}$. This decrease of $\langle F_{\text{ext}} \rangle$ for given N_t is observed

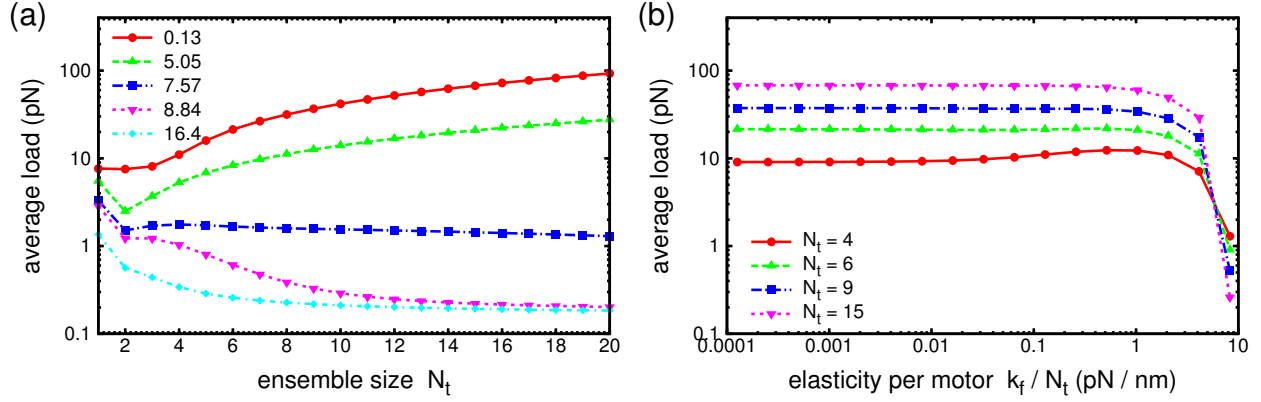


FIG. 20. Numerical results for the parallel cluster model with linear external load: average external load $\langle F_{\text{ext}} \rangle$ for $\eta = 0$. (a) $\langle F_{\text{ext}} \rangle$ as function of ensemble size N_t for values $k_f/N_t = 0.13 \text{ pN nm}^{-1}$, 5.05 pN nm^{-1} , 7.57 pN nm^{-1} , 8.84 pN nm^{-1} and 16.4 pN nm^{-1} of the external elastic constant per motor. (b) $\langle F_{\text{ext}} \rangle$ as function of external elastic constant per motor k_f/N_t for ensemble size $N_t = 4, 6, 9$ and 15 . Constant parameters are listed in Tab. I.

in the trajectories of Fig. 25. At the critical external elastic constant, $k_f/N_t \simeq k_f^c/N_t$, the average external load is independent of N_t . Above the critical threshold, the LTE transition towards the weakly-bound state occurs already at $z = 0$ so that ensemble movement is severely reduced. Here, $\langle F_{\text{ext}} \rangle$ decreases with increasing N_t . Fig. 20 (b) plots the average external load as function of k_f/N_t for different N_t . For small $k_f/N_t < k_f^c/N_t$, the average external load is independent of k_f/N_t . Close to the critical value, $\langle F_{\text{ext}} \rangle$ breaks down because ensemble movement is effectively impossible.

Fig. 21 (a) plots the average external load as function of ensemble size N_t for different values of k_f/N_t for the case that the ensemble is reset to its initial position $z = 0$ after complete detachment. This corresponds to the limit of large mobility $\eta \rightarrow \infty$. The values of k_f/N_t are below the critical value $k_f^c(z = 0)/N_t$ and from a range in which $\langle F_{\text{ext}} \rangle$ at $\eta = 0$ was independent of k_f/N_t . For small external elastic constant, the isometric state corresponds to a large ensemble position z . Therefore, ensembles detach frequently during the long transient movement towards the isometric state. Because detached ensembles are reset to $z = 0$, this reduces the average external load, as observed in Fig. 16 (a). Because detachment becomes less likely with increasing N_t and ensembles are stabilized in the isometric state, $\langle F_{\text{ext}} \rangle$ increases with N_t and eventually jumps discontinuously to the average load for $\eta = 0$. With increasing k_f/N_t , the average external load grows in proportion to k_f/N_t at given N_t . This means that the movement of the ensemble during the initial transient

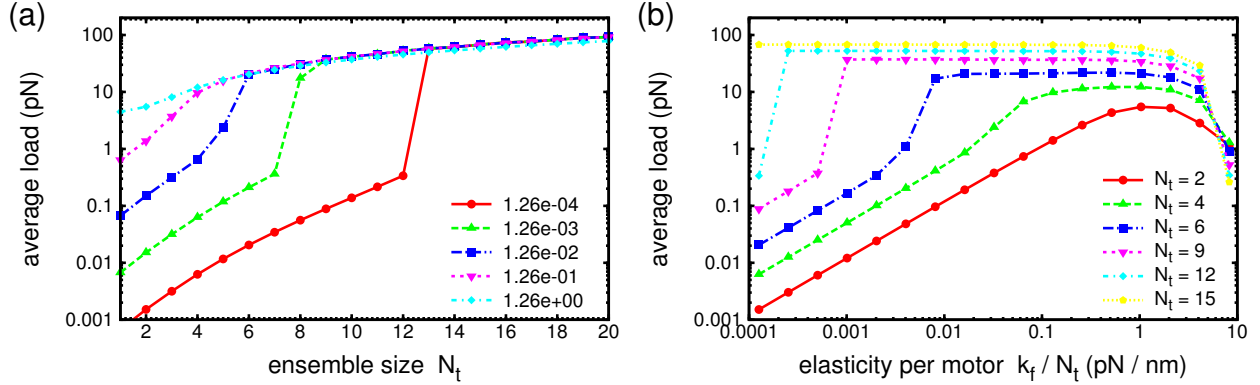


FIG. 21. Numerical results for the parallel cluster model with linear external load: average isometric load $\langle F_{\text{ext}} \rangle$ for $\eta \rightarrow \infty$. (a) $\langle F_{\text{ext}} \rangle$ as function of ensemble size N_t for values $k_f/N_t = 1.26 \times 10^{-4}$ pN nm $^{-1}$, 0.00126 pN nm $^{-1}$, 0.0126 pN nm $^{-1}$, 0.126 pN nm $^{-1}$ and 1.26 pN nm $^{-1}$. (b) $\langle F_{\text{ext}} \rangle$ as function of external elastic constant per motor k_f/N_t for ensemble size $N_t = 4, 6, 9$ and 15 . Constant parameters are listed in Tab. I.

is hardly affected by the small external load. Because the isometric state corresponds to smaller ensemble position z , however, the discontinuous jump to the curve for $\eta = 0$ occurs at smaller values of N_t and becomes less pronounced. Fig. 21 (b) plots the average external load for $\eta \rightarrow \infty$ as function of k_f/N_t for different N_t . For small k_f/N_t , $\langle F_{\text{ext}} \rangle$ increases linearly towards the average isometric load. For larger N_t , $\langle F_{\text{ext}} \rangle$ for given k_f/N_t increases and jumps discontinuously towards isometric load. The discontinuity becomes more pronounced with increasing N_t and the position of the jump decreases.

IV. DISCUSSION AND SUMMARY

In this paper we have introduced and analyzed a stochastic model for ensembles of non-processive motors such as myosin II working against an external load. The model allows us to investigate in detail the effect of a finite number of motors in an ensemble, most importantly the stochastic binding dynamics of the motors. Introducing the parallel cluster model and using the local thermal equilibrium approximation allowed us to reduce the complexity of the model significantly, eventually leading to efficient numerical simulations and analytical results for stationary properties. In detail, we have analyzed two paradigmatic situations in which the motor-ensemble works against either a constant or a linear external load. Both situations are highly relevant for a

large class of experiments.

For constant external load, our results for large ensemble sizes are in good qualitative agreement with previous model results for large assemblies of myosin II^{19,44}. Due to the local thermal equilibrium assumption, however, our model is not able to describe, e.g., the synchronization of motors under large external load which is due to the kinetic hindrance of the power stroke. Average quantities, however, are well represented. In particular the force-velocity relation of an ensemble follows the characteristic concave shape which is described by a Hill relation and is found experimentally for muscle fibers⁵⁵ as well as for small ensembles of myosin II⁴⁶. The parallel cluster model makes it easy to identify the relevant quantities determining the force-velocity curve. In particular the role of the load-sensitivity of unbinding from the post-power-stroke state and the increase of the number of bound motors under load for the adaption of the dynamic range of an ensemble becomes clear. Due to the strong bias of the LTE distribution towards the post-power-stroke state, myosin II as a whole behaves as a catch bond for the whole range of constant external load considered in this manuscript. This induces the increase of the number of bound motors under load, which is the basis for the concave shape of the force-velocity relation. At small external load, a small number of bound motors is able to work against the external load and the large number of unbound motors generates fast ensemble movement with little resistance from the bound motors. At large external load, on the other hand, the increase of the number of bound motors allows to increase the stall force of the ensemble relative to the case of a constant number of bound motors. Thus, the mechanosensitive response of myosin II to a constant external load greatly increases the dynamic range over which myosin II ensembles can operate and the robustness of ensemble movement. As demonstrated in Appendix B 1, the apparent load-sensitivity of myosin II becomes stronger for small duty ratios, for which a stronger increase of the number of bound motors is observed. The relevance of this mechanism of mechanosensitivity for the efficiency of motor ensembles is underlined by the experimental observation of the increase of the number of bound motors in muscle filaments which use myosin II¹⁴ and the recent identification of a similar load-sensitive step in myosin I⁶⁰. This last result indicates that the mechanisms described here might have wider applications. In addition to reproducing previous results for large ensembles, our model in particular allows to identify the range of ensemble sizes in which stochastic detachment of ensembles is relevant and reduces the efficiency of ensembles. As demonstrated in Appendix B, this range depends strongly on the duty ratio of the single motor. The smaller the single motor duty ratio, the larger is the number of motors in an ensemble that is needed to ensure practically permanent

attachment. For the model parameters used in the main part of the manuscript, the single motor duty ratio is similar but slightly larger than reported for non-muscle myosin II³¹. Here, it turns out that roughly $N_t = 15$ motors are needed for almost permanent attachment. This number is in the range of the size of minifilaments, in particular if one considers that due to spatial restrictions, not all motors which are contained in a minifilament can actually bind to a substrate at the same time. Thus, unbinding will be relevant for cytoskeletal myosin II minifilaments. Interestingly, due to the load-sensitivity of myosin II minifilaments, detachment of the ensembles will occur most frequently for ensemble under small load whereas ensembles working against large external load are stabilized by the catch bond character of myosin II so that they can form efficient crosslinkers of actin fibers.

For linear external load, it has been shown that the load-sensitivity of the unbinding step is less relevant for the behavior of a motor ensemble. Rather, the reverse transition from the post-power-stroke state to the weakly-bound state, which is induced by the stiffness of the external spring or by large external load, eventually stalls the ensemble in the isometric state. As long as the stiffness of the external spring is below the critical threshold, ensembles can move forward until the isometric state is reached. Because ensembles adapt their position dynamically towards the isometric state, characteristic dynamic properties such as the detachment time or the typical number of bound motors in the isometric state are independent of the external elastic constant state and increases significantly only when the critical stiffness is reached. Thus, measuring the change of the number of bound motors with the stiffness of the external force is a characteristic sign of the relative size of the unbinding rates from the different bound states of the motors. The critical value of k_f above which ensemble are no longer able to generate force allows to determine the free energy bias towards the post-power-stroke state. The qualitative change of behavior of the ensemble should allow to observe this experimentally even in noisy data, e.g. in extensions of the three bead assay with better control over the number of motors. Typical stochastic trajectories reveal a behavior which is qualitatively similar to previously predicted or experimentally observed types of behavior. For relatively large ensembles which do not unbind, a sort of irregular oscillation pattern has been observed, similar to the oscillation predicted using a ratchet model for large ensembles of motors⁴⁰. The linear increase of stress followed by a fast stress relaxation which is observed in three bead assays³² and in active gels³⁴ has been reproduced for the case that unbinding from the substrate occurs before the ensemble reaches its equilibrium position.

The sequence of reaction in our basic crossbridge model is compatible with experiments^{20,48}.

Compared to other models, we have neglected one additional post-power-stroke state, which will be important for detailed descriptions of the force-velocity relation in skeletal muscle¹⁹ or inclusion of the ATP dependence of the motor cycle⁴⁶. The ATP dependence, however, could also be included in our model via an ATP dependent off-rate from the post-power-stroke state. On the other hand, our model explicitly includes the weakly-bound state (or pre-power-stroke state) as a load bearing state, which is omitted by Walcott et al.⁴⁶. Because for constant external load, the weakly-bound state is hardly occupied so that motors bind effectively directly to the post-power-stroke state as in Walcott et al.⁴⁶. For linear external load, however, the isometric state of the ensemble is determined by the transition from the post-power-stroke to the weakly-bound state, which could not be described without a model for the power stroke. Without the weakly-bound state, which is stable under load, this transition would destabilize the ensemble instead of stabilizing it. The choice of the set of parameters used in our model was motivated by previous modeling approaches and did not aim at a description of a specific molecular motor. However, the basic conclusions of the model do not depend on the exact choice of parameters. The only prerequisite for the application of the model is that transitions between the bound states are fast so that the local thermal equilibrium can establish. Comparison with simulations without PCM or LTE have shown that this requires a forward rate k_{12} for the power stroke which is faster than the off-rate k_{10} from the weakly-bound state. Thus, our model can be used with different choices of parameters. This is demonstrated in Appendix B for different choices of the single motor duty ratio. The discussion of the result has demonstrated the dependence of experimentally measurable quantities such as the number of bound motors, the load free velocity or the stall force on the model parameters so that the parameters can be adapted to describe a desired behavior of the motor ensemble.

Ensembles of non-processive motors behave very similarly to processive motors with a specific force-velocity relation and a typical walk length. The analytical expressions allow to integrate such ensembles in larger systems in a similar manner as it has been done for processive motors^{9,11}. In such a systems, ensembles of ensembles would be multiply coupled either in series or in parallel through forces that they generate. Such model could be used to describe, e.g. tension generation in a stress fibers or the cell actin cortex. Since the relaxation to the stationary values is relatively fast, slow external stimuli, changing for example the motor activity, could be included to mimic signaling events which a cell experiences, e.g. during cell migration.

REFERENCES

- ¹R. Lipowsky and S. Klumpp, *Physica A* **352**, 53 (2005).
- ²J. Howard, *Nature* **389**, 561 (1997).
- ³R. D. Vale and R. A. Milligan, *Science* **288**, 88 (2000).
- ⁴T. Guérin, J. Prost, P. Martin, and J.-F. Joanny, *Curr. Opin. Cell Biol.* **22**, 14 (2010).
- ⁵R. D. Vale, *Cell* **112**, 467 (2003).
- ⁶K. Svoboda, C. F. Schmidt, B. J. Schnapp, and S. M. Block, *Nature (London)* **365**, 721 (1993).
- ⁷R. D. Vale, T. Funatsu, D. W. Pierce, L. Romberg, Y. Harada, and T. Yanagida, *Nature (London)* **380**, 451 (1996).
- ⁸A. Ashkin, K. Schütze, J. M. Dziedzic, U. Euteneuer, and M. Schliwa, *Nature (London)* **348**, 346 (1990).
- ⁹S. Klumpp and R. Lipowsky, *Proc. Natl. Acad. Sci. U.S.A.* **102**, 17284 (2005).
- ¹⁰Y. Chai, R. Lipowsky, and S. Klumpp, *Journal of Statistical Physics* **135**, 241 (2009).
- ¹¹G. Koster, M. van Guijn, B. Hofs, and M. Dogterom, *Proc. Natl. Acad. Sci. U.S.A.* **100**, 15583 (2003).
- ¹²C. Leduc, O. Campás, K. B. Zeldovich, A. Roux, P. Jolimaitre, L. Bourel-Bonnet, B. Goud, J.-F. Joanny, P. Bassereau, and J. Prost, *Proc. Natl. Acad. Sci. U.S.A.* **101**, 17096 (2004).
- ¹³T. A. McMahon, *Muscles, Reflexes, and Locomotion* (Princeton University Press, Princeton, New Jersey, 1984).
- ¹⁴G. Piazzesi, M. Reconditi, M. Linari, L. Lucii, P. Bianco, E. Brunello, V. Decostre, A. Stewart, D. B. Gore, T. C. Irving, M. Irving, V. Lombardi, *Cell* **131**, 784 (2007).
- ¹⁵A. F. Huxley, *Prog. Biophys.* **7**, 255 (1957).
- ¹⁶A. F. Huxley and R. M. Simmons, *Nature* **233**, 533 (1971).
- ¹⁷M. A. Geeves and K. C. Holmes, *Adv. Protein Chem.* **71**, 161 (2005).
- ¹⁸S. Leibler and D. A. Huse, *J. Cell Biol.* **121**, 1357 (1993).
- ¹⁹T. A. J. Duke, *Proc. Natl. Acad. Sci. U.S.A.* **96**, 2770 (1999).
- ²⁰C. Veigel, J. E. Molloy, S. Schmitz, and J. Kendrick-Jones, *Nature Cell Biology* **5**, 980 (2003).
- ²¹B. Guo and W. H. Guilford, *Proc. Natl. Acad. Sci. U.S.A.* **103**, 9844 (2006).
- ²²M. Vicente-Manzanares, X. Ma, R. S. Adelstein, and A. R. Horwitz, *Nature Reviews Molecular Cell Biology* **10**, 778 (2009).
- ²³S. L. Gupton and C. M. Waterman-Storer, *Cell* **125**, 1361 (2006).

- ²⁴T. Wakatsuki, R. B. Wysolmerski, and E. L. Elson, *J. Cell Sci.* **116**, 1617 (2003).
- ²⁵E. Paluch, M. Piel, J. Prost, M. Bornens, and C. Sykes, *Biophysical Journal* **89**, 724 (2005).
- ²⁶S. Pellegrin and H. Mellor, *J. Cell Sci.* **120**, 3491 (2007).
- ²⁷L. J. Peterson, Z. Rajfur, A. S. Maddox, C. D. Freel, Y. Chen, M. Edlund, C. Otey, and K. Burridge, *Molecular Biology of the Cell* **15**, 3497 (2004).
- ²⁸A. B. Verkhovsky and G. G. Borisy, *J. Cell Biol.* **123**, 637 (1993).
- ²⁹T. Thoresen, M. Lenz, and M. L. Gardel, *Biophysical Journal* **100**, 2698 (2011).
- ³⁰T. Thoresen, M. Lenz, and M. L. Gardel, *Biophysical Journal* **104**, 655 (2013).
- ³¹M. Soares e Silva, M. Depken, B. Stuhmann, M. Korsten, F. C. MacKintosh, and G. H. Koenderink, *Proc. Natl. Acad. Sci. U.S.A.* **108**, 9408 (2011).
- ³²J. T. Finer, R. M. Simmons, and J. A. Spudich, *Nature* **368**, 113 (1994).
- ³³E. P. Debold, J. B. Patlak, and D. M. Warshaw, *Biophysical Journal* **89**, L34 (2005).
- ³⁴D. Mizuno, C. Tardin, C. F. Schmidt, and F. C. MacKintosh, *Science* **315**, 370 (2007).
- ³⁵T. Duke, T. E. Holy, and S. Leibler, *Phys. Rev. Lett.* **74**, 330 (1995).
- ³⁶P.-Y. Plaçais, M. Balland, T. Guérin, J.-F. Joanny, and P. Martin, *Phys. Rev. Lett.* **103**, 158102 (2009).
- ³⁷D. Hexner and Y. Kafri, *Phys. Biol.* **6**, 036016 (2009).
- ³⁸T. Erdmann and U. S. Schwarz, *Phys. Rev. Lett.* **108**, 188101 (2012).
- ³⁹F. Jülicher and J. Prost, *Phys. Rev. Lett.* **75**, 2618 (1995).
- ⁴⁰F. Jülicher and J. Prost, *Phys. Rev. Lett.* **78**, 4510 (1997).
- ⁴¹M. Badoual, F. Jülicher, and J. Prost, *Proceedings of the National Academy of Sciences of the United States of America* **99**, 6696 (2002).
- ⁴²A. Vilfan, E. Frey, and F. Schwabl, *EPL (Europhysics Letters)* **45**, 283 (1999).
- ⁴³A. Vilfan and E. Frey, *Journal of Physics: Condensed Matter* **17**, S3901 (2005).
- ⁴⁴T. Duke, *Phil. Trans. Roy. Soc. Lond. B* **355**, 529 (2000).
- ⁴⁵A. Vilfan and T. Duke, *Biophysical Journal* **85**, 818 (2003).
- ⁴⁶S. Walcott, D. M. Warshaw, and E. P. Debold, *Biophysical Journal* **103**, 501 (2012).
- ⁴⁷B. Chen and H. Gao, *Biophysical Journal* **101**, 396 (2011).
- ⁴⁸J. R. Sellers and C. Veigel, *Nature Structural and Molecular Biology* **17**, 590 (2010).
- ⁴⁹B. Colombini, M. A. Bagni, G. Romano, and G. Cecchi, *Proc. Natl. Acad. Sci. U.S.A.* **104**, 9284 (2007).
- ⁵⁰T. Erdmann and U. S. Schwarz, *Phys. Rev. Lett.* **92**, 108102 (2004).

- ⁵¹T. Erdmann and U. S. Schwarz, *J. Chem. Phys.* **121**, 8997 (2004).
- ⁵²T. Erdmann and U. S. Schwarz, *Biophysical Journal* **91**, L60 (2006).
- ⁵³N. G. van Kampen, *Stochastic Processes in Physics and Chemistry* (Elsevier Ltd, Amsterdam, 2003).
- ⁵⁴D. T. Gillespie, *J. Chem. Phys.* **22**, 403 (1976).
- ⁵⁵A. V. Hill, *Proc. R. Soc. Lond. B* **127**, 434 (1939).
- ⁵⁶F. Berger, C. Keller, S. Klumpp, and R. Lipowsky, *Phys. Rev. Lett.* **108**, 208101 (2012).
- ⁵⁷A. Kunwar and A. Mogilner, *Phys. Biol.* **7**, 016012 (2010).
- ⁵⁸See Supplementary Material Document No. _____ for additional results with the same set of parameters as used in the main text and further results demonstrating the effect of changing the parameter values, in particular the single motor duty ratio. For information on Supplementary Material, see <http://www.aip.org/pubservs/epaps.html>.
- ⁵⁹M. Caruel, J. M. Allain, and L. Truskinovsky, *Physical Review Letters* **110**, 248103 (2013).
- ⁶⁰J. M. Laakso, J. H. Lewis, H. Shuman, and E. M. Ostap, *Science* **321**, 133 (2008).

Appendix A: Supplemental results for standard parameters

1. Constant load

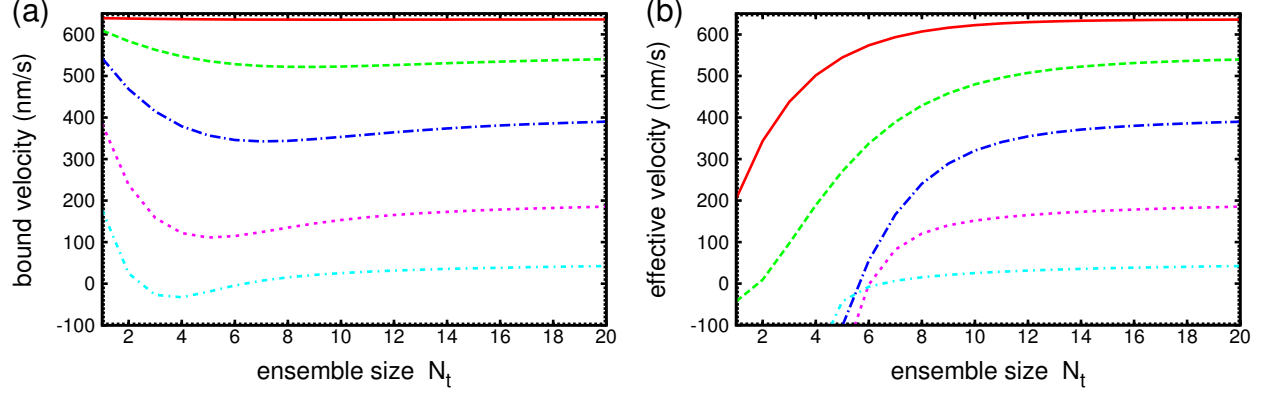


FIG. 22. Analytical results for the parallel cluster model with constant external load. (a) Bound velocity v_b and (b) effective velocity v_{eff} as function of ensemble size N_t for values $F_{\text{ext}}/N_t = 0.0126$ pN, 1.262 pN, 3.787 pN and 8.835 pN (top to bottom curves) of the external load per motor. For v_{eff} the viscous mobility of detached ensembles is $\eta = 10^3$ nm pN $^{-1}$ s $^{-1}$. Constant parameters are listed in Tab. I of the main text.

Fig. 22 (a) plots the bound velocity v_b as function of ensemble size N_t for different values of the external load per motor F_{ext}/N_t . For finite external load, v_b varies markedly only at small N_t but approaches a constant value for large N_t . The variation is non-monotonic at large external loads and the bound velocity can be negative for intermediate values of N_t . Fig. 22 (b) plots the effective velocity v_{eff} as function of N_t for different F_{ext}/N_t . For all values of the force, v_{eff} increases quickly at small N_t and approaches constant for $N_t \geq 15$.

2. Validation of the parallel cluster model: Kramers' type off-rate

In the simulations for the validation of the parallel cluster model, we have used an off-rate from the post-power-stroke state which decreases for negative strain but remained constant for positive strain of the motor (see Eq. (55)). Here, we demonstrate the effect of a Kramers' type off-rate

$$k_{20}(\xi_n) = k_{20}^0 \exp(-k_t \xi_n), \quad (\text{A1})$$

for all values of the strain ξ_n on the dynamics of the ensemble. Because within the PCM, the strain of the post-power-stroke motors is always positive, the behavior of $k_{20}(\xi_n)$ for $\xi_n > 0$ is not

relevant for the PCM.

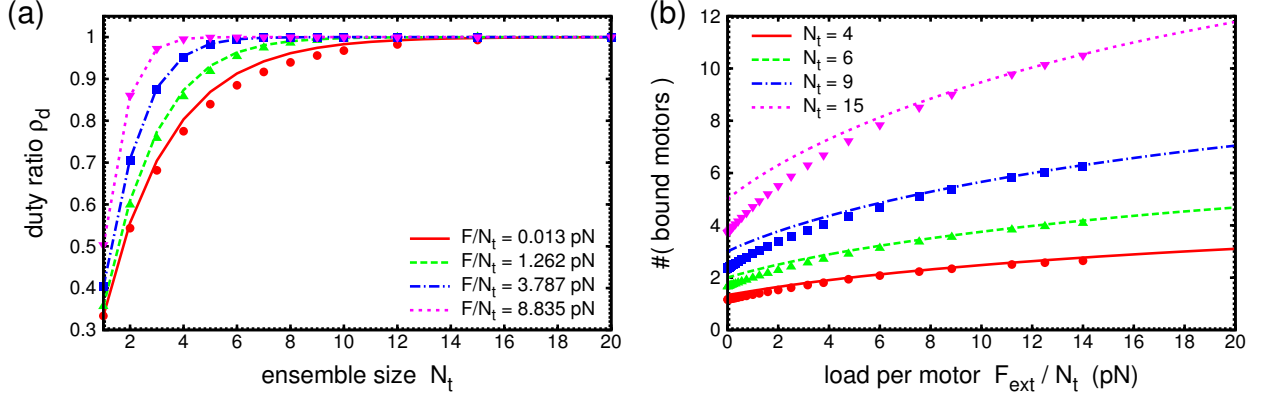


FIG. 23. Validation of the parallel cluster model: comparison of analytical results using the PCM (lines) with computer simulations with individual motor strains (symbols). (a) Duty ratio ρ_d as function of ensemble size N_t for the values $F_{\text{ext}}/N_t = 0.0126$ pN, 1.262 pN, 3.787 pN and 8.835 pN of the external load per motor. (b) Average number of bound motors N_b as function of external load per motor F_{ext}/N_t for ensemble sizes $N_t = 4, 6, 9$ and 15. Constant parameters are listed in Tab. I.

Fig. 23 (a) compares analytical results for the average number of bound motors as function of ensemble size for different values of the constant external load F_{ext}/N_t to results of simulations without PCM or LTE with the off-rate from Eq. (A1) from the post-power-stroke state. While the average number of bound motors with the asymmetric off-rate from Eq. (55) was increased, the Kramers' type off-rate from Eq. (A1) leads to a clearly reduced number of bound motors at small values of the external load. This is confirmed by Fig. 23 (b) which plots N_b as function of F_{ext}/N_t for different values of N_t . At small F_{ext}/N_t , N_b is reduced in comparison to the results from the PCM. This decrease is caused by the internal strains of motors at different positions which are working against each other. For the rate in Eq. (55), this induced an increase of N_b compared to the PCM. For the Kramers' type rate in Eq. (A1), the increase of the off-rate for negative strain dominates so that N_b is reduced. For large external load, most motors are subject to negative strain so that the effect of the internal strains is mitigated.

Fig. 24 plots the bound velocity in (a) and the effective velocity in (b) as function of the constant external load F_{ext} . Due to the smaller number of bound motors at small values of the external load, the bound velocity as well as the effective velocity are strongly increased in comparison with the results from the PCM. Because the effect of the internal strains becomes negligible for large

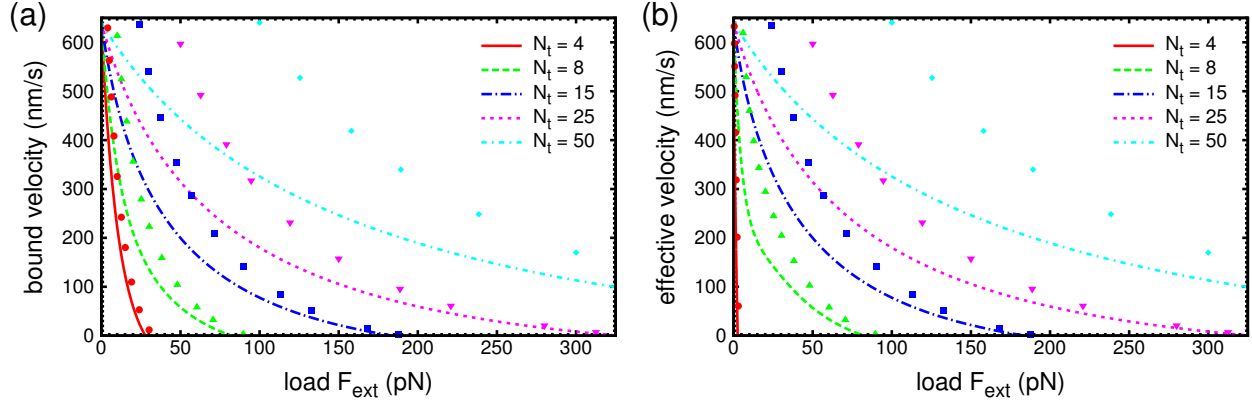


FIG. 24. Validation of the parallel cluster model: comparison of analytical results using the PCM (lines) with computer simulations with individual motor strains (symbols). Analytical results for the parallel cluster model with constant external load. (a) Average bound velocity v_b and (b) average effective velocity v_{eff} as function of the external load per motor F_{ext}/N_t for ensemble sizes $N_t = 4, 8, 15, 25$ and 50 . The mobility of the free ensemble entering v_{eff} is $\eta = 10^3 \text{ nm pN}^{-1} \text{ s}^{-1}$. Constant parameters are listed in Tab. I.

external load, the stall force is unchanged by the different choice of the off-rate.

3. Linear load

Fig. 25 (a) shows a trajectory for an ensemble with $N_t = 15$ motors working against the external elastic constant $k_f/N_t = 1.26 \text{ pN nm}^{-1}$ (that is $k_f = 18.9 \text{ pN nm}^{-1}$). For such a large ensemble size, detachment is irrelevant even for $z = 0$. Due to the large external elastic constant, the transient towards the isometric state is very short. The typical load $k_f z \simeq 60 \text{ pN}$ in the isometric state corresponds to the ensemble position $z \simeq 3.2 \text{ nm}$ and the critical elastic constant $k_f^c/i \simeq 2 \text{ pN nm}^{-1}$. For $k_f = 18.9 \text{ pN nm}^{-1}$, the LTE distribution shifts towards the weakly-bound state for $i \leq 9$ so that only states with $i > 9$ can contribute to ensemble movement. Because of the slow unbinding from the weakly-bound state, values of $i \leq 9$ are only observed when z fluctuates to values below $z \simeq 3.2 \text{ nm}$. Fig. 25 (b) shows a trajectory for $N_t = 15$ with $k_f/N_t = 5.05 \text{ pN nm}^{-1}$ (that is $k_f = 75.8 \text{ pN nm}^{-1}$). Even for $i = N_t$, this k_f is close to the critical elastic constant for $z = 0$ and the load in the isometric state is significantly reduced in comparison to (a). The typical value of $k_f z \simeq 19 \text{ pN}$ corresponds to an ensemble position $z \simeq 0.25 \text{ nm}$ for which the critical elastic constant for the LTE transition is $k_f^c/i \simeq 6 \text{ pN nm}^{-1}$. Therefore, the LTE distribution

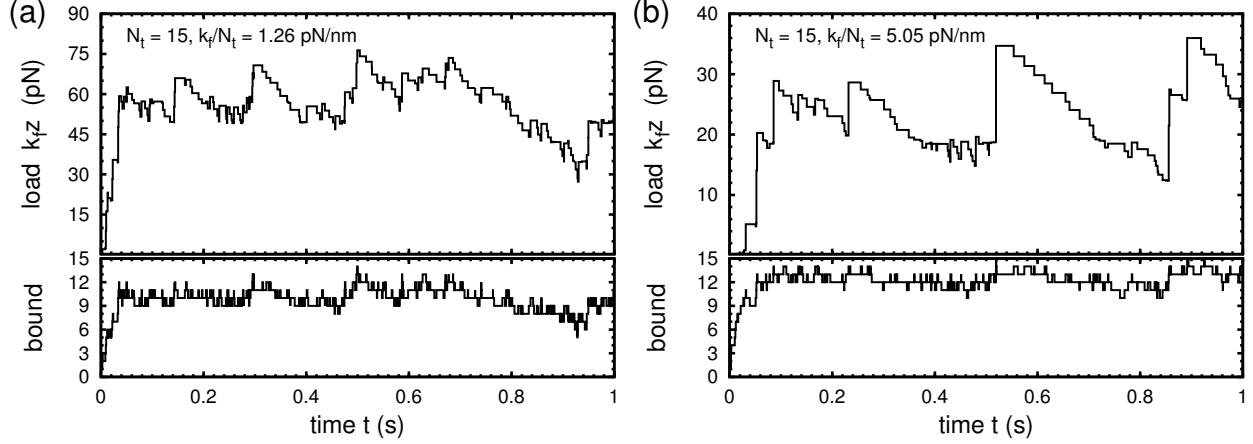


FIG. 25. Stochastic trajectories for linear external load. External load $k_f z$ on the ensemble (upper panel) and number i of bound motors (lower panel) as function of time t for ensemble size $N_t = 15$ and external elastic constant per motor (a) $k_f/N_t = 1.26 \text{ pN nm}^{-1}$ and (b) $k_f/N_t = 5.05 \text{ pN nm}^{-1}$. In (a) and (b) detached ensembles are stationary with mobility $\eta = 0$. Constant parameters are listed in Tab. I.

shifts towards the weakly-bound state for $i \leq 12$. Because unbinding is slowed down for a larger number of states, the typical number of bound motors increases relative to (a). The isometric load, on the other hand, reduces because only a few states with $i > 12$ can contribute to the forward movement. For the large ensemble sizes shown in Fig. 25, the alternating forward and backward motion in the isometric state displays a characteristic pattern of rapid increase of $k_f z$ concomitant with an increase of i , followed by a gradual decrease of $k_f z$ accompanied by a decrease of i . This pattern, which becomes more pronounced for larger values of the external elastic constant, is reminiscent of oscillation pattern for ensembles of motors working against an elastic element⁴⁰. A Fourier analysis, however, has not shown any characteristic time scale for the fluctuations.

Fig. 26 plots two trajectories for ensembles with finite mobility $\eta = 10^3 \text{ nm pN}^{-1} \text{ s}^{-1}$. The other parameters are as in Fig. 16 of the main text. For a small filament stiffness, the detached ensemble is usually rescued before $z = 0$ is reached. The typical external load is thus larger than for $\eta \rightarrow \infty$ but still smaller than the isometric load. For a larger external elastic constant, the trajectory is identical to the one for $\eta \rightarrow \infty$ because the backsteps are large and reset the ensemble to $z = 0$.

Fig. 27 compares the dependence of the average external load on ensemble size N_t and external elastic constant k_f/N_t for finite mobility $\eta = 10^3 \text{ nm pN}^{-1} \text{ s}^{-1}$ to the limits $\eta = 0$ and $\eta \rightarrow \infty$. As

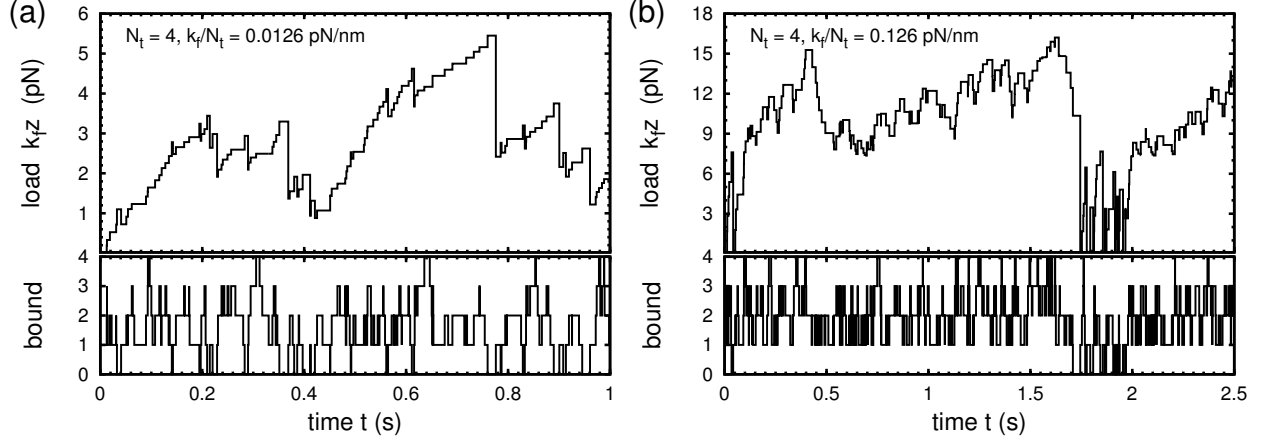


FIG. 26. Stochastic trajectories for linear external load. Elastic load $k_f z$ on the ensemble (upper panel) and number i of bound motors (lower panel) as function of time t for ensemble size $N_t = 4$ and external elastic constant per motor (a) $k_f/N_t = 0.126 \text{ pN nm}^{-1}$ and (b) $k_f/N_t = 1.26 \text{ pN nm}^{-1}$. In (a) and (b) detached ensembles slide backwards with mobility $\eta = 10^3 \text{ nm pN}^{-1} \text{ s}^{-1}$. Constant parameters are listed in Tab. I.

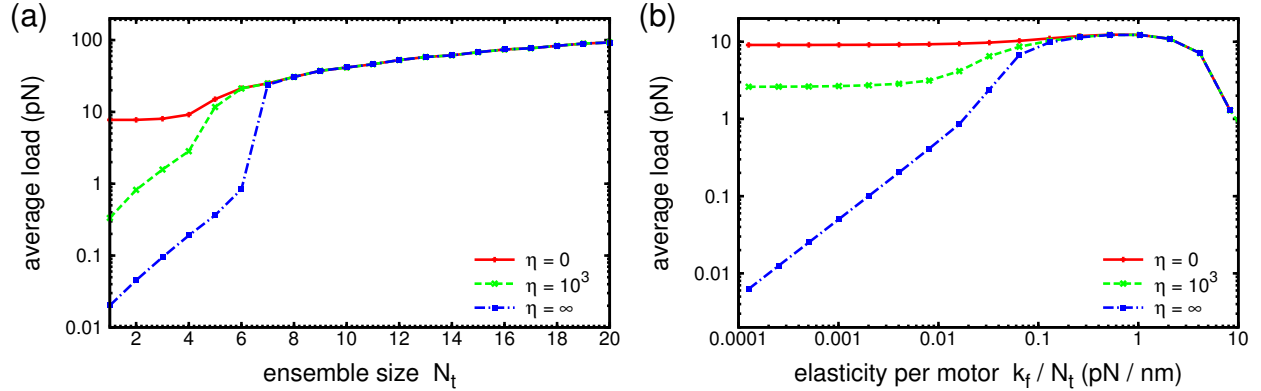


FIG. 27. Numerical results for the parallel cluster model with linear external load: average external load $\langle F_{\text{ext}} \rangle$ for $\eta = 0$, $\eta = 10^3 \text{ nm pN}^{-1} \text{ s}^{-1}$ and $\eta \rightarrow \infty$. (a) $\langle F_{\text{ext}} \rangle$ as function of ensemble size N_t for $k_f/N_t = 0.00379 \text{ pN nm}^{-1}$ of the external elastic constant. (b) $\langle F_{\text{ext}} \rangle$ as function of external elastic constant for $N_t = 4$. Constant parameters are listed in Tab. I.

expected, the average external load for finite mobility is intermediate between the extreme limits. As function of N_t for constant k_f/N_t , the dependence of $\langle F_{\text{ext}} \rangle$ at finite η resembles that of $\langle F_{\text{ext}} \rangle$ for $\eta \rightarrow \infty$: it increases linearly for small N_t and jumps to the isometric value at smaller k_f/N_t that $\langle F_{\text{ext}} \rangle$ for $\eta \rightarrow \infty$. As function of k_f/N_t at given N_t , the average external load for finite η is

constant as for $\eta = 0$ but smaller than the isometric load. The transition to the isometric value occurs at the same N_t as for $\eta \rightarrow \infty$.

Appendix B: Variation of model parameters

In the main body of the manuscript, one set of parameters was used to describe the dynamics of myosin II ensembles and only the dependence on F_{ext} , k_f and η was investigated. There are, however, many different types of myosin II motors for which the exact parameter values vary and indeed different sets of parameters are used in models (see Tab. I). The discussion of the force-velocity relation for constant external load following Fig. 10 has already demonstrated how experimentally accessible quantities such as load free velocity $v_b(F = 0)$ and stall force F_s are determined by our model parameters. A particularly characteristic quantity for different types of myosin II is the duty ratio ρ_d^{single} of individual motors. For example, the duty ratio of smooth muscle myosin II has been measured as $\rho_d^{\text{single}} \simeq 0.04$ (see Ref.²⁹) while for non-muscle myosin II a duty ratio of $\rho_d^{\text{single}} \simeq 0.23$ was found (see Ref.³¹). Moreover, the single motor duty ratio depends on ATP concentration through the off-rate from the post-power-stroke state, which is a first order function of ATP concentration⁴⁶. While the ATP concentration is rather stable *in vivo*, it can be varied *in vitro* over several orders of magnitude, thus varying ρ_d^{single} . For our set of model parameters, the single motor duty ratio for vanishing load was $\rho_d^{\text{single}} \simeq 0.33$. In this appendix, we discuss analytical results for constant external load for $\rho_d^{\text{single}} \simeq 0.1 < 0.33$ and $\rho_d^{\text{single}} \simeq 0.67 > 0.33$. The single motor duty ratio is change through the unloaded off-rate k_{20}^0 from the post-power-stroke state, because it is accessible experimentally and it is the most convenient determinant of ρ_d^{single} in our model. Changing the off-rate k_{10} from the weakly-bound state is not very efficient, because unbinding proceeds mainly from the post-power-stroke state. Changing the on-rate k_{01} , on the other hand, would also change the unloaded velocity $v_b(F = 0)$ directly and not only through the ensemble duty ratio.

1. Small duty ratio

In this section, we demonstrate the effect of a small duty ratio on the analytical results for constant external load. The unloaded off-rate from the post-power-stroke state is set to $k_{20}^0 \simeq 360 \text{ s}^{-1}$ so that the single motor duty ratio is $\rho_d^{\text{single}} \simeq 0.1$. Other parameters are as in Tab. I.

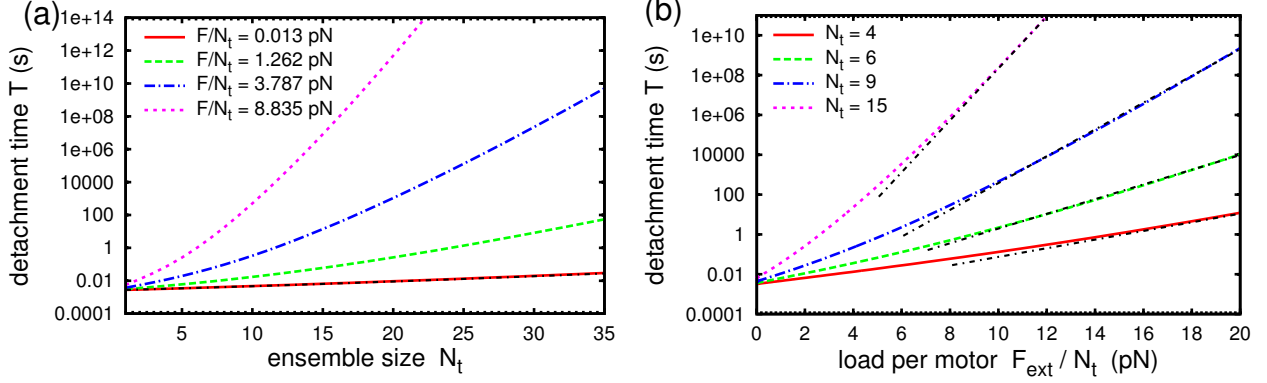


FIG. 28. Analytical results for the parallel cluster model with constant external load at reduced duty ratio of individual motors: average detachment time T_{10} . (a) T_{10} as function of ensemble size N_t for the values $F_{\text{ext}}/N_t = 0.0126$ pN, 1.262 pN, 3.787 pN and 8.835 pN of the external load per motor. The black, dash-dotted curve is the approximation of Eq. (51) for $F_{\text{ext}}/N_t = 0$. (b) T_{10} as function of the external load per motor F_{ext}/N_t for ensemble sizes $N_t = 4, 6, 9$ and 15 . Black, dash-dotted curves are exponential approximations. The unloaded off-rate from the post-power-stroke state is $k_{20}^0 = 360 \text{ s}^{-1}$ so that the duty ratio of a single, unloaded motor is $\rho_d^{\text{single}} \simeq 0.1$. Other parameters are as listed in Tab. I.

Fig. 28 (a) plots the detachment time as function of ensemble size for different values of the external load per motor. The qualitative dependence of T_{10} on N_t is the same as for $\rho_d^{\text{single}} \simeq 0.33$ (see Fig. 5), although T_{10} is significantly smaller at $N_t = 1$ and the increase of T_{10} with N_t is weaker. This is particularly striking for $F_{\text{ext}}/N_t \simeq 0.013$ where T_{10} increases by less than an order of magnitude from $N_t = 1$ to $N_t = 35$. Nevertheless, T_{10} at $F_{\text{ext}}/N_t \simeq 0.013$ pN is very well described by the approximation for vanishing load in Eq. (51). Fig. 28 (b) plots the detachment time T_{10} as function of F_{ext}/N_t for different N_t . Again, the increase of T_{10} with F_{ext}/N_t is weaker than for $\rho_d^{\text{single}} \simeq 0.33$ but does proceed exponentially for large enough F_{ext}/N_t .

Fig. 29 (a) plots the ensemble duty ratio as function of N_t for different F_{ext}/N_t . Due to the small detachment time, ρ_d at $N_t = 1$ is reduced in comparison to the case of $\rho_d^{\text{single}} \simeq 0.33$ (see Fig. 6). For $F_{\text{ext}}/N_t = 0.013$ pN, ρ_d follows the approximation for vanishing load from Eq. (53): it relaxes exponentially from the single motor duty ratio $\rho_d^{\text{single}} \simeq 0.1$ and reaches $\rho_d \simeq 1$ for ensemble sizes $N_t > 35$. For $\rho_d^{\text{single}} \simeq 0.33$, permanent attachment was achieved already for $N_t \geq 15$. With increasing external load, the duty ratio increases more rapidly with N_t . For very large F_{ext}/N_t , $\rho_d \simeq 1$ is reached for values of N_t that are comparable to the case of $\rho_d^{\text{single}} \simeq 0.33$. Fig. 29 (b)

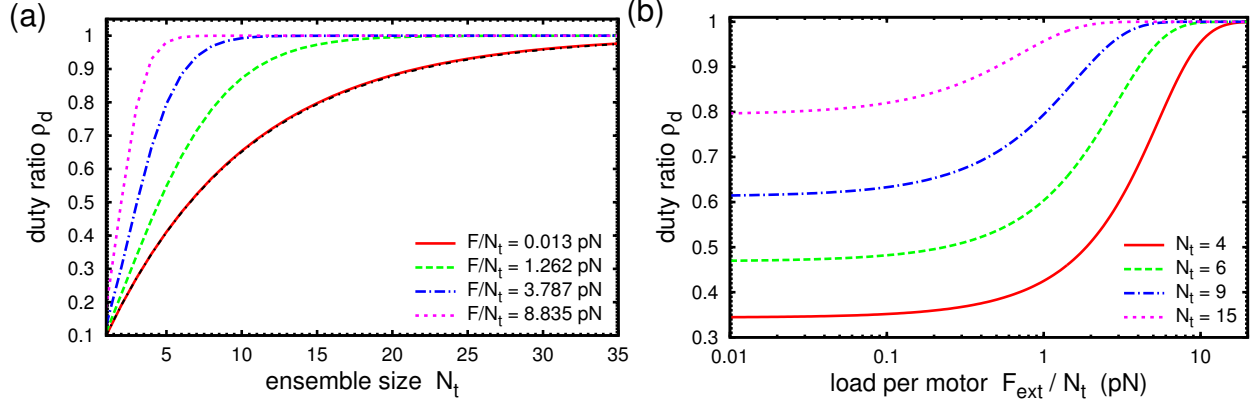


FIG. 29. Analytical results for the parallel cluster model with constant external load at reduced duty ratio of individual motors: ensemble duty ratio ρ_d . (a) ρ_d as function of ensemble size N_t for the values $F_{\text{ext}}/N_t = 0.0126$ pN, 1.262 pN, 3.787 pN and 8.835 pN of the external load per motor. The black, dash-dotted curve is the approximation of Eq. (53). (b) ρ_d as function of the external load per motor F_{ext}/N_t for ensemble sizes $N_t = 4, 6, 9$ and 15. The unloaded off-rate from the post-power-stroke state is $k_{20}^0 = 360 \text{ s}^{-1}$ so that the duty ratio of a single, unloaded motor is $\rho_d^{\text{single}} \simeq 0.1$. Other parameters are as listed in Tab. I.

plots the ensemble duty ratio as function of F_{ext}/N_t . Although at small external load, the duty ratio is significantly smaller than for $\rho_d^{\text{single}} \simeq 0.33$ in Fig. 6, the threshold for permanent attachment is reached at similar values of $F_{\text{ext}}/N_t \simeq 15$ pN.

Fig. 30 plots the average number of bound motors as function of ensemble size for different values of the external load per motor in (a) and as function of F_{ext}/N_t for different N_t in (b). As function of N_t , the average number of bound motors increases linearly. The slope increases with increasing F_{ext}/N_t . This increase is more pronounced than for $\rho_d^{\text{single}} \simeq 0.33$ (see Fig. 7). This is confirmed by the plot of N_b on F_{ext}/N_t . Over the range of external load shown in Fig. 30 (b), N_b increases about 6 fold while in Fig. 7 it increased about 2.5 fold. This apparently stronger mechanosensitive response of myosin II for smaller ρ_d^{single} is due to the saturation of N_b towards N_t , which has a stronger effect for large duty ratios.

Fig. 31 (a) plots the average bound velocity as function of the external load per motor for different ensemble sizes. Due to the smaller number of bound motors at vanishing load, $N_b \simeq 0.1N_t$, the load free velocity $v_b(F_{\text{ext}} = 0) \simeq [(N_t - N_b)/N_b] k_{01} = 9dk_{01} = 2880 \text{ nm s}^{-1}$ is significantly larger than for $\rho_d^{\text{single}} \simeq 0.33$ (see Fig. 10). Because N_b is also smaller at the stall force, F_s/N_t is reduced to $F_s/N_t \simeq 6$ pN for large N_t . The inset shows that v_b can again be fitted

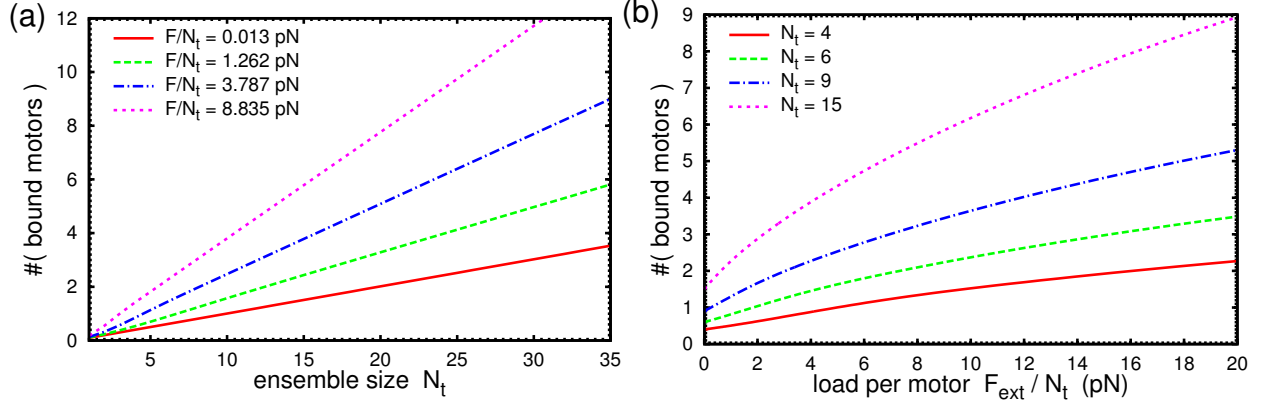


FIG. 30. Analytical results for the parallel cluster model with constant external load at reduced duty ratio of individual motors: average number of bound motors N_b . (a) N_b as function of ensemble size N_t for the values $F_{\text{ext}}/N_t = 0.0126$ pN, 1.262 pN, 3.787 pN and 8.835 pN of the external load per motor. (b) N_b as function of external load per motor F_{ext}/N_t for ensemble sizes $N_t = 4, 6, 9$ and 15. The unloaded off-rate from the post-power-stroke state is $k_{20}^0 = 360 \text{ s}^{-1}$ so that the duty ratio of a single, unloaded motor is $\rho_d^{\text{single}} \simeq 0.1$. Other parameters are as listed in Tab. I.

to the Hill relation from Eq. (54). The fit parameter α for large N_t is smaller than in Fig. 10, indicating a stronger curvature of $v_b(F_{\text{ext}})$. Due to the more frequent detachment of ensembles, the influence of the off-step $\Delta z_{1j}^{\text{off}}$ from Eq. (28) on the bound velocity is already observed for $N_t \leq 25$, which reveals itself by the larger values of α . Fig. 31 (b) plots the effective velocity v_{eff} of an ensemble as function of the external load per motor, F_{ext}/N_t . Due to the more frequent detachment of ensembles with smaller ρ_d^{single} , the deviations of v_{eff} from v_b due to the backward slips are larger than for $\rho_d^{\text{single}} \simeq 0.33$ in Fig. 10. The differences between effective and bound velocity become negligible only for $N_t > 25$.

2. Large duty ratio

In this section, we discuss the effect of a large duty ratio on the analytical results for constant external load. The unloaded off-rate from the post-power-stroke state is set to $k_{20}^0 \simeq 20 \text{ s}^{-1}$ so that the single motor duty ratio is $\rho_d^{\text{single}} \simeq 0.67$. All other parameters are as in Tab. I.

Fig. 32 (a) plots the detachment time as function of ensemble size for different values of the external load per motor. Despite the larger values of ρ_d at $N_t = 1$ and the steeper increase with

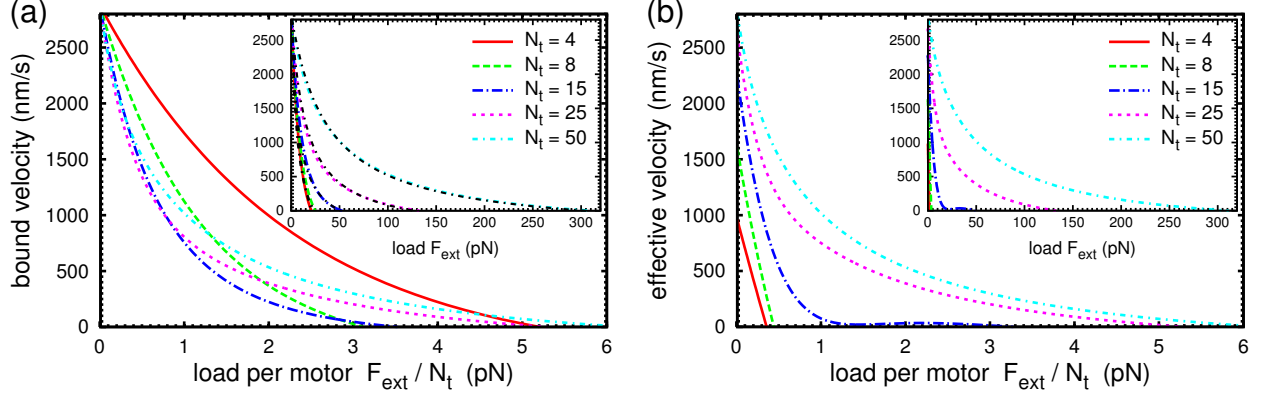


FIG. 31. Analytical results for the parallel cluster model with constant external load at reduced duty ratio of individual motors. (a) Average bound velocity v_b and (b) average effective velocity v_{eff} as function of the external load per motor F_{ext}/N_t for ensemble sizes $N_t = 4, 8, 15, 25$ and 50 . The mobility of the free ensemble entering v_{eff} is $\eta = 10^3 \text{ nm pN}^{-1} \text{ s}^{-1}$. The insets show v_b and v_{eff} as function of external load F_{ext} . Black, dash-dotted curves in the inset of (a) show the Hill-relation from Eq. (54) with $\alpha = 0.46 \text{ pN}, 0.25 \text{ pN}, 0.14 \text{ pN}, 0.12 \text{ pN}$ and 0.12 pN for $N_t = 4, 8, 15, 25$ and 50 . The unloaded off-rate from the post-power-stroke state is $k_{20}^0 = 360 \text{ s}^{-1}$ so that the duty ratio of a single, unloaded motor is $\rho_d^{\text{single}} \simeq 0.1$. Other parameters are as listed in Tab. I.

increasing N_t , T_{10} has the same qualitative dependence on N_t as for $\rho_d^{\text{single}} < 0.67$. For $F_{\text{ext}}/N_t \simeq 0.013$, T_{10} is very well described by the approximation for vanishing load from Eq. (51). Fig. 32 (b) plots the detachment time T_{10} as function of F_{ext}/N_t for different N_t . The increase of T_{10} with F_{ext}/N_t is significantly more rapid than for smaller ρ_d^{single} and is described by an exponential over the whole range of F_{ext}/N_t .

Fig. 33 (a) plots the ensemble duty ratio as function of N_t for different values of F_{ext}/N_t . For all values of F_{ext}/N_t , the same qualitative behavior of T_{10} is observed as for $\rho_d^{\text{single}} \simeq 0.33$ (see Fig. 6. For small load, ρ_d follows the approximation for vanishing load in Eq. (53) and reaches $\rho_d \simeq 1$ already for $N_t \simeq 5$. Fig. 29 (b) plots the ensemble duty ratio as function of F_{ext}/N_t . For all values of N_t , the ensemble duty ratio is practically unity over the whole range of F_{ext}/N_t .

Fig. 34 plots the average number of bound motors N_b as function of ensemble size N_t for different values of the external load per motor F_{ext}/N_t in (a) and as function of F_{ext}/N_t for different N_t in (b). As function of N_t , the average number of bound motors increases linearly but the slope shows a weak dependence on F_{ext}/N_t . This is confirmed by the plot of N_b on F_{ext}/N_t . Due to the

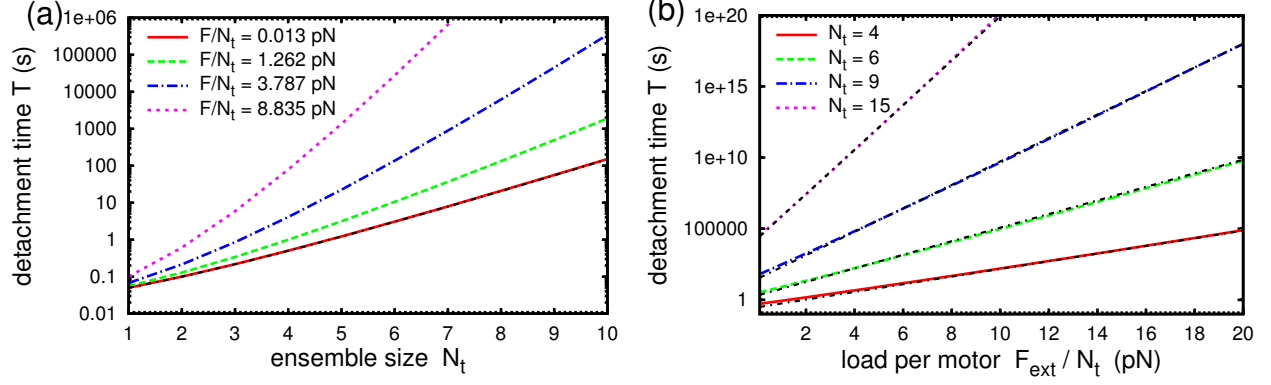


FIG. 32. Analytical results for the parallel cluster model with constant external load at increased duty ratio of individual motors: average detachment time T_{10} . (a) T_{10} as function of ensemble size N_t for the values $F_{\text{ext}}/N_t = 0.0126$ pN, 1.262 pN, 3.787 pN and 8.835 pN of the external load per motor. The black, dash-dotted curve is the approximation of Eq. (51) for $F_{\text{ext}}/N_t = 0$. (b) T_{10} as function of the external load per motor F_{ext}/N_t for ensemble sizes $N_t = 4, 6, 9$ and 15 . Black, dash-dotted curves are exponential approximations. The unloaded off-rate from the post-power-stroke state is $k_{20}^0 = 20 \text{ s}^{-1}$ so that the duty ratio of a single, unloaded motor is $\rho_d^{\text{single}} \simeq 0.67$. Other parameters are as listed in Tab. I.

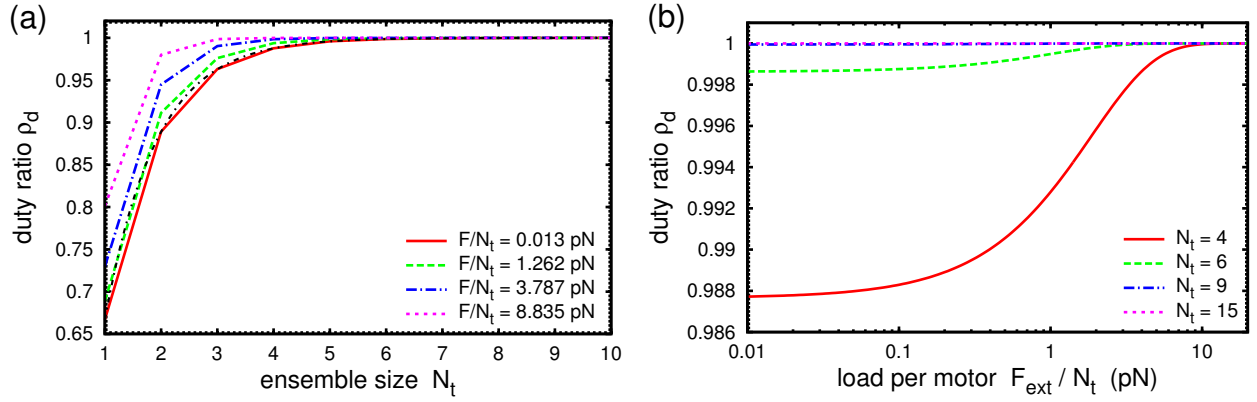


FIG. 33. Analytical results for the parallel cluster model with constant external load at increased duty ratio of individual motors: ensemble duty ratio ρ_d . (a) ρ_d as function of ensemble size N_t for the values $F_{\text{ext}}/N_t = 0.0126$ pN, 1.262 pN, 3.787 pN and 8.835 pN of the external load per motor. The black, dash-dotted curve is the approximation of Eq. (53). (b) ρ_d as function of the external load per motor F_{ext}/N_t for ensemble sizes $N_t = 4, 6, 9$ and 15 . The unloaded off-rate from the post-power-stroke state is $k_{20}^0 = 20 \text{ s}^{-1}$ so that the duty ratio of a single, unloaded motor is $\rho_d^{\text{single}} \simeq 0.67$. Other parameters are as listed in Tab. I.

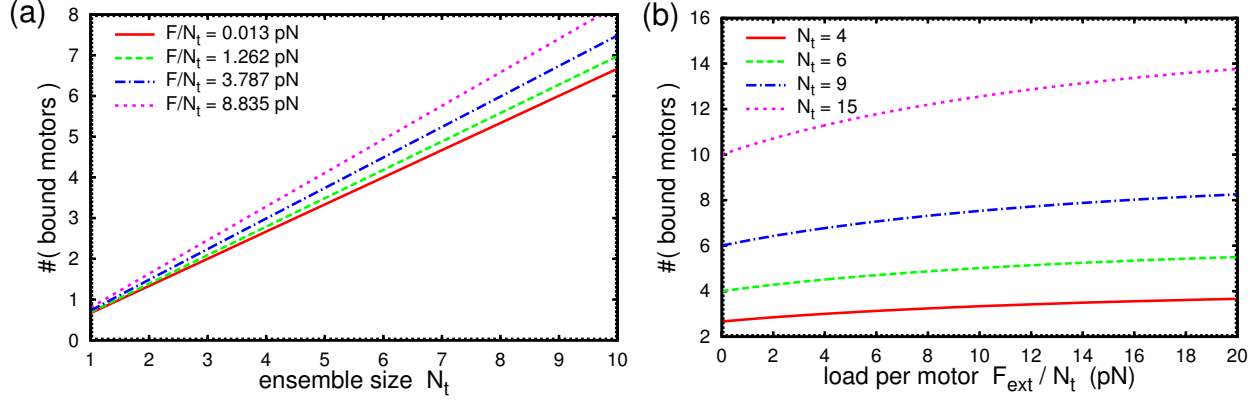


FIG. 34. Analytical results for the parallel cluster model with constant external load at increased duty ratio of individual motors: average number of bound motors N_b . (a) N_b as function of ensemble size N_t for the values $F_{\text{ext}}/N_t = 0.0126$ pN, 1.262 pN, 3.787 pN and 8.835 pN of the external load per motor. (b) N_b as function of external load per motor F_{ext}/N_t for ensemble sizes $N_t = 4, 6, 9$ and 15. The unloaded off-rate from the post-power-stroke state is $k_{20}^0 = 20 \text{ s}^{-1}$ and the duty ratio of a single, unloaded motor is $\rho_d^{\text{single}} \simeq 0.67$. Other parameters are as listed in Tab. I.

larger number of bound motors at $F_{\text{ext}}/N_t = 0$, the N_b can only increase weakly with F_{ext}/N_t so that the ensemble with large ρ_d^{single} appears to be weakly mechanosensitive.

Fig. 35 (a) plots the average bound velocity as function of external load per motor for different ensemble sizes. Due to the larger number of bound motors at $F_{\text{ext}}/N_t = 0$, the load free velocity $v_b(F_{\text{ext}} = 0) \simeq [(N_t - N_b)/N_b] k_{01} = 0.5dk_{01} = 160 \text{ nm s}^{-1}$ is significantly smaller than for $\rho_d^{\text{single}} \simeq 0.33$ (see Fig. 10). Because of the larger number of bound motors at the stall force, F_s/N_t is increased to $F_s/N_t \simeq 16$ pN for large N_t . The force-velocity relation is constant for ensemble sizes above $N_t \geq 8$. The inset shows that v_b can again be fitted to the Hill relation from Eq. (54). The fit parameter α is generally larger than in Fig. 10, indicating a smaller curvature of $v_b(F_{\text{ext}})$. Because detachment is rare even for $N_t = 4$, there are no significant deviations from the shape of the force-velocity curve for large N_t . Also the effective velocity deviates from the bound velocity only for $N_t = 4$.

The comparison of the results for constant external load for different values of the single motor duty ratio ρ_d^{single} has shown that the qualitative behavior of the motor ensembles is robust to changes of ρ_d^{single} , although the quantitative results do change. In particular the stochastic effects from ensemble detachment become more pronounced for smaller ρ_d^{single} . The results for the force-

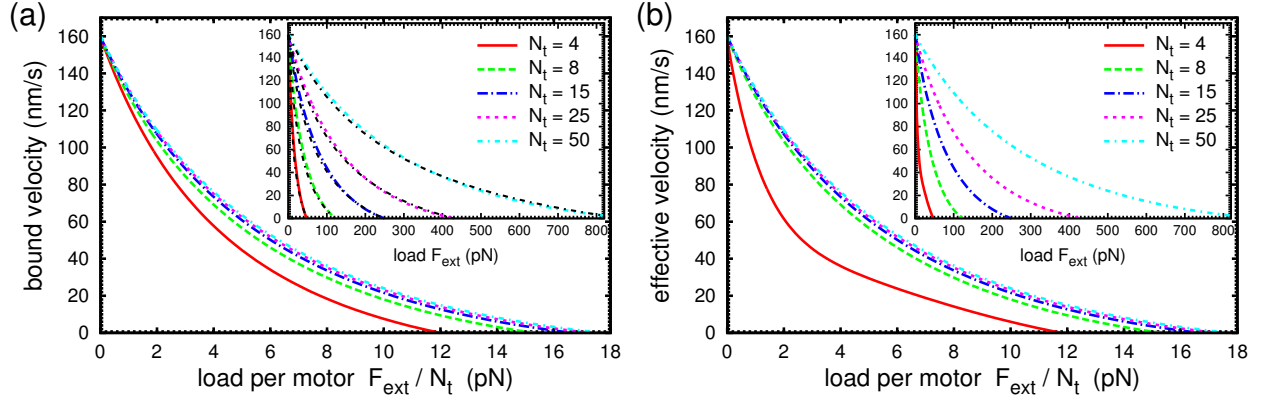


FIG. 35. Analytical results for the parallel cluster model with constant external load at increased duty ratio of individual motors. (a) Average bound velocity v_b and (b) average effective velocity v_{eff} as function of the external load per motor F_{ext}/N_t for ensemble sizes $N_t = 4, 8, 15, 25$ and 50 . The mobility of the free ensemble entering v_{eff} is $\eta = 10^3 \text{ nm pN}^{-1} \text{ s}^{-1}$. The insets show v_b and v_{eff} as function of external load F_{ext} . Black, dash-dotted curves in the inset of (a) show the Hill-relation from Eq. (54) with $\alpha = 0.28 \text{ pN}, 0.28 \text{ pN}, 0.30 \text{ pN}, 0.32 \text{ pN}$ and 0.34 pN for $N_t = 4, 8, 15, 25$ and 50 . The unloaded off-rate from the post-power-stroke state is $k_{20}^0 = 20 \text{ s}^{-1}$ so that the duty ratio of a single, unloaded motor is $\rho_d^{\text{single}} \simeq 0.67$. Other parameters are as listed in Tab. I.

velocity relation confirm the dependence of the load free velocity and the stall force on the model parameters.